Vector Drop-on-Demand Production of Tungsten Carbide-Cobalt Tooling Inserts by Three Dimensional Printing

by

David Guo

B. S. Mechanical Engineering
The University of Texas at Austin, 1998

Submitted to the Department of Mechanical Engineering in
Partial Fulfillment of the Requirements for the Degree of

MASTER OF SCIENCE IN MECHANICAL ENGINEERING

at the

MASSACHUSETTS INSTITUTE OF TECHNOLOGY

June 2004

Signature of Author: ....
Department of Mechanical Engineering
May 7, 2004

Certified by: ....
Professor Emanuel M. Sachs
Professor of Mechanical Engineering
Laboratory for Manufacturing and Productivity
Thesis Supervisor

Accepted by: ....
Professor Ain A. Sonin
Chairman, Committee for Graduate Students
Department of Mechanical Engineering

Vector Drop-on-Demand Production of Tungsten Carbide-Cobalt Tooling Inserts by Three Dimensional Printing

by

David Guo

ABSTRACT

Three Dimensional Printing (3DP) is a solid freeform fabrication process used to generate solid parts directly from three-dimensional computer models. A part geometry is created by selectively depositing binder into sequentially spread layers of powder. In slurry-based 3DP, a suspension of powder in a solvent is used to form the powderbed layer. This slurry-based powderbed yields higher green density and part resolution than dry powder-based 3DP because of smaller particle size. Vector printing requires that the printhead trace and define the external geometries of a part before raster filling the interior, a new approach in comparison to conventional, raster-only printing. Drop-on-demand (DOD) printheads allow binder droplets to be ejected when needed rather than relying upon charge-and-deflect mechanisms used in continuous jet printheads. Integrating these concepts for vector, DOD printing has the potential to enhance the 3DP process by providing greater part resolution and surface finish. The 3DP slurry-based process and vector, drop-on-demand printing are examined as potential methods to produce Tungsten Carbide-Cobalt (WC-Co) tooling inserts.

The research focuses on three fundamental process steps: (1) development of a stable slurry, (2) determination of jetting parameter values for optimal powderbed deposition, and (3) implementation of vector, DOD printing for the binder. Due to unforeseen circumstances, the first two objectives are only briefly introduced in Chapter 1 and summarized in Chapter 3. Further details may be found in the Diplomarbeit document of Olaf Dambon. Two approaches are explored to develop a stable, jettable slurry. One method involves using a water-based Tungsten Carbide slurry and a Cobalt Acetate binder; the other method utilizes an alcohol-based Tungsten Carbide-Cobalt slurry and an organic binder. Various suspension properties, such as sedimentation density and viscosity, are measured to assess the degree of slurry stability. After adequate slurry formulations are developed, an investigation of powderbed formation is conducted. Due to the low solubility limit of the Cobalt salt in water and the persistent defects in water-based slurry powderbeds, the alcohol-based approach is pursued and, because of its greater efficacy, is used for optimizing powderbed jetting parameters. An effective combination of line spacing, flow rate, and drying time is determined for producing powderbeds with minimal surface roughness and high packing density. Experiments are subsequently conducted in vector DOD printing of various geometries using a piezo-actuated, drop-on-demand printhead and Bridgeport three-axis milling machine. A Hewlett-Packard inkjet cartridge is initially used for vector testing of the milling machine; a Siemens PT-88S printhead is used to assess and optimize binder droplet formation parameters, such as voltage waveform and fluid properties. Functional conditions for vector printing and DOD droplet generation are developed and deliver acceptable performance. Successfully printed geometries with high-definition lines (140-170 μm line width) and smooth surface finish are produced using sanded, jetted alumina slurry powderbeds. Following necessary refinements in slurry redispersion and slurry-binder compatibility, the same vector process can be repeated with jetted WC-Co slurry powderbeds.

Thesis Supervisor: Emanuel M. Sachs
Title: Professor of Mechanical Engineering

ACKNOWLEDGMENTS

Many people contributed to making my graduate experience a success. I would require many more pages to properly thank all of those who touched my life during these past two years. I can only begin by paying some small tribute to all of you.

First and foremost, I wish to thank Professor Emanuel Sachs for his tolerance, commitment, and understanding. You have taught me a great deal about the importance of believing in what you can accomplish and what it takes to be successful at anything in life. I will forever continue to make efforts to improve in this direction.

I must also give a great thanks to Professor Michael Cima for providing an insightful material science perspective in analyzing my experimental data. Your comments and suggestions have undoubtedly increased my understanding in this field of interest.

Dave Brancazio and Jim Serdy have my gratitude for providing invaluable assistance and advice in setting up experiments. They are—without a doubt—the foundation of this lab. I also thank Jim for broadening my perspective on life and the world, and I will surely miss Dave for his knowledge of electronics and his impressive musical talent.

I wish to thank Pat Saxton and Bjorn Debear for helping me get situated in the beginning of my graduate studies. Both of you were great to work with. The background knowledge you shared (and the laughs you sometimes had at my expense) made my transition into 3DP an enjoyable (and entertaining) one.

To alumni Jason Grau, Scott Uhland, Richard Holman, and Sherry Morissette, your knowledge of material science, suspension stability, and slurry-based 3DP has been an extraordinary resource. Without your assistance, I could not have achieved the milestones that have brought 3DP tooling inserts closer to fruition.

Olaf Dambon, I cannot imagine what things would have been like if I had not had the chance to work with you. You were a fundamental part of this thesis work. Without you, I do not believe I could have achieved as much. You are a great friend with whom I will cherish many memories both inside and outside of lab. You have my eternal respect and gratitude.

A special note for the additional Germans in our group: Bernd Heid, Markus Werner, Andreas Straube, and René Apitz. Having gained an immense affection for your culture during my time in Munich, I believe you all represent the best of what Germans are, and you have my utmost respect and admiration. Beyond being great colleagues, you have all been great friends.

Another note of gratitude goes to Mark Belanger and Gerry Wentworth for their invaluable assistance in the Laboratory for Manufacturing & Productivity machine shop. You have taught me a great deal about and given me a new appreciation for the art and skill of machining.

For Huaijun Wu, Xiaorong Xu, Costas Hadjiloucas, Garth Grover, Ben Polito, Adam Lorenz, Ram Chilukuri, Diana Buttz, David Ables, and all the great people in the basements of Buildings 12 and 35, though I did not have the opportunity to work extensively with you, I thank you for your willingness to help and feel incredibly fortunate to have had the chance to know you.

Finally, I would like to thank John Keane of Valenite and Russ Yeckley of Kennametal for your continued support and for making this research possible.

For those now in my life who have made this once distant goal a reality, no words will ever be able to express my gratitude.

It has been a pleasure and a great honor working with all of you.

TABLE OF CONTENTS

LIST OF FIGURES

11

LIST OF TABLES

15

1 INTRODUCTION

1.1. THE THREE DIMENSIONAL PRINTING PROCESS

Similar to other rapid prototyping (RP) technologies such as stereolithography and selective laser sintering, Three Dimensional Printing (3DP) is a solid free-form fabrication technique developed at the Massachusetts Institute of Technology that produces three-dimensional parts directly from computer-generated models [1]. This unique RP process has successfully fabricated parts using various materials, including ceramics, metals, and polymers [2]. Every part is manufactured by "inkjet" printing droplets of binder into a sequence of two-dimensional powder layers [2-7]. The binder placement information for each layer is determined by applying a slicing algorithm to the computer-generated model [6]. Two basic types of Three Dimensional Printing exist (1) dry powder-based 3DP and (2) slurry-based 3DP.

In dry powder-based 3DP, the first of the two processes developed, a thin layer of powder is evenly distributed across a piston. A nozzle then selectively deposits binder into the powder to define the part geometry. After drying the binder, the piston is subsequently lowered by a one-layer increment, and a new powder layer is spread over the surface of the previously printed one. Unbound powder from the preceding layers can support portions of the binder-printed part, thereby allowing overhangs, undercuts, and internal volumes to be created [2]. This procedure is repeated until the complete part geometry is printed. The excess powder, which lacks binder, is then removed to extract the finished part [4]. Figure 1.1 illustrates the basic, dry powder-based 3DP process. Subsequent post-processing steps, such as de-binding and sintering, are performed if necessary [5].
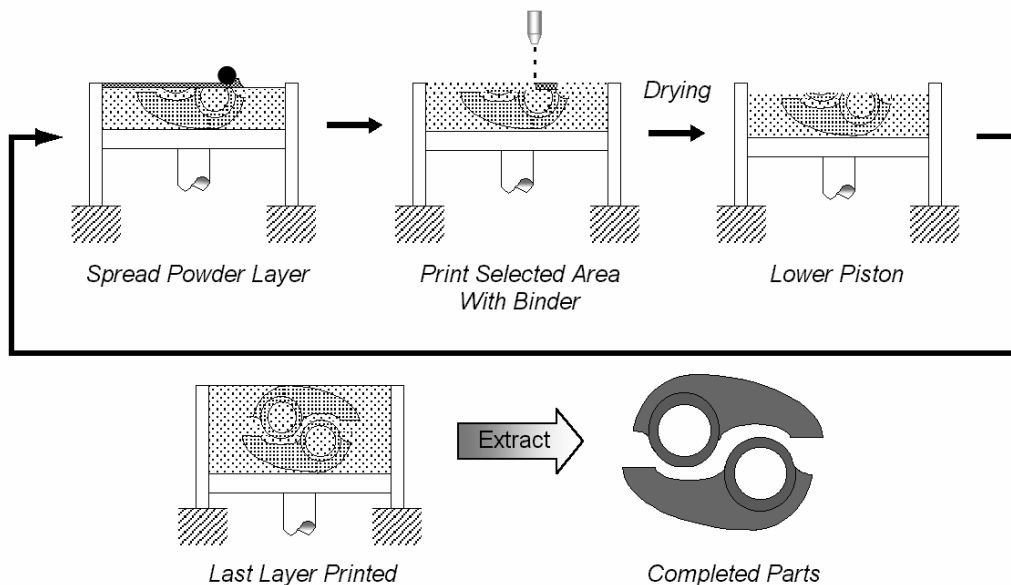
Figure 1.1 Illustration of the dry powder-based Three Dimensional Printing (3DP) process.

Spreading smooth, uniform layers of dry powder becomes a problem when the particle size decreases below approximately 50 microns [4]. This difficulty arises from the high surface area to volume ratio of and van der Waals attraction between particles, which tend to agglomerate. This uneven spreading phenomenon results in a low packing density and thus poor part definition within the powderbed. In response to this problem, a new approach has been developed that modifies the dry powder-based 3DP process by using a slurry, a flowable liquid suspension of particles in a solvent, instead of dry powder to deposit a powderbed layer.

In slurry-based 3DP, the suspension is produced by mixing a powder, a solvent (i.e. water or alcohol), and a dispersant. The dispersant prevents particles from flocculating in the slurry, thus allowing the mixture to be easily jetted from a small orifice nozzle—typically 100 to 200 microns in diameter. The slurry (otherwise known as a dispersion) is then raster printed across a porous substrate. The pores in the surface beneath the jetted slurry absorb the liquid portion of the slurry, leaving a thin, even, and compact layer of powder. A period of heat-assisted drying ensures adequate removal of moisture from the powderbed layer and protects against crack formation [8]. The binder is then selectively printed into the layer. The layer is once again dried to remove binder liquid from the powderbed. These steps are repeated until the part is defined [8]. Figure 1.2 depicts this process.
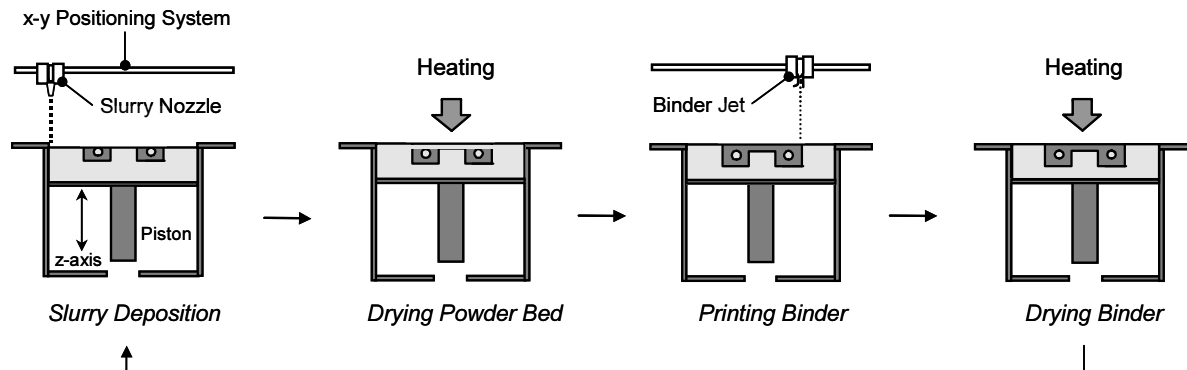
Figure 1.2　　Illustration of the slurry-based Three Dimensional Printing part production process.

An additional step is necessary in order retrieve the part from the resulting powderbed. Since the slurry powderbed has significant cohesive strength, the printed part cannot be removed by brushing away the unbound powder. The entire powderbed must instead be submerged in a redispersing agent that separates the excess powder while preserving the binder printed regions. Figure 1.3 on the following page illustrates this extraction procedure. A more detailed explanation of slurry-based 3DP and its fundamental development may be found in Jason Grau's thesis [8].

Printed Part

Jetted Unbound Powderbed

Porous Substrate

Solvent

Completed Part Embedded in Powderbed

Redispersion of Powderbed in Solvent

Printed Part Retrieved
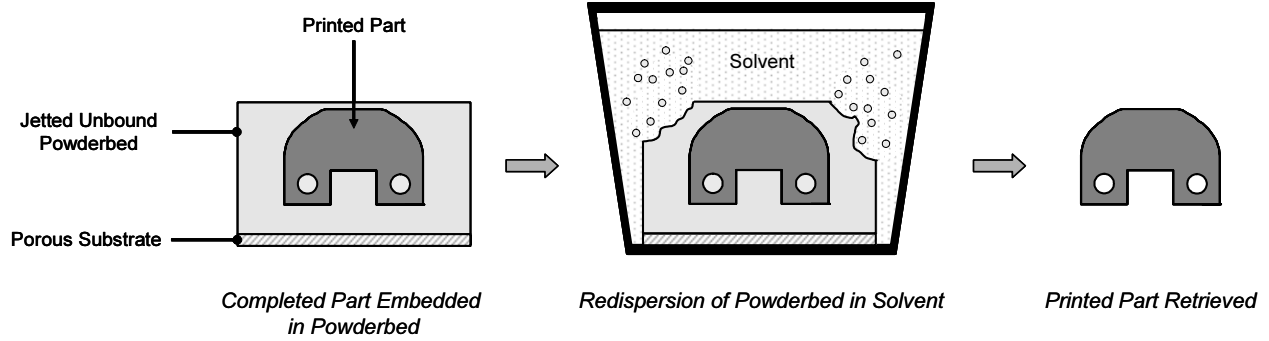
Figure 1.3   Redispersion technique for the slurry-based 3DP process that removes unbound regions of powder by submerging the entire assembly in solvent to retrieve the printed part.

1.2.   VECTOR DROP-ON-DEMAND PRINTING VS. STANDARD 3DP METHOD

In terms of how geometry can be defined by 3DP, two basic approaches exist: raster printing or vector printing. In addition, two different types of printheads—a continuous jet (CJ) and a drop-on-demand (DOD)—can be used to print the binder. Vector drop-on-demand printing requires that the process of vector definition and drop-on-demand droplet generation work in unison to define the shape of a part. This printing style is being explored as a new binder deposition process for Three Dimensional Printing. The current 3DP process utilizes raster printing to define shapes and a continuous jet nozzle to generate droplets. There are several fundamental differences between these two printing methods.

Raster printing involves an iterative, stepwise movement along a part's geometry. In a simplified model, given the designated area to be printed in a layer, the shape is divided into a set of equal, parallel lines that each represents approximately one line spacing of binder droplets (see Figure 1.4). For either printing method, the line spacing created by binder droplets is determined by measuring the width of bound powder resulting from a single line of printed binder and then using a certain amount of overlap to ensure adequate stitching between lines.

T O P   V I E W

Single Binder Droplet Line Spacing

Part Geometry

Loose Powderbed
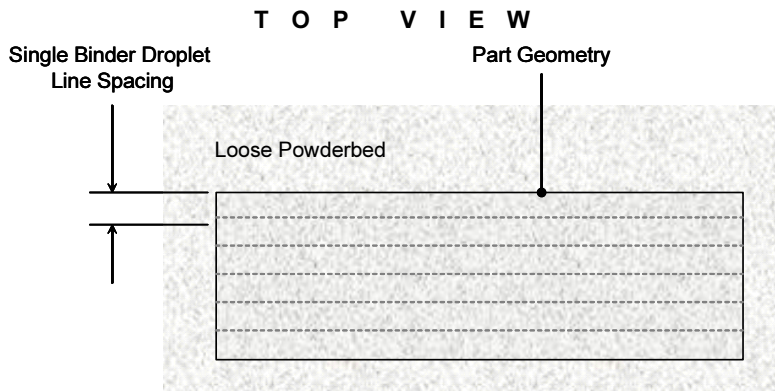
Figure 1.4   Single dashed lines indicate the division of the desired rectangular shape into a set of parallel lines that are each less than one binder droplet line spacing wide to introduce overlap. These lines are the paths that the nozzle will follow to define the part geometry in this layer.

The binder nozzle moves along each parallel line selectively depositing binder to delineate the shape and, after completely traversing across the powderbed, shifts over one line spacing to deposit the next binder dose. This process is repeated for each layer until the entire part has been printed. Figure 1.5 depicts how raster printing is performed as described above.

TOP VIEW
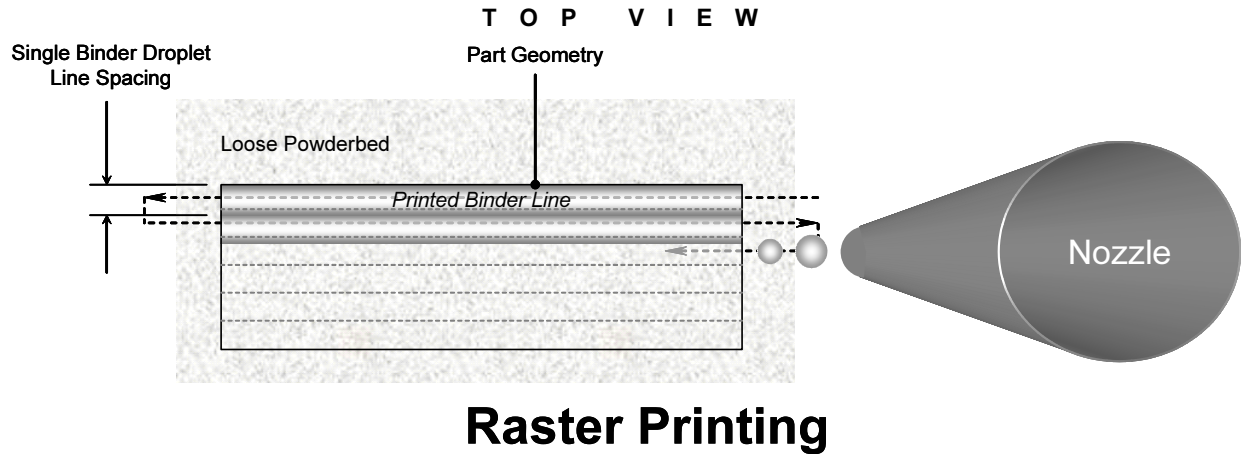
Raster Printing

Figure 1.5   Illustration of raster printing. The nozzle places binder droplets by moving along the parallel line divisions depicted in Figure 1.4.

In addition to raster printing, the standard 3DP method employs a continuous jet nozzle. This type of nozzle uses pressure to move binder through a cylindrical piezo that breaks the stream into a series of droplets [9]. Electrical signals charge the droplets and control their movement by directing them to either the powderbed or a catcher. Figure 1.6 illustrates this printing process. This charge-and-deflection scheme allows any desired geometry to be defined by selectively placing droplets onto the powderbed. For a more detailed discussion of continuous jet operation and characterization, refer to [9].
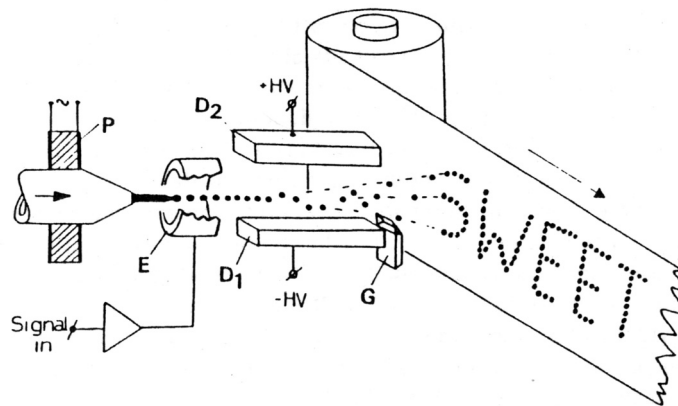
Figure 1.6   A continuous inkjet breaks up into droplets inside the control electrode E. Due to mechanical vibrations generated by the piezoelectric ceramic P, all droplets have equal mass. Each droplet can be charged individually by applying a suitable control voltage to electrode E at the moment the droplet is formed. Depending on this charge, the droplet will be deflected in the transverse electric field between electrodes D_1 and D_2, either onto the paper or into the gutter G [9].

In contrast to the parallel slicing, linear method of raster printing, vector printing involves moving the nozzle along the part contour to trace the desired geometry. The nozzle thus progresses in a primarily nonlinear fashion with adjacent parallel lines along the contour. The line spacing for each vector line is determined in the same manner as raster printing. Figure 1.7 shows how a vector trace for a rectangular part could be defined.

T O P   V I E W

Single Binder Droplet
Line Spacing

Part Geometry

Loose Powderbed
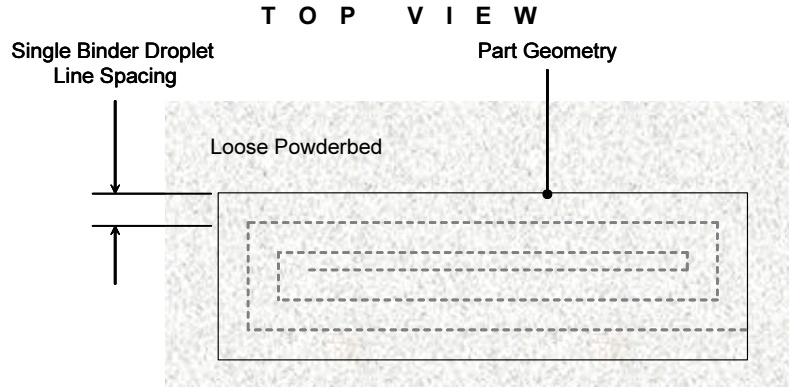
Figure 1.7   Dashed line defines the imaginary division of a desired rectangular shape into a spiraling vector trace with line spacing less than one binder droplet line spacing wide. This line depicts the path that the nozzle will follow to define the part's shape in this layer.

Using the trace in Figure 1.7, the nozzle moves along the part contour, deposits binder, and gradually moves inward along progressively smaller contour lines to fill the interior of the geometry. This process is repeated in each layer until the entire part has been printed. Figure 1.8 illustrates this printing process for a single layer.

T O P   V I E W

Single Binder Droplet
Line Spacing

Part Geometry

Loose Powderbed

Nozzle

Printed Binder Line
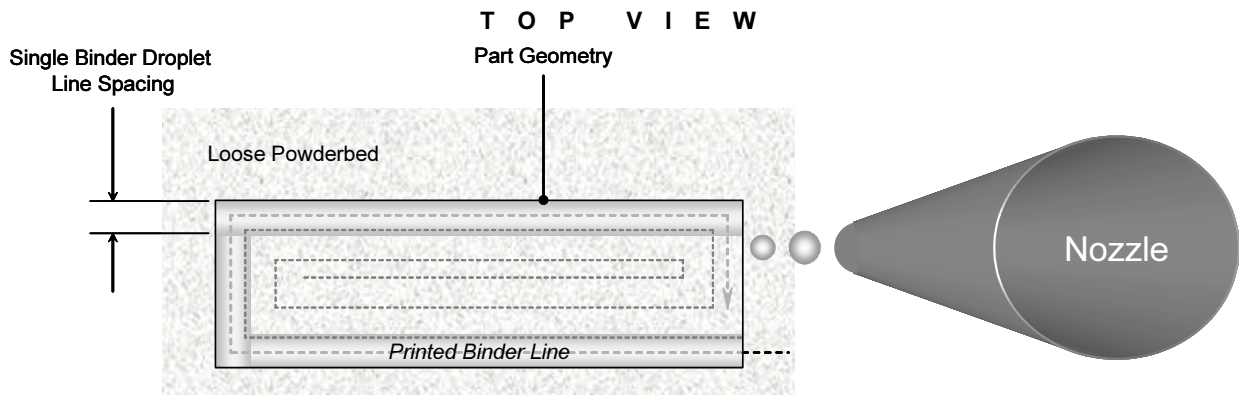
Vector Printing

Figure 1.8   Illustration of vector printing. The nozzle places binder droplets by moving along the adjacent, parallel contour lines depicted in Figure 1.7.

Vector printing is complemented by the use of drop-on-demand droplet production. Drop-on-demand systems use electrical signals "to control the moment when an individual drop is ejected" [9].

The fluid is dispensed from the nozzle by activating a transducer, commonly a piezoelectric device that changes shape with an applied charge. Instead of using high pressure to eject a continuous stream of droplets as before, a DOD nozzle uses a pressure impulse generated by the transducer to accelerate and then separate the fluid from the nozzle to form a drop [9]. This signal is only sent when a droplet is required to define the geometry so no "catcher," as required in CJ printheads, is necessary. The signal is represented by an electrical waveform that causes the piezo to contract upon an applied positive voltage. Figure 1.9 provides a simplified cross-section of a typical DOD printhead and its components. A more detailed discussion of drop-on-demand operation and characterization can be found in [9].
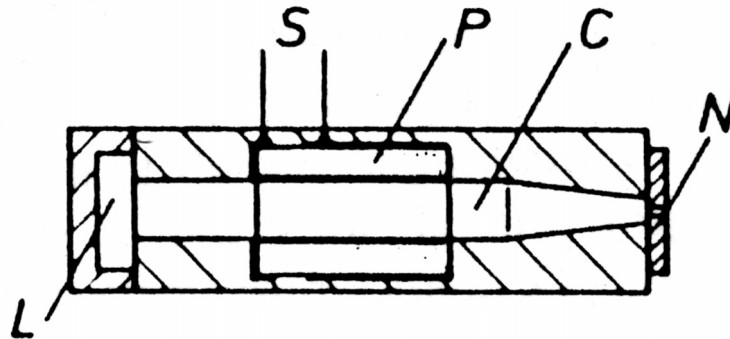
Figure 1.9   A thick piezo-tube cast in a plastic unit (Heinzl, 1975) as a type of drop-on-demand system containing a nozzle N, ink chamber or ink channel C, ink conduit L, and piezoelectric transducer P, which is excited by short electrical signals S [9].

The combination of vector printing and drop-on-demand droplet generation presents a new method by which to produce 3DP parts. In comparison to the conventional raster, continuous jet printing process, several potential advantages exist which will be discussed in Section 1.4. An investigation into the operating parameters for this printing process is one portion of the research presented in this thesis. The primary effort, however, has been to incorporate this technology into the production of tungsten carbide-cobalt tooling inserts.

1.3.   TUNGSTEN CARBIDE-COBALT TOOLING INSERTS

Tungsten Carbide-Cobalt (WC-Co) tooling inserts are machining tools used for metal removal when manufacturing hard steels. Insert geometries typically have a rectangular or diamond shape. When compared to steel, tungsten carbide tools have several superior characteristics: (1) strength in compression, (2) rigidity and abrasion resistance, (3) heat resistance, (4) machine tool accuracy, (5) reduced machine downtime and maintenance, (6) chemical stability, and (7) reduced scrap. The Cobalt acts as a binder material in the insert to hold the tungsten carbide particles together. Tooling inserts are commonly used in automotive, aeronautic, medical, and farming applications [10, 11]. Figure 1.10 shows two standard tooling inserts in their sintered and unsintered forms.
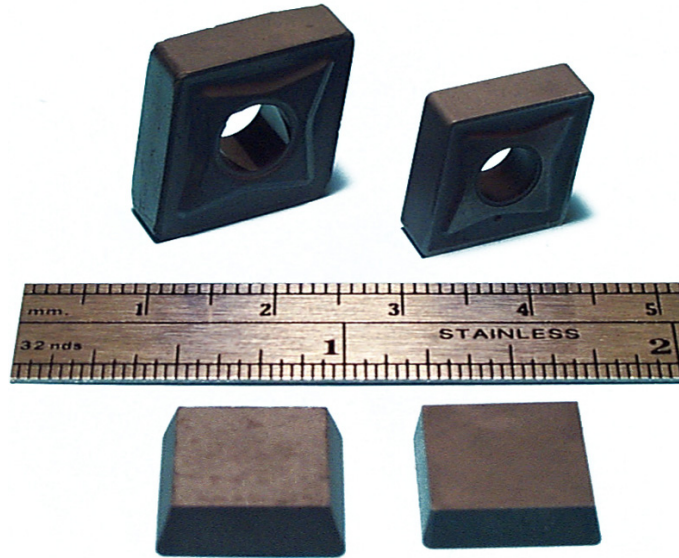
Figure 1.10   Two conventional types of WC-Co tooling inserts. Each set consists of an unsintered (left) and a sintered (right) form. Tooling inserts provided courtesy of Valenite, Inc.

Conventional Tungsten Carbide-Cobalt components, also known as cemented carbides, are manufactured through a powder metallurgy (PM) process, which involves powder processing, production of grade powders, powder consolidation, sintering, and finishing [10, 11]. This process usually takes an average of three to four days to complete. These cemented carbide inserts are composed of three fundamental constituents: the ceramic-phase tungsten carbide, the metallic binder Cobalt, and various alloying elements (such as Titanium Carbide or Vanadium Carbide) [10]. Other impurities, such as sulfur, calcium, or phosphorus, may be present in miniscule amounts without weakening final tool properties [12]. Complex chemical reactions are involved to produce these basic powder components. The prepared ingredients are then combined in a slurry and milled in a conventional ball mill, attrition mill, or vibratory mill for a few hours to produce a homogeneous mixture. The slurry contains a protective solvent (i.e. acetone) that minimizes heating and oxidation and a dissolved lubricant (i.e. paraffin wax) that solidifies when dried and also impedes oxidation. The solvent is subsequently removed from the mixture by a process known as spray drying. A nozzle atomizes the slurry by spraying it into a stream of hot nitrogen gas and forms dried spherical aggregates of powder and wax approximately 150 to 250 microns in diameter [10, 11]. Many references provide detailed descriptions of variations in this slurry processing technique [10, 13-15]. Through several types of consolidation techniques, such as hydraulic isostatic pressing, extrusion, or injection molding, the grade powder is formed into the desired shape. This billet is then machined to a net shape if necessary. Sintering operations first de-wax at 400 to 500 °C and then sinter the parts to full density at 1300 to 1600 °C. This final sintering temperature depends on the Cobalt content. The Cobalt binder begins to melt, and liquid

phase sintering occurs. During this time, the WC particles rapidly coalesce and form a "fully dense, virtually porosity-free microstructure" [10]. Hot isostatic pressing (HIP) may also be performed after or during the sintering process to eliminate residual porosity, pits, or defects [10, 11]. Finishing operations, such as diamond grinding, are performed to yield appropriate material and surface properties for the final production piece [10].

Valenite and Kennametal are two companies that produce these tooling inserts. As joint sponsors of this research, they seek to explore the capabilities of Three Dimensional Printing as a new method for manufacturing their products. The slurry-based 3DP method and vector drop-on-demand printing previously discussed introduce several advantages compared to the conventional tooling insert production process.

1.4. MOTIVATION

Many enhancements to the 3DP method and to manufacturing WC-Co tooling inserts can be realized through pursuit of this research. The slurry-based 3DP method generates high-density green parts that are necessary for sintering to full density [16]. The slurry processing route permits high definition, small featured part production because of the sub-micron powder used [16] and is well suited to fabricating multiple copies of miniature parts [17]. Vector printing represents a new and improved method for defining part geometry by tracing the outline directly instead of by raster printing (refer to the comparison in Section 1.2). This vectoring technique offers the potential for higher quality surface finish and edge definition for printed parts. Drop-on-demand printhead technology provides a simpler mechanism for starting and stopping the binder stream, which in turn leads to more accurate droplet placement. With a smaller droplet size compared to standard CJ printing, finer features may be constructed, and the resolution of printed parts will increase. Using these three technologies, the final implementation would likely utilize a single DOD printhead per part for vector tracing and raster filling of binder onto a smooth jetted slurry powderbed [17]. Multiple parts would be produced simultaneously by arranging nozzles in a grid array with center-to-center spacing slightly greater than the dimensions of a part. Each nozzle is dedicated to a single part, so if one nozzle fails, only one part is lost. The nozzle configuration moves in a coordinated vector motion with each nozzle printing the same pattern, thus making high production rates possible [17]. In comparison to the industrial tooling insert production process, the advent of 3DP tooling inserts will reduce inventory and permit mass customization of orders. Research into new tooling geometries can be more easily performed, and more complex-featured tools may be generated with this new method. Many challenges exist, however, to make this vision a reality. Several of these issues are addressed in this research with recommendations for future or alternative work discussed in Chapter 3. Inspired by the preceding motives, the specific goals addressed by this thesis are outlined in the following section.

1.5. OBJECTIVES

The long-term, ultimate goal of this research is to manufacture WC-Co tooling inserts by Three Dimensional Printing. Slurry-based 3DP and vector drop-on-demand printing are two major elements being investigated. In order to meet this objective, other people have and are currently contributing to this effort by looking at specific aspects of these elements. Their work has laid a foundation and supplemented the research reported in this thesis. Several tasks have been and also need to be accomplished. The primary purpose of this thesis is to examine three of the initial, fundamental issues in producing WC-Co tooling inserts by 3DP:

- Tungsten Carbide-Cobalt slurry development
- Tungsten Carbide-Cobalt powderbed production
- Vector drop-on-demand printing of Tungsten Carbide-Cobalt tooling inserts.

These objectives are studied in this order. The following paragraphs provide a brief discussion of the topics examined for each objective.

The first step in making 3DP tooling inserts is to develop a slurry that can be jetted through a nozzle in order to create a powderbed. To produce a jettable slurry, two approaches are considered. Many factors, such as redispersion and binder interaction, must be considered in adapting a material system for slurry-based 3DP. One method utilizes a water-based slurry composed of WC powder. One major disadvantage is that Cobalt cannot be used in an aqueous slurry because of its reactivity with water. Instead, a Cobalt salt solution is printed into the powderbed to introduce the Cobalt, bind the WC powder, and define the part geometry. The solubility limit of the Cobalt salt in solution is measured as it limits the amount of Cobalt that can be introduced in the final part. In the second approach, a non-aqueous based slurry composed of WC-Co powder is explored. This process negates the issue of including Cobalt in the slurry by using an organic non-reactive solvent. An organic binder would then be printed into the powderbed. To evaluate slurry stability, density, particle size, and viscosity measurements as well as jetting experiments are performed.

After a suitable slurry has been devised, parameters for powderbed production are considered. The influence of factors, such as saturation thickness, flow rate, drying time, and line spacing, on the quality of a powderbed surface are identified and observed. Two different slurry-jetting setups are used to conduct this study: the rotary machine for preliminary tests and the hood machine for later, more precise slurry jetting experiments. Powderbeds are produced with both aqueous and non-aqueous slurry systems. The effect of each factor in producing a smooth powderbed surface is measured, and the most

important factors and their appropriate values are identified. A set of reproducible smooth powderbeds is created using an alcohol-based slurry.

The issues relevant to vector drop-on-demand printing of binder are examined next. The parameters required for vector printing using a three-axis milling machine and for drop generation using a DOD printhead are investigated. In order to evaluate the vector printing capabilities of the 3-axis milling machine, a standard DOD inkjet printhead is used to generate ink droplets that are deposited onto paper. The vector printing setup also incorporates function generators and a CCD camera to control and verify binder droplet formation, respectively. Various test shapes to be vector printed are created using both the internal machine programming language and automated tool path definition software. Different electrical waveforms for actuating the piezo are evaluated for their respective DOD droplet formation characteristics. Each waveform is subjected to a range of voltages and frequencies to define conditions for stable single droplet formation. After functional vector printing and droplet formation specifications are established, the first geometries are printed onto slurry-jetted alumina powderbeds, and the single layers are successfully extracted. A set of vector geometries is then created on jetted WC-Co powderbeds. The results from these two experiments are examined for surface finish and line quality.

1.6. ORGANIZATION OF THE THESIS

Originally, the thesis was arranged into three main sections corresponding to the objectives described above with each chapter covering a specific goal. In light of extenuating circumstances, the scope of this thesis has consequently been focused towards presenting material concerning only vector, drop-on-demand printing, the third main goal described in Section 1.5. The majority of the two previous goals, especially investigations into aqueous WC slurry powderbed deposition, non-aqueous WC-Co slurry formulation, and WC-Co slurry powderbed deposition, are covered in Olaf Dambon's Diplomarbeit document [18]. The remaining portions of this section discuss the previous thesis organization in further detail.

Chapter 2 addressed the issues of WC-Co and WC only slurry development. Experiments and results are reported for formulating jettable versions of both aqueous and non-aqueous slurries. Chapter 3 discussed powderbed production and its associated factors. Important constraints are determined, and non-aqueous WC-Co powderbeds with a smooth surface finish are ultimately produced, although subsequently discovered reactivity complications involving the associated dispersant make alternative dispersant evaluations necessary. Segments of the information presented in Chapters 2 and 3 are covered in greater detail by Olaf Dambon in his report [18], and all relevant data will be identified accordingly. The implementation of vector drop-on-demand printing for producing tooling inserts is presented in Chapter 4 (*now* Chapter 2). An investigation of vector printing and DOD binder droplet generation is conducted, and single layers of various geometries are successfully printed and extracted from jetted

alumina powderbeds. Chapter 5 (*now* Chapter 3) finally summarizes the work performed and discusses upcoming developments that will influence this research. Finally, recommendations for future work and further investigation are made.

2 VECTOR DROP-ON-DEMAND PRINTING OF TUNGSTEN CARBIDE-COBALT TOOLING INSERTS

2.1. VECTOR DROP-ON-DEMAND PRINTING PROCESS PARAMETERS

In addition to the material considerations of slurry and binder system development, the goal of manufacturing WC-Co tooling inserts by Three Dimensional Printing also involves implementing vector, drop-on-demand printing technology. This process requires integrating accurate, vector-capable translation equipment for performing printhead-powderbed relative movement with a versatile DOD printhead that can produce droplets from various binder systems. Many possible solutions exist to address these needs. In conducting this research, the necessary functionality is extracted from commercially available tools, including a milling machine and a conventional inkjet printhead. To use this method effectively for producing 3DP parts, a number of associated parameters must be examined. Each of the following sections deals with one of these primary topics.

Section 2.2 details the component specifications of the vector printing configuration and provides an evaluation of their respective capabilities. The primary vectoring instrument is a Bridgeport 3-axis milling machine. The remaining equipment includes a switch mechanism for DOD control, a function generator and amplifier for printhead activation signaling, a camera-LED visualization system for verifying droplet stability, and two different DOD printheads. The programming of various geometries is performed first manually for simple shapes and then, for more complex structures, by using conventional computer-aided manufacturing (CAM) software, in which virtual milling functions translate a desired vector or raster path into a series of equivalent machine commands. A series of ink-based vector DOD tests are conducted on the milling machine and provide valuable insight into the vectoring limitations of this setup.

Binder droplet generation is another important aspect of this printing process and is discussed in Section 2.3. Mechanical actuation and fluid property considerations affect the viability of printing a particular binder system through the DOD printhead. The two most pertinent fluid characteristics are the bulk viscosity and surface tension. Mechanical energy is imparted to the binder through a piezoelectric element present within the DOD printhead that deforms based on a user-defined voltage waveform geometry at a certain frequency. The compression and expansion of the fluid is the driving force for droplet formation. The complex interdependencies between all associated droplet formation variables make optimization difficult. To conduct droplet formation experiments, a specially designed test stand known as the Droplet Observation Station, or Nozzle Test Station, is used. A multitude of waveform timings and voltages are analyzed over a range of frequencies with several binders in order to develop an understanding of how droplet stability is affected. To address function generator limitations, a second function generator is added to the vector printing setup to prevent waveform degradation at

low frequencies. These experiments yield a functional set of droplet formation parameters for the DOD printhead, which is used to conduct vector printing experiments with alumina as outlined in the following section.

The application of vector drop-on-demand printing for 3DP production of test geometries on a single alumina layer is explained in the final Section 2.4. The process begins with slurry processing and powderbed jetting to prepare an alumina substrate for vector printing. Several geometries are programmed for vector outline definition and interior raster fill: (1) a simple square, (2) a tooling insert cross-section, and (3) a central grid with external frame designed to print and preserve individual lines for width measurements. Using the droplet formation parameters previously determined through extensive testing, two sets of experiments are performed: one with as-jetted alumina powderbeds and a follow-up with sanded powderbeds to permit a more lucid evaluation of vector printing quality independent of the original powderbed surface texture.

2.2. VECTOR DROP-ON-DEMAND PRINTING EQUIPMENT & CONFIGURATION

As a functional, preliminary design, the vector drop-on-demand printing configuration used for this research consists of a collection of standard commercial equipment, each customized for a particular task. Vector movement functions are carried out by a Bridgeport EZ-Trak programmable milling machine. A comprehensive listing of its relevant features is given in the following sections. Along with its engineered specifications, a practical evaluation of its vectoring behavior is performed, which identifies an issue with velocity control that leads to a compromise between production rate and part quality. To control the drop-on-demand printhead, a mechanical micro switch is attached to the milling machine vertical quill and connected to the printhead signal circuit. The printhead activation state is therefore controlled by the height of the quill and the position of the micro switch. Initially, only one function generator is used to send the printhead waveform signal at a set frequency. This arrangement causes the waveform signal to deteriorate as the frequency decreases. The problem is resolved with the addition of another function generator, so that one controls the droplet frequency while the other defines the waveform geometry. The first function generator sends an input signal at the desired frequency to the second. The voltage waveform is generated at the specified trigger rate and is subsequently amplified. A separate, large-scale amplifier is required for actuation of the binder system printhead, while a transistor chip provides signal magnification for the ink-based DOD printhead. The correct voltage waveform and frequency is confirmed with an oscilloscope connected to the function generator and amplifier. In order to verify stable printhead operation, the droplet stream is observed with a CCD camera and LED strobe situated on the opposite side of the printhead. To generate the normally large amount of machine code that controls the milling machine during vector and rastering movement, MasterCAM manufacturing software is used to build a model and then automatically calculate the

appropriate tool paths based on a desired printing method. Two printheads with different DOD actuation mechanisms are used for consecutive stages of the vector, DOD study. For evaluating the vector printing DOD setup, a standard black inkjet cartridge manufactured by Hewlett-Packard is chosen to trace ink paths onto paper. Subsequent vector printing DOD experiments using 3DP binder systems employ a more robust and durable printhead made by Siemens. A general overview of the entire final vector printing setup without DOD actuation control is shown in Figure 2.1.
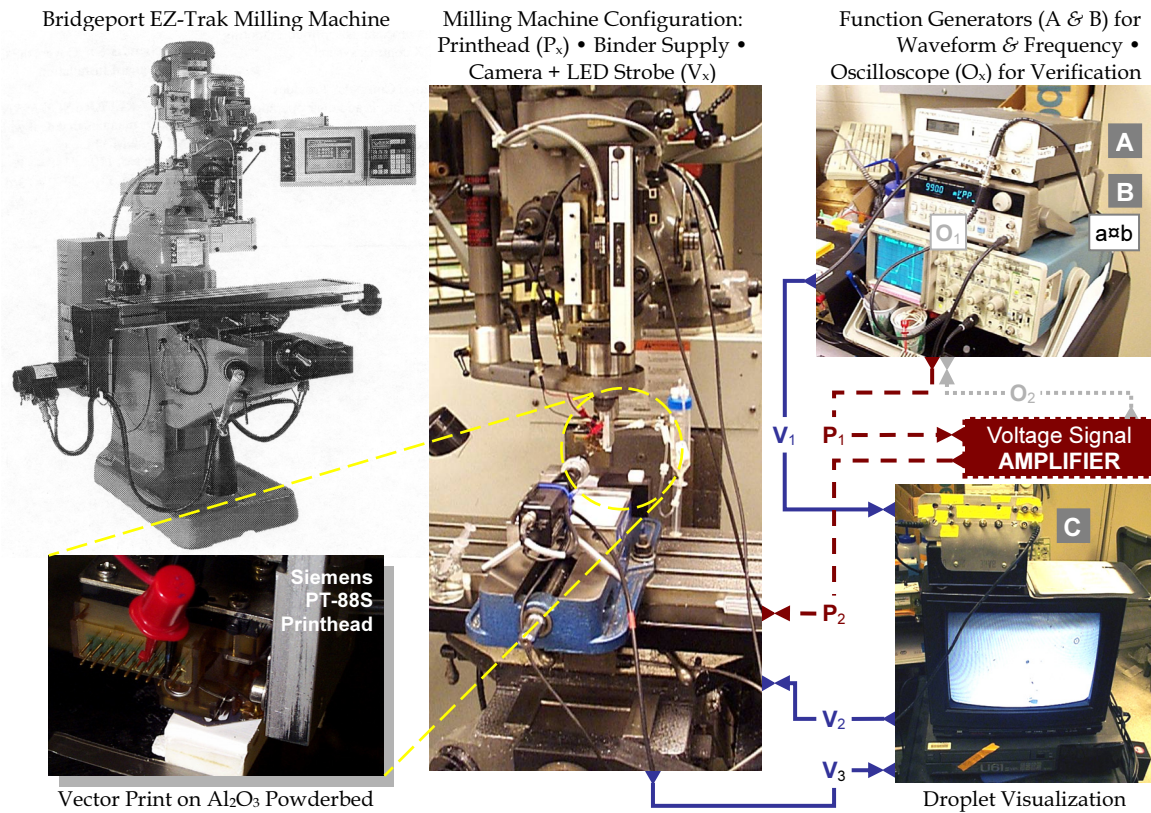
Figure 2.1   Overview of the equipment and connections for vector drop-on-demand printing using a conventional 3DP powderbed and binder system. Essentially, a Bridgeport EZ-Trak 3-axis milling machine provides vector movement, while a Siemens PT-88S printhead ejects drop-on-demand binder droplets onto the powderbed substrate. The process begins with function generator A, which sends frequency input signals to function generator B. Function generator B sends the printhead voltage waveform to the amplifier (P_1) at the rate specified by the trigger frequency received from A. The voltage signal amplifier multiplies the waveform 100 times to the required operating level and transfers it to the printhead (P_2). Two oscilloscope verification connections check the droplet frequency (O_1) and amplified voltage waveform (O_2). The droplet visualization setup has a control circuit C that takes the input frequency (V_1) from function generator A and signals the LED to strobe at a particular time and length offset (V_2). The CCD camera sends the LED-illuminated droplet image back to a television screen for verification (V_3) of binder deposition accuracy and droplet consistency. Note that the drop-on-demand control functions provided by a micro switch and positioning of the quill are not pictured above (refer to Section 2.2.1.3 for implementation details).

The following sections explain in greater detail the specifications and functions for each of the components shown above, including the incorporation of the micro switch with the milling machine quill for controlling DOD printhead activation. A summary of the ink-based vector DOD printing results along with corresponding analyses is included in the concluding Section 2.2.6. The overall performance of this setup with respect to ink-based testing is an important measure for future reference, especially for vector motion, because similar phenomena will likewise be reflected in the quality of the final printed, binder-based alumina geometries discussed in Section 2.4 since the modifications to this setup will only involve the DOD printing conditions and the deposition media.

2.2.1. *Bridgeport Series I EZ-Trak DX 3-Axis Milling Machine*

As a tool available for general 3DP research, the Bridgeport Series I EZ-Trak DX Milling, Drilling, and Boring machine [19] (henceforth referred to as a "milling machine" for brevity) possesses a number of features essential for providing vector printing functionality. The milling machine consists of the following major structural components: the base, the knee with table, the turret, the ram, and the spindle-quill assembly. The operator's control box and the CRT display with keypad provide critical control functions and automated input-output feedback. The main power switch and computer hardware interface for transferring program files by floppy are located in the large metal control cabinet attached to the back of the turret column. The knee allows for z-axis adjustment and supports the X-Y table, which provides the requisite vector-raster translation motions. The operator's control box specifically houses both the green spindle start button, which must be activated to execute any programmed machine code, and the red emergency stop button. As part of the electronic hardware interface, the 9" monochrome CRT display and keypad present status information and control functions, automate axis motion, and allow programming of machining operations using the native EZTRAK® Software [20]. The spindle-quill assembly, identified as (b) in Figure 2.2, has several important functions. First, the printhead is situated on the spindle axis by fashioning a holding device (refer to Figure 2.1 for the Siemens printhead mount) that is then secured in the spindle by a collet. To keep the printhead stationary and before powering the spindle motor with the operator's control box start button, the spindle must be disconnected from the motor by placing the Speed Range Lever, located on the right-hand side of the spindle-quill assembly, in NEUTRAL (refer to the "Hi-Neutral-Lo Lever" in Figure 2.2 (b) for further identification). Please note, to prevent potential equipment damage and/or personal injury, the SPINDLE MUST **NOT** BE ENGAGED. Second, the spindle motor speed can, and should, be reduced to a minimum while the motor is powered by using the Speed Change Handwheel. Beyond providing safety benefits and energy conservation, lowering the rotational speed reduces the external vibrations on the printhead and thus helps preserve droplet stability and placement accuracy. Third, the quill raises and lowers the printhead to an appropriate operating level and, as described in Section 2.2.1.3, also serves as an interface for micro

switch DOD control. The two illustrations referenced and enhanced from [20] in Figure 2.2 identify a significant number of Bridgeport controls.

(a)   (b)
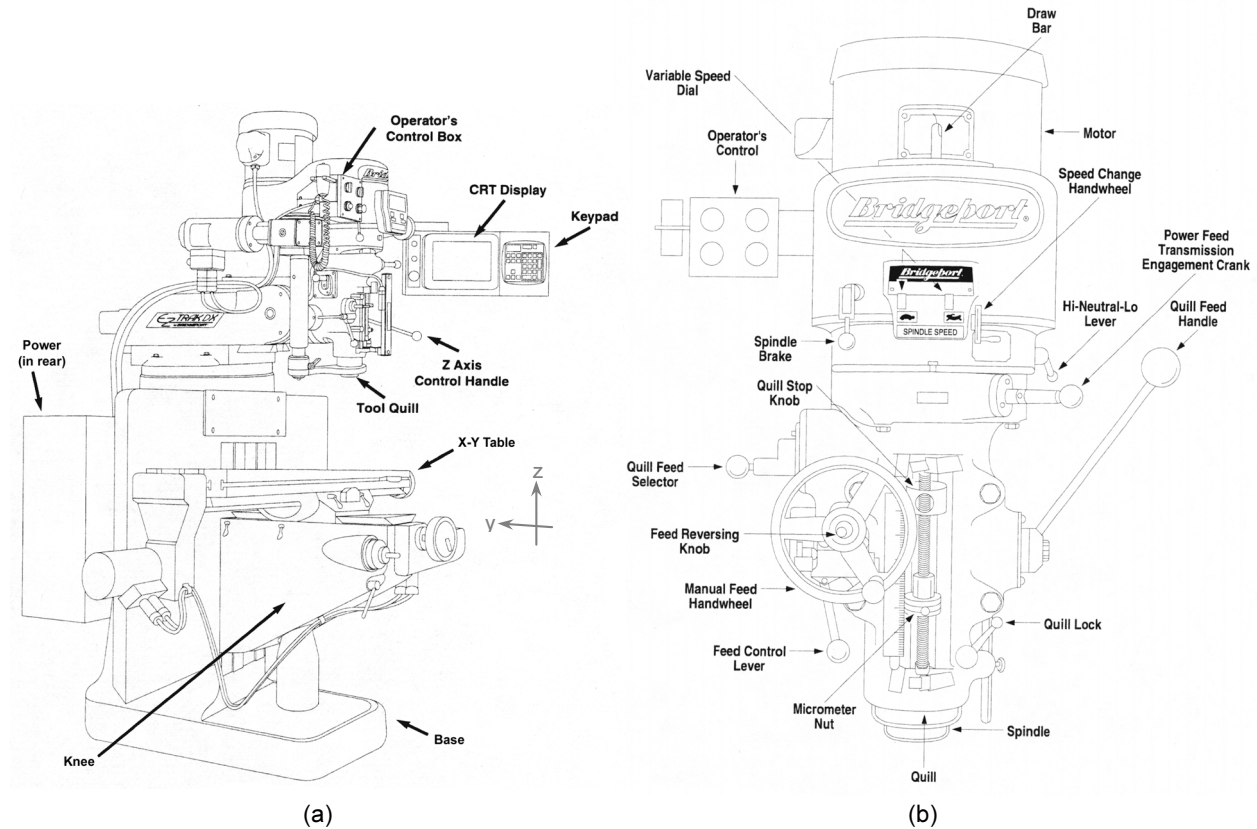
Figure 2.2   Two illustrations of the Bridgeport Series I EZ-Trak DX 3-Axis Milling Machine with basic components identified: (a) the entire machine and (b) the spindle-quill assembly. The tool quill primarily serves as an attachment point for the DOD printhead. The z-axis distance between the powderbed and printhead is adjusted by changing the vertical extension of the quill. The quill movement also functions as the activation mechanism for a micro switch that provides printhead start-stop control (refer to Section 2.2.1.3). The precision, motorized X-Y table supplies vectoring and rastering capability by positioning the powderbed under the stationary printhead. The y-z axes shown in (a) establish the correlation between machine and geometry orientation for all vector printing experiments discussed.

With the level of integrated hardware and software available, the Bridgeport Series I EZ-Trak DX is capable of processing complex computer numerical control (CNC) programs to direct its movement. This automated manufacturing function is adapted for the vector 3DP process. The computing hardware includes a standard 80486 DX-based PC system along with a 32-bit 68030 Bridgeport Motor Drive Controller (BMDC) that is tied directly to the PC data bus [20]. The EZTRAK® Software contains various program routines that allow for sequential or simultaneous movement in three-dimensions, directional speeds or feed rates, tooling changes, and geometry scaling. These available motion functions are sufficient to meet the demands of the current study. The machine programs for vector printing

experimentation are created either manually for simple vector-only geometries by using the Bridgeport Graphical User Interface (GUI) or by using additional computer-aided manufacturing software (refer to Section 2.2.4 for details and for input conditions used for later vector tests). This latter method is particularly well suited to generating the normally large number of tool paths needed for the internal geometry raster fill.

In terms of motion performance for the Bridgeport milling machine, the specifications provided by the manufacturer [19] appear sufficient for the purposes of vector printing geometries on the scale of WC-Co tooling inserts. The three axes, defined as table travel (x-axis), saddle travel (y-axis), and spindle travel (z-axis), have 762 mm, 305 mm, and 127 mm of possible movement, respectively. The positioning rate for the X-Y table ranges from 2 to 2,540 mm/min with a minimum increment of 0.001 mm (1 micron). For control and machine precision, the input, servo, and display functions provide 0.001 mm resolution measurements with a positioning accuracy of ± 0.025 mm and a positioning repeatability of ± 0.02 mm. The degree of accuracy may contribute to errors in the placement of DOD binder droplets and thus affect the edge quality of printed parts, but with respect to other possible sources of error in the process, this deficiency should not be a major factor.

2.2.1.1.   Operating Conditions for Vector Printing Experimentation

Given the performance characteristics and features of the milling machine detailed in the previous section, a range of suitable operating conditions are determined in relation to the functionality of other components. To explore the vector-raster capabilities of the Bridgeport milling machine, a basic setup is devised to trace lines and shapes onto paper using a DOD printhead; this arrangement is later enhanced with the introduction of a printhead start-stop control mechanism which completes the requirements for "drop-on-demand" printing functionality (refer to Section 2.2.1.3 for details). A standard Hewlett-Packard (HP) inkjet cartridge, with a nozzle array of resistive heating elements [21], is chosen as the visualization mechanism. A corresponding wiring interface and a cartridge holder are appropriated from a commercial inkjet printer to connect the inkjet printhead to a basic waveform generation circuit. The HP cartridge and interface apparatus are held by a three-prong test tube clamp whose stem is then inserted into a collet and mounted on the spindle of the milling machine. To address connectivity issues between the circuit and printhead, the interface connector and cartridge mount are later replaced with a pair of wires that are soldered to specific pins on the back of the printhead to actuate a single nozzle. A function generator sends the required frequency and voltage waveform signals through the circuit to generate droplets. Detailed information about the printhead and its actuating waveform is provided in Section 2.2.5.1.

During the initial course of testing, the question of printhead reliability arises due to the unexpected failure of multiple nozzles. The reasons for this occurrence may be attributable to improper

cleaning of the nozzle array, which may have inadvertently damaged the printing mechanism, drying of the ink in the nozzle, communication issues between the printhead and control circuit, or the degradation of nozzle resistor performance through continual use [21]. The potential for nozzle failure is minimized by improving maintenance procedures and by changing the connection between the printhead and circuit as previously mentioned. Another cause for printhead failure, known as switch bounce, develops with the subsequent introduction of a micro switch for start-stop droplet control. The implementation of this DOD function and the associated circuit used to remove this negative side effect are explained in Section 2.2.1.3.

Using this configuration with and without the micro switch, the process of printing lines and geometries with the milling machine and DOD printhead is studied with ink as the "binder" and paper as the "powderbed substrate." The ink and paper, as well as the printhead, are later replaced with more representative 3DP items, as discussed in Section 2.4, but for initial testing, these conditions permit configuration and vector printing issues, which are of primary concern, to be diagnosed and addressed. To simulate and accurately model binder printing parameters, the size of an ink drop "primitive" on paper is measured; the average size of a drop is approximately 115 microns. The printhead frequency and milling machine vector speed are thereby coordinated to obtain various droplet distributions and to check for geometry and spacing consistencies over a wide range of conditions. A variety of shapes, including lines, rectangles with straight and curved corners, and a tooling insert, are programmed and executed over a span of vectoring speeds (from 100 mm/min to 2,400 mm/min) and orientations (0° to 50° rotation). An example of one such vector geometry is shown in Figure 2.3.


```
                    092399.pgm
0000 EZTRAK    1 MODE|MM  |TUE SEP 07 20:28:44 1999
0010 || STOP
0020 RAPID ABS X0. Y0. Z0.
0030 RAPID ABS X11.112 Y.794 Z0
0040 || STOP
0050 LINE ABS X.510 Y9.689 Z0 F360
0060 BLEND|LN ABS X0 Y10.117 Z0 R.794 CCW F360
0070 LINE ABS X-11.112 Y.794 Z0 F360
0080 BLEND|LN ABS X-12.058 Y0 Z0 R.794 CCW F360
0090 LINE ABS X-.510 Y-9.689 Z0 F360
0100 BLEND|LN ABS X0 Y-10.117 Z0 R.794 CCW F360
0110 LINE ABS X11.112 Y-.794 Z0 F360
0120 BLEND|LN ABS X12.058 Y0 Z0 R.794 CCW F360
0130 LINE ABS X11.112 Y.794 Z0 F360
0140 RAPID ABS X0 Y-3 Z0
0150 CIRCLE OUT X0 Y0 Z0 Z-.0001 Z0 R3 P0 P0 D0. F360 F360
```

Figure 2.3   Illustration of a vector printed, ink-droplet geometry using the HP 51626A printhead without DOD activation control. The corresponding program (092399.pgm) details the commands entered manually through the Bridgeport programming GUI and processed by the milling machine. The movements for the above tooling insert shape are performed at a vectoring speed of 360 mm/min and droplet frequency of 26.09 Hz.

Note that additional z-axis positioning commands would be necessary to incorporate DOD control functionality into the above tooling insert outline to eliminate the connecting droplet path between ❶ and ❷. Approaches for raster filling the interior—using methods such as a zigzag, spiral, or section-based fill—are also studied by compiling more extensive machine programs. An extensive summary of these ink-based tests is provided in Section 2.2.6. Based on the examination of droplet spacing at several speeds, notable Bridgeport milling machine limitations exist that can limit part accuracy and are discussed in the next section.

2.2.1.2. Evaluation of Vector Printing Limitations

With the aforementioned setup using a standard HP cartridge to print ink onto paper, a series of lines and shapes are generated to evaluate the vectoring capabilities of the Bridgeport EZ-Trak milling machine (refer to Table 2-A for an overview).

Table 2-A:
BRIDGEPORT SERIES I EZ-TRAK DX MILLING MACHINE VECTOR EVALUATION PARAMETERS
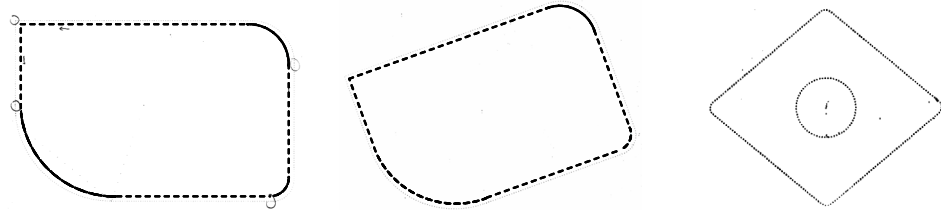
	ABSTRACT GEOMETRY	ABSTRACT ROTATED GEOMETRY	TOOLING INSERT GEOMETRY
Ink Droplet Frequency	10 Hz	2.5 Hz	7.13 Hz
Frequency Variations	40 Hz	2.5 Hz[1], 5 Hz[2], 10 Hz[3], 40 Hz[4]	5 Hz to 452 Hz
Vectoring Speed	600 mm/min	150 mm/min	120 mm/min
Speed Variations	2400 mm/min	150[1], 300[1&2], 600[3], 2400[4] mm/min	120 to 2,400 mm/min
Associated CNC Machine Program	819992.pgm	819995.pgm	090799.pgm
Purpose & Notes	Transformation of the rectangle geometry with various corner radii; evaluation of vectoring capabilities for more complex geometry definition; observed a speed reduction (as indicated by droplet spacing) before each change in direction executed by the milling machine; vector deceleration scales proportionately with increasing default vectoring speed	ABSTRACT GEOMETRY[1, 2, & 4] rotated 20° from horizontal; also tested at 10° and 50° from horizontal with 600 mm/min vectoring speed; evaluation of vectoring capabilities at a various angles to test x- & y-axis independence, stability, and control; observed that vector deceleration before each direction change is independent of geometry orientation relative to milling machine axes	Actual tooling insert geometry; evaluation and verification of desired vector geometry; dimensions derived manually from actual tooling insert; vector deceleration observed at speeds of 300 mm/min and above; lack of drop-on-demand control implementation leads to connecting trace between external outline and internal circle

NOTE: ❶ & ❷ contain manually drawn, dashed traces of the inkjet-printed geometry to aid in visualization.

Using droplet separations mostly between 230 microns (2x the average droplet diameter) and 1 mm, multiple rectangles, abstracts, and tooling insert geometries are printed. The rectangle with sharp and rounded corners represents the basic four-sided polygon necessary for tooling insert definition, while the abstract shape provides a more complex variation with differing corner radii. This latter shape is also

printed at several angles of rotation to evaluate the geometric accuracy of the milling machine independent of its default axes. The tooling insert is programmed based on manual measurements made on an unsintered sample and successfully illustrates the ultimate geometric requirement for this research.

Although the Bridgeport milling machine is clearly capable of vector printing the necessary geometry, the overall accuracy in part definition and consistency in droplet spacing decline proportionately with increasing speed. By comparing the printed droplet spacing with the intended value (based on a set frequency and speed), a noticeable deceleration is observed to occur just prior to any direction change starting at speeds of 300 mm/min. This phenomenon is less obvious, though no less present, at the juncture of a sharp corner versus the region before a curve. For a circular geometry, the decrease in speed only occurs at the end of the trace before starting another command. Tests with the rotated abstract shape indicate that the speed deviation is independent of the machine axes and occurs at any angle. At 2,400 mm/min, the deceleration effect is greatly magnified with an associated distortion in form, especially evident with the tooling insert center hole definition. Figure 2.4 illustrates the deceleration effect at various speeds on the corner profile of a tooling insert geometry.
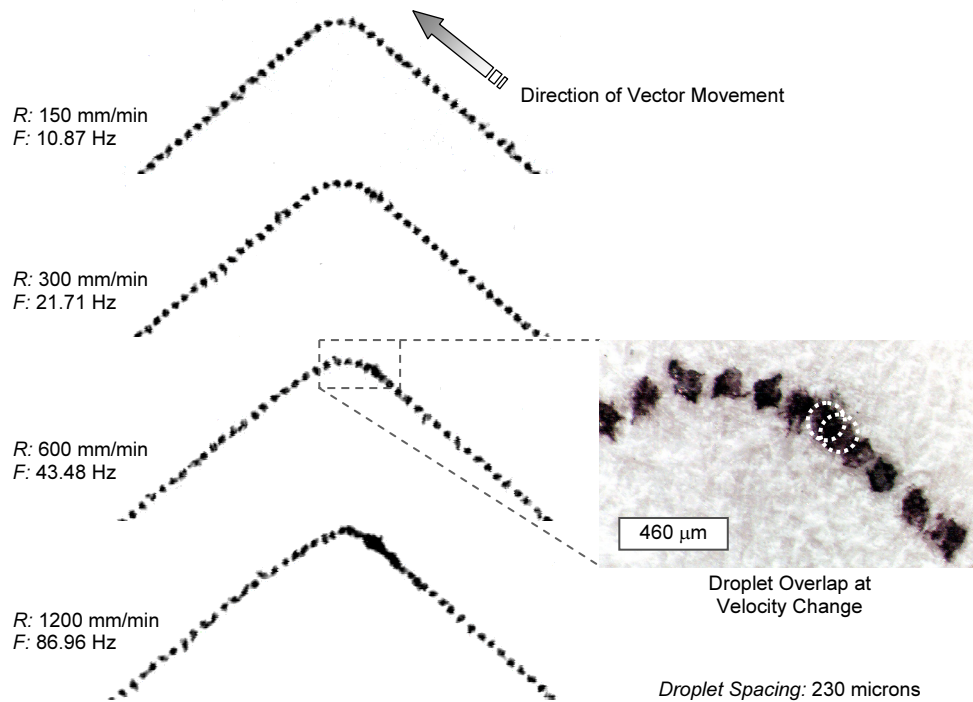
Figure 2.4   Depiction of Bridgeport milling machine vector movement limitations. One curved edge of the tooling insert geometry is shown. Ink droplet spacing is used to measure velocity consistency. At speeds below approximately 254 mm/min, the droplet spacing remains constant regardless of direction changes. Above 254 mm/min, observable deceleration occurs immediately preceding a change of direction. For the above samples, the frequencies (F) and feed rates (R) maintain a designated droplet spacing of 230 μm for visual comparison.

The milling machine motion limitation can be generalized as follows: the faster the speed, the larger the deceleration and the less accurate the geometry. This consideration restricts the maximum 3DP vector printing rate to that which will preserve an acceptable uniform binder distribution and minimize possible distortions. This behavior also necessitates another important compromise.

The determination of an acceptable vectoring speed requires reconciling the demand for binder droplet accuracy with the now conflicting goal of maximizing production rate. By evaluating the degree of droplet spacing error at various speeds, a value of 4.2 mm/sec (254 mm/min) is interpolated to be the fastest setting that guarantees uniform droplet spacing. Based on an acceptable overlap of 50% as observed with a 230-micron droplet spacing, it is determined that 600 mm/min would be an appropriate compromise between binder placement accuracy and production rate for experimentation with this setup.

Although the deceleration effect occurs as a function of speed, another possible way to compensate is to consider droplet size. In tests of the abstract geometry, at 300 mm/min and 2.5 Hz, the relatively large droplet spacing of 2 mm makes the deceleration virtually imperceptible. So even though the deceleration still occurs, its presence is minimized because of low droplet frequency, or in other words, large droplet spacing. In this manner, the undesired effects of speed change can be reduced by decreasing droplet frequency with a corresponding increase in droplet volume, so that binder placement is not as dependent on speed consistency. In light of other 3DP considerations, however, this solution may not be practical since high frequency, low volume droplets can produce parts with higher resolution and detail than low frequency, high volume droplets.

For further discussion of these vector printing results, along with an examination of other ink-based milling machine experiments, refer to Section 2.2.6.

2.2.1.3. Implementation of Drop-on-Demand Controls

Another aspect of the vector drop-on-demand printing process to be addressed is the operational control of the printhead. In considering the numerous options available to satisfy this objective, the decision is made to implement a mechanical micro switch into the existing milling machine vector setup. The Honeywell 1SM2 Micro Switch is the particular switch version chosen. The switch interfaces with the vertical movement of the quill and, depending on the plunger state, starts or stops the DOD printhead function. The ability to integrate easily with the Bridgeport milling machine along with the minimal and effective control requirements dictated by the positioning of a mechanical snap-action contact make this a highly practical and effective solution.

The quill of the milling machine controls the z-axis positioning of the attached tool or, in this case, printhead. Mounted on an aluminum bar that is fastened to a magnetic block, the Honeywell 1SM2 Micro Switch is configured so that the control circuit remains functional when the plunger is released, or

in the normally closed position, thereby allowing droplet generation to occur. When the quill column is raised, the micro switch plunger becomes depressed against the upper ledge of the quill (labeled as *Part A* in Figure 2.5) and causes the mechanical contact to move from the normally closed to the normally open terminal. Current flow to the printhead circuit is stopped thereby halting printhead droplet formation. The location of the micro switch relative to the quill, magnetic support assembly, and part identification and dimensions supplied by Honeywell are depicted below in Figure 2.5.
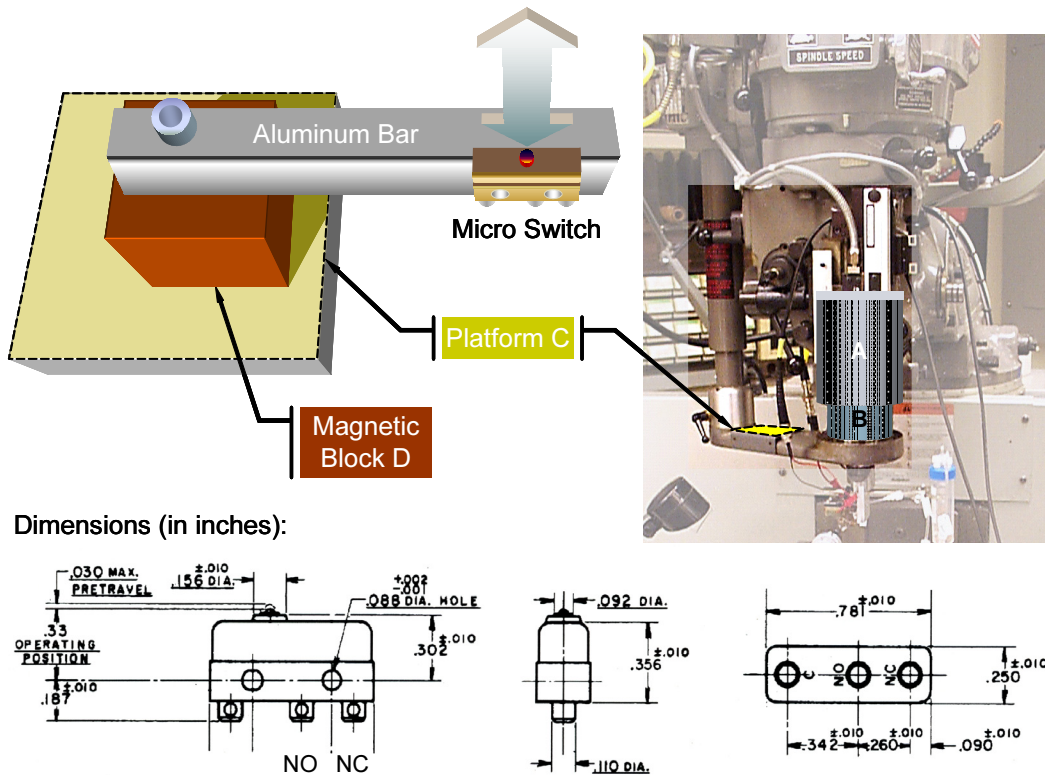
Figure 2.5   Graphical representation of the DOD control method along with detailed dimensions of the Honeywell 1SM2 Micro Switch. Some measurements are omitted for clarity; refer to Honeywell Catalog Listing 1SM2 [7025] (Issue 13, Drawing Number M) for further details. Fastened to an *aluminum bar*, the micro switch is positioned and held magnetically by *Block D* onto *Platform C* of the milling machine. When *Column B* of the quill moves up or down, the micro switch plunger is depressed by or released from *Part A*, respectively. The current setup permits printhead operation when the micro switch is released. Drop-on-demand control is therefore dependent on the vertical position of the quill in relation to the micro switch.

To ensure reliable DOD control, the actuation of the plunger must conform to the operating specifications of the Honeywell design. First, with the plunger completely released, or in the *free position*, the common contact is in the normally closed (NC) state. As the plunger is depressed, it reaches its *operating point* but beforehand must move a distance known as *pretravel*, which is 0.03″ max [22]. At the operating point, the common contact accelerates from the normally closed to the normally open (NO)

contact and within milliseconds strikes, bounces, and comes to rest in the NO position. Moving down past the operating point does not change the state of the common contact; the amount of this *overtravel* is 0.10″ min [22]. In order to return the micro switch to the NC position, the plunger must be allowed to reach its *release point*, which is above the operating point. The distance between the operating and release points is called *differential travel*, which is 0.004″ max [22]. Of these measurements, the most important value for determining z-axis quill movement is the differential travel (0.004 inch). To guarantee that adequate displacement occurs in the micro switch, the z-axis is programmed to travel ± 0.01 inch after positioning the quill (1) to account for pretravel tolerances and (2) to depress the plunger just past the operating point, but before the minimum overtravel. Therefore, when the z-axis moves down to start printing, the plunger is released a distance greater than the differential travel and subsequently returns the switch state to the normally closed position. The reverse also applies for subsequently stopping the printhead: by raising the quill the same distance from its previously set position, the plunger moves down once again past the switch operating point.

By introducing this control device into the current vector DOD printing setup with the HP printhead, the likelihood of printhead failure increases—as observed in practice—because of the phenomenon known as switch bounce. When the common contact of the micro switch moves from one terminal to another due to plunger actuation, the physical connection requires time to stabilize, and the associated mechanical vibrations lead to unpredictable electrical signal oscillations. The resulting voltage fluctuation increases the probability of nozzle failure, especially in the case of the HP printhead. An electrical circuit is thus constructed to eliminate this problem and provide a stable switching signal for DOD control.

The circuit design utilizes two microchip components. First, a dual J-$\overline{\text{K}}$ positive-edge-triggered flip-flop with preset and clear (SN74109) removes the transient switch contact signals that are input through Pins 1 and 5 and outputs on Pin 6 a high- or low-level state to the second chip. The quadruple 2-input positive-NAND gate then processes the signal from the flip-flop input on Pin 1 with the printhead pulse frequency input from a function generator on Pin 2. The output from the first NAND gate is evaluated through a second NAND gate. The resulting output, an active (H) or inactive (L) state, is sent back to the printhead circuit through Pin 6. For integration with the HP printhead, the input source for Pin 2 of the first NAND gate comes from the function generator that supplies the frequency TTL signal, and the output is returned to the input of the drive circuit (refer to Section 2.2.5.1 for printhead circuit details). To implement this micro switch control with the Siemens printhead, the input to the first NAND gate through Pin 2 is taken from the frequency trigger signal sent from the first function generator. The output from the second NAND gate is returned to the external trigger input of the second function generator that holds the arbitrary waveform. Information about the two function generator setup for the

Siemens printhead is provided in Section 2.2.2 with a detailed explanation in Section 2.3.7. The pin designations and logic conditions are referenced from Texas Instruments data sheets obtained in the lab. Refer to Figure 2.6 for relevant chip identification, wiring connections, and associated function tables.
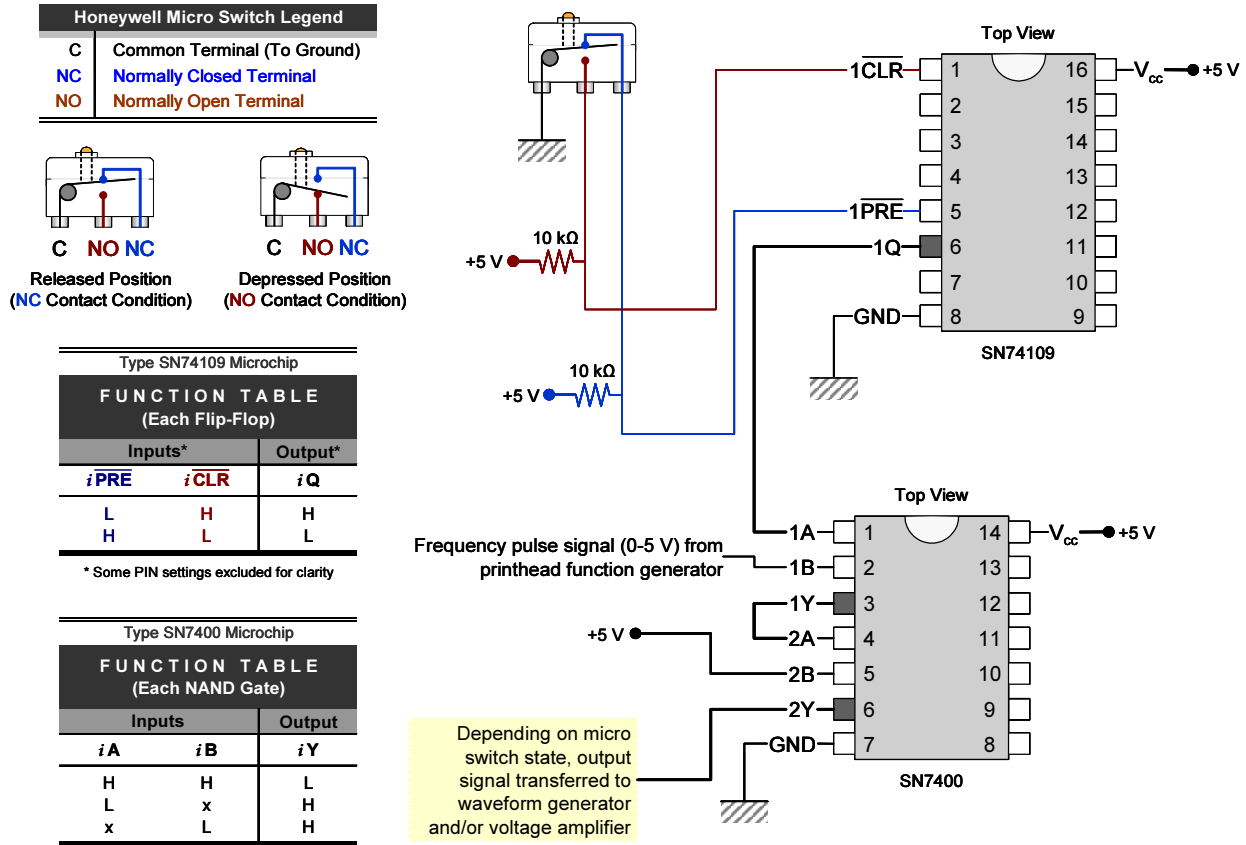
Figure 2.6   Electrical circuit diagram designed to eliminate switch bounce and control DOD printhead signal delivery using two microchip components. Switch bounce increases the likelihood of printhead failure due to the voltage oscillation that occurs when the mechanical common contact changes from one terminal to the other. First, the switch signal is processed through a flip-flop contained in the Type SN74109 chip to isolate and send only the initial transition pulse. The output is then filtered along with the printhead frequency pulse signal through two NAND gates in the Type SN7400 chip to achieve the desired logical output: the printhead activates only when the micro switch plunger is in the released position.

To add a drop-on-demand control function to the existing configuration requires addressing several issues with the HP and Siemens printheads. In both cases, the reliability and consistency of droplet generation upon initiation and re-activation must be improved. For the HP inkjet cartridge, the fragile nature of the resistive elements in its nozzles requires careful introduction of the voltage signal to prevent permanent damage. Another issue with the HP printhead is the possibility of nozzle clogging due to dried ink. The alterations to the printhead interface and the development of a switch debouncing circuit have mitigated the severity of these obstacles. Unfortunately, a less functional situation exists for

the Siemens printhead. On the one hand, the debouncing circuit is applicable to the Siemens printhead and prevents possible piezo damage from the mechanical switching process. On the other hand, to adapt the piezo-driven system to different binder fluids involves an intensive study of various droplet formation parameters. As demonstrated by the efforts described later in Section 2.3, the complex relationship between and cursory knowledge of these parameters in actuating the piezo for stable droplet generation compounds the difficulty of establishing an equilibrium condition without the consideration of such a dynamic contribution. Further discussion of the considerations related to DOD control with each respective printhead is presented in Sections 2.2.6 and 2.3.6.

With the nominal implementation of DOD activation control for the Hewlett-Packard printhead, the possibility of vector representations possessing several distinct external profiles can be studied, such as the tooling insert geometry with center hole.

2.2.2. *Function Generators & Amplifier*

The specifications and purpose of the function generators and amplifier differ slightly for each printhead. A few basic requirements, however, are identical for both systems. At least one function generator is necessary to send a frequency pulse signal that controls the rate of droplet generation. In both instances, a standard TTL waveform is output from the function generator to be processed. The respective amplifiers subsequently magnify the low voltage actuation waveform to the appropriate levels for printhead operation. Beyond these similarities, the contrasting designs of each printhead lead to significant differences in component selection.

The Hewlett-Packard printhead only requires a common feature found on many function generators: output of a TTL level square wave frequency signal. Thus, no specific model is necessary as long as a suitable frequency range can be designated; any of the following function generators used with the Siemens printhead will work. The voltage square wave output is sent to the customized HP control circuit and modified to produce the appropriate waveform geometry while preserving the set frequency (refer to Section 2.2.5.1 for further circuit details). The proper actuation waveform is then delivered to the amplifier for additional processing.

The signal amplification for the HP printhead is integrated into the control circuit design used for waveform processing. A transistor chip is used to increase the signal voltage; no additional equipment is needed. The output is passed on to the printhead for droplet generation. An oscilloscope is connected to the transistor output for waveform geometry, amplification, and frequency verification.

The Siemens printhead also possesses a standard control circuit for waveform creation and processing with frequency input, but in the course of evaluating stable droplet generation for various binder systems, an examination of waveform modification, discussed in Section 2.3, necessitates an alternative method for inducing printhead actuation. To define a custom waveform for DOD printing,

the Hewlett-Packard 33120A 15 MHz Function Generator/Arbitrary Waveform Generator is utilized. This function generator has four 16,000 data point storage areas for retaining desired waveform patterns [23]. Because of its arbitrary waveform capability, the HP 33120A function generator is also used in the design of a test station for droplet observation that includes an efficient method for programming arbitrary waveforms. Discussed in the following Section 2.3.1, this Nozzle Test Station is used extensively in the study of binder droplet generation with the Siemens printhead. Initially, a single HP function generator is programmed with the actuation waveform, and the voltage signal is sent to the amplifier at a set frequency. The degradation of waveform geometry with decreasing frequency prompts the addition of another function generator to separate these two parameters. The second function generator sends a TTL square wave frequency signal to the external input of the HP function generator. The high-resolution, frequency independent arbitrary waveform is triggered at this rate and is subsequently sent to the amplifier. Since the second function generator only provides frequency control for the Siemens printhead by interfacing with the HP 33120A, a number of different models are acceptable for this task. Over the course of this research, three different function generators are used for this purpose: (1) another HP 33120A 15 MHz Function Generator, (2) a Lodestar FG-2102AD 0.2 Hz - 2 MHz Function Generator, and (3) an Inster FG-8016G 2 MHz Function Generator. Specific details on the process and parameters used in this two function generator setup and the correlation between arbitrary waveform resolution and frequency in the HP 33120A are explained in Section 2.3.7.

In contrast to the HP printhead transistor, the amplifier used for the Siemens printhead is a Krohn-Hite Model 7500 Wideband Power Amplifier (DC to 1 MHz • 140 V_{rms} • 75 Watts). The amplification settings specified for the printhead waveform are 100x (40 dB ± 0.2 dB) Fixed Gain, DC input coupling (with low frequency cutoff at approximately 1 Hz), and zero Volts DC offset [24]. As a result, the arbitrary waveform scale is thus magnified 100 times and sent to the Siemens printhead. An oscilloscope is once again connected to the Krohn-Hite output to verify waveform geometry, amplification, and frequency.

2.2.3. *Droplet Visualization Setup*

During the first stages of vector DOD printing with the HP printhead, droplet visualization as an inspection of printhead stability is not as important in comparison with the following binder-based droplet generation tests performed with the Siemens printhead. The HP inkjet cartridge operates under fairly normal conditions using the conventional waveform geometry and fluid chemistry for droplet formation. The presence and consistency of droplets are easily verified by visual inspection of the ink deposited on paper. The Siemens printhead is evaluated using various 3DP binder systems and non-standard waveform shapes in an attempt to generate a stable droplet stream in unfamiliar conditions. Therefore, to measure and confirm droplet stability and uniformity, a visualization setup is devised as an

important tool for vector DOD printing experiments using the Siemens printhead on the Bridgeport EZ-Trak milling machine.

The functional components of this visualization system are adapted from equipment specifications used in the Droplet Observation Station, or Nozzle Test Station (refer to Section 2.3.1). The Siemens printhead visualization system consists of a CCD camera, LED attachment, control circuit, and television monitor. Images of these components, their orientation, and their connections, identified with blue V_x arrows, are shown in Figure 2.1. The camera with LED attachment is mounted on a tripod and temporarily secured to the milling machine X-Y table with tape. The printhead is positioned between the camera lens and the LED. In order to align the droplet stream with the focus plane of the camera, a piece of paper is attached to the side of the printhead parallel to and in line with the row of orifice nozzles. The camera focus is then calibrated on the vertical plane denoted by the paper, which approximates the plane of droplet formation from any orifice. The diode pulse is synchronized with and activates at the droplet waveform frequency. The control circuit receives the frequency setting from the printhead function generator and provides pulse width and delay modulation for the LED so different states of droplet development can be observed, and the CCD camera captures this stroboscopic image and displays it on the monitor screen.

2.2.4.   *Vector Geometry Composition & Programming*

To compose the geometries used for vector testing, initial machine programs are created manually using the Bridgeport EZTRAK® Software within the native milling machine GUI. A collection of vector-only shapes are designed, ranging from a rectangle to a tooling insert, primarily for assessing the effectiveness of the Bridgeport Series I EZ-Trak DX milling machine as a vector definition tool and the incorporation and testing of other components to the process. The discussion of this configuration development and refinement is presented throughout Section 2.2.1. With the increasing functionality of the vector DOD printing configuration using the HP printhead, more complex printing programs are developed which more accurately represent the 3DP production process with vector profile definitions and interior raster fills. Composing these machining procedures efficiently requires the implementation of external CAM software.

The software used to design and compile machine programs for outline vector printing and raster interior fills is MasterCAM version 7.2 by CNC Software, Inc. This CAM package allows for versatile design and modeling of any geometry for production with CNC-capable machines, using a collection of representative virtual machine tools. The 3DP vectoring and rastering of binder droplets on a powderbed substrate is simulated as a subtractive milling procedure with the tool diameter equivalent to the ink or binder droplet diameter. Three geometries are designed with MasterCAM for vector DOD printing implementation: (1) a square, (2) a tooling insert, and (3) a centered, perpendicular grid design

with support frame. Each of these geometries are examined in detail and defined with the appropriate parameters for use with each printhead before creating the corresponding Bridgeport machine program. To define the position of the printhead above the substrate, the z-axis origin is set as the top surface of the powderbed with the printhead orifice ideally positioned 500 microns above. In practice, the distance is slightly increased because the origin cannot be precisely calibrated without damaging either the powderbed or printhead.

To define an adequate line spacing and overlap between consecutive parallel vector or raster lines, the diameter of a binder droplet must be known. Ideally, the measurement should reflect the as-printed condition of the droplet absorbed in the powderbed. To make this determination for one specific binder system, considerable time and effort is required to analyze and account for the behavior of liquid infiltration in a particular powderbed composition, not only to calculate the diameter for individual droplets, but also to formulate a theory for optimal line definition. For the vector DOD printing experiments conducted in this thesis, particularly with the binder system used in Section 2.4, taking into account the number of variables already present for examination, such an accurate diameter assessment must be postponed and substituted with a best guess approximation for droplet size and line spacing.

Fortunately, for ink-based tests using the HP printhead, this measurement, while not representative of actual binder-powderbed interactions, is easily determined by measuring the ink drop size left on paper. With an average 115 micron droplet size, as calculated earlier in Section 2.2.1.1, all MasterCAM geometry files prepared for vector DOD printing using the HP printhead assume a 58 micron separation (or 50% overlap) between consecutive sets of parallel lines. Using this droplet spacing, relevant observations can be made concerning the potential distribution of binder based on the vector and raster performance of the current experimental setup (refer to Section 2.2.6 for a summary). The spacing between adjacent droplets in a single line may be controlled by varying either the droplet frequency or speed of the milling machine.

In contrast, the basis for an average droplet size used for binder printing with the Siemens printhead is less accurate though still fairly reasonable. The relevant vector DOD printing experiments using several MasterCAM-designed geometries are outlined in Section 2.4. The particular binder system used is functionally composed of Polyacrylic Acid (PAA) with glycerol, which is deposited into slurry-jetted alumina powderbeds. The binder droplet size as generated by the printhead in air is chosen to determine the line spacing and overlap parameters in MasterCAM. To determine this droplet diameter, two separate measurements are taken, and both yield similar results. One method of calculating the droplet size involves manual measurement of a scaled image as seen on the Droplet Observation Station (refer to Section 2.3.1 for details). The second approach to determining the average droplet size in air uses the mass of binder ejected at a certain frequency over a known time period. Section 2.3.8 includes a detailed explanation of this calculation. With a stable voltage waveform, the average droplet size of the

PAA binder from the Siemens printhead is 44 microns. This size estimation, though not optimal, essentially reflects the smallest diameter possible for a binder droplet in the powderbed because the droplet is believed to expand in diameter upon impact. The same conventions used for the HP inkjet printhead are applied for each Siemens binder-based machine program: a 50% overlap, or 22-micron line spacing, between adjacent parallel lines. Therefore, assuming the same droplet spacing is used for consecutive binder drops, the printed powderbed geometries resulting from this droplet diameter assumption will likely be cohesive.

Each of the three geometries designed in MasterCAM serves a purpose. The square is developed to test a basic, fundamental shape for 3DP part production. Geometric distortion can be easily identified; edge quality and corner sharpness are also important characteristics to assess. For vector DOD printing using either printhead, the square is programmed with a reinforcing set of exterior vector traces followed by a linear, horizontal zigzag raster fill starting from the bottom and progressing upward. The tooling insert geometry signifies the primary reason for this study of vector DOD printing. The MasterCAM design is based on the CNMA 432 tooling insert provided by Valenite with an increase in dimensional scale to reflect green density and to account for the expected decrease in sintered size. Figure 2.7 provides a cross-sectional illustration of the CNMA 432 insert labeled with sintered dimensions.
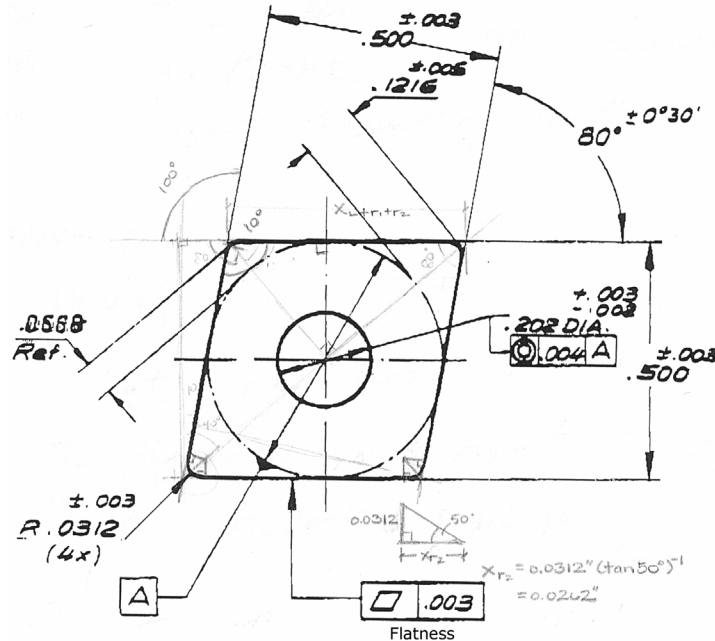
Figure 2.7   Technical diagram of a finished, conventional WC-Co tooling insert cross-section. Unit measurements are provided in inches. The dimensions and geometry depicted above serve as the basis for the model and machine tool paths generated by MasterCAM for vector printing the tooling insert shape. Dimensions for the 3DP model are scaled to compensate for shrinkage during sintering. Data for the CNMA 432 Tooling Insert provided courtesy of Valenite, Inc.

Based on an ideal, jetted powderbed with 55% green density, calculations for as-printed part dimensions assume that complete sintering provides a 45% reduction in volume to achieve full density with constant mass. In actuality, the part mass will decrease slightly with the decomposition of organic components in the slurry and binder. Since these component quantities are relatively small, however, the associated mass change is negligible and is currently ignored. Using these assumptions,

VARIABLES $\quad \rho_b \quad =$ Density before sintering $\qquad V_b \quad =$ Volume before sintering $= x_b * y_b * z_b$
$\qquad\qquad\quad \rho_s \quad =$ Density after sintering $\qquad\quad V_s \quad =$ Volume after sintering $\quad = x_s * y_s * z_s$

$$\rho_b = 0.55 \cdot \rho_s$$

$$\frac{V_s}{V_b} = \frac{x_s \cdot y_s \cdot z_s}{x_b \cdot y_b \cdot z_b} = 0.55$$

If the ratio of corresponding dimensions (sintered : unsintered) is defined as $R_{\frac{s}{b}}$,

$$\left(\frac{x_s}{x_b}\right) \cdot \left(\frac{y_s}{y_b}\right) \cdot \left(\frac{z_s}{z_b}\right) = R_{\frac{s}{b}}^{\ 3} = 0.55$$

$$R_{\frac{s}{b}} = \frac{x_s}{x_b} = \frac{y_s}{y_b} = \frac{z_s}{z_b} = 0.819$$

$$x_b = (0.819)^{-1} \cdot x_s = 1.22 x_s$$
$$y_b = 1.22 y_s$$
$$z_b = 1.22 z_s$$

Therefore, if the shrinkage occurs isotropically, then the green dimensions should be 22% larger than their sintered counterparts. Note that this calculation also does not account for how the interior hole affects the volume decrease.

The MasterCAM tooling insert model is adapted for use with both printheads. For the HP inkjet cartridge, a more accurate model of the tooling insert with inclusion of the center hole can be printed as the result of effective DOD control functionality and relatively stable droplet generation. Moreover, simpler tooling insert models without the center hole are programmed to compare various raster fill methods, including angled zigzag, spiral, and sectioned fills. For the Siemens printhead, the tooling insert model is programmed without the center hole for printing PAA binder into alumina using a 130° raster-fill method. The center grid design with support frame is a specialized geometry intended for the Siemens printhead to preserve individual vector DOD printed lines of PAA binder into alumina so that corresponding line width measurements can be taken.

2.2.5. *Drop-On-Demand Printheads*

Two printheads serve as the primary droplet generation mechanisms for this research: (1) a Hewlett-Packard 51626A Black Inkjet Printhead and (2) a Siemens PT-88S Printhead. Based on the principles of DOD operation discussed in Section 1.2, each printhead is used for a separate portion of vector DOD printing development. The HP 51626A is employed mainly for equipment evaluation and testing, while the Siemens PT-88S is utilized first for investigation of droplet generation with various binders and second for the functional implementation of vector printing PAA binder into alumina. Both printheads do similarly perform vector DOD printing experiments with the milling machine setup using machine programs of various geometries designed in MasterCAM, but with differences in fluid systems and droplet generation performance, the specified vector and rastering parameters for each printhead contrast greatly. It should be noted that a prototype printhead being developed by Hiro Tsuchiya, a visiting scientist from TDK, is also used briefly for an examination of droplet formation. His printhead design is intended to function with the TDK Slurry-Vector Printing Machine currently in development (refer to Section 3.2 for information). The amount of work conducted with his customized printhead in this research is significantly less than the collection of results obtained with the other two. Hiro's DOD design does share a common actuation process with the Siemens printhead, and a brief comparison is given between the two printheads in Section 2.3. This similarity in piezo-actuated droplet formation may allow possible correlations to be made between behaviors, parameters, and measurements made with each printhead although further research and analysis is required to draw any conclusions.

With the common ability to exert droplet production control over a range of frequencies, the two DOD printheads achieve this objective differently. The HP printhead produces droplets by heating fluid with individually accessible resistive elements [21]. In contrast, a piezoelectric element induces pressure fluctuations in the fluid to control droplet formation for the Siemens printhead. In addition, as discussed previously in Section 2.2.2, the waveform generation process differs greatly as well with a significant departure from normal operating conditions for the Siemens PT-88S in order to accommodate different binder systems. Figure 2.8 provides an illustration of these two printheads and their respective components.

PART NO.	DESCRIPTION
1	Orifice Array Plate
2	Clear Rubber Seal
3	Bail
4	Retainer Spring
5	Black Rubber O-Ring I
6	Mesh Filter
7	Metal Punch Plate
8	Black Plastic Choke Plate
9†	Black Rubber O-Ring II
10	Plastic Membrane
11	Rubber Seal

† Item not shown in diagram
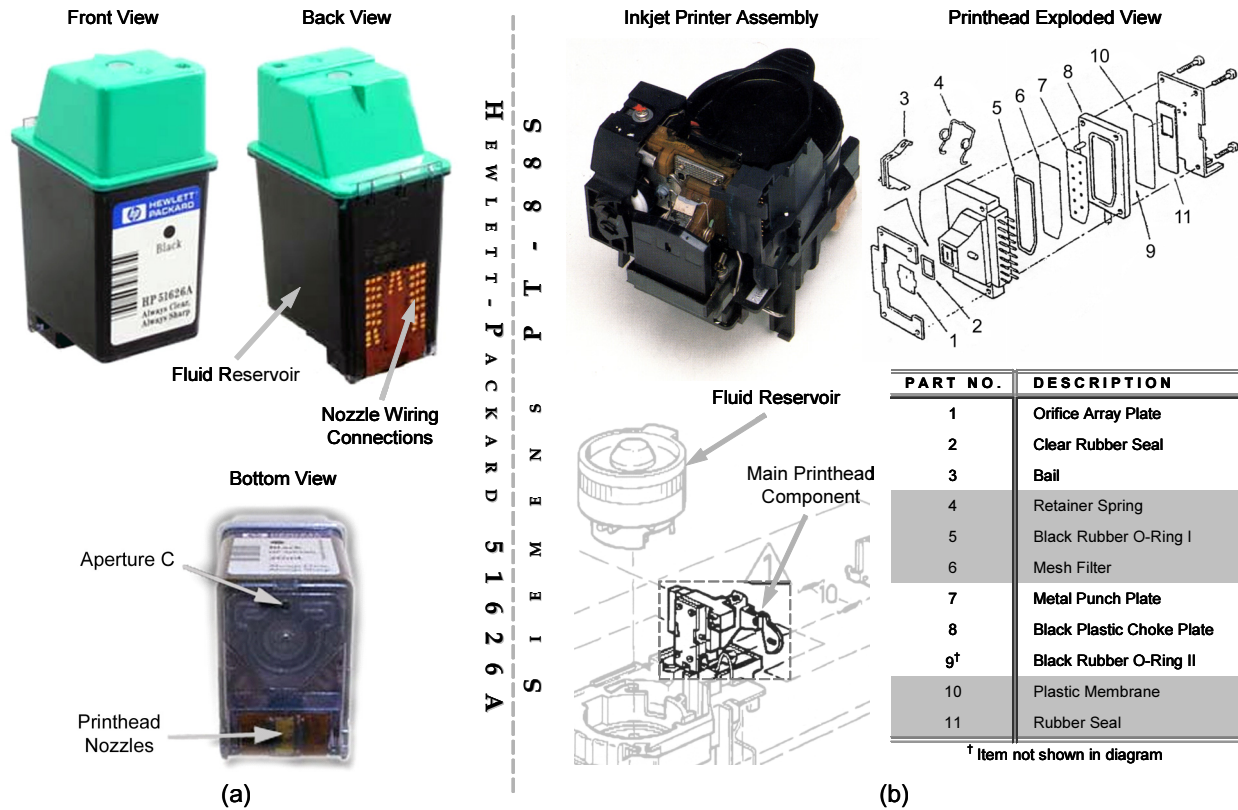
Figure 2.8 Illustrations and part identification of the two drop-on-demand printheads used for experimentation: (a) the Hewlett-Packard 51626A Black Ink Inkjet Printhead, used primarily for geometry and vector evaluation tests with ink and paper, and (b) the Siemens PT-88S Printhead, used ultimately for generating a single 3DP vector printed layer by depositing liquid organic binder onto a dried slurry powder substrate. Essential components of the HP 51626A printhead are identified in the three different views shown above. Pictured in composite and expanded form, the Siemens PT-88S printhead provides only droplet generation functionality as a sub-system of a more modular Siemens inkjet printer assembly.

As seen from the construction of each printhead in the figure, by including the ink reservoir with the DOD nozzles, the Hewlett-Packard 51626A Black Ink inkjet cartridge is a more compact and integrated design compared to the Siemens PT-88S. In contrast, the Siemens PT-88S is a more specialized and modular sub-component of a complex assembly. Other distinctions between the two printheads are outlined in the following sections.

2.2.5.1. Hewlett-Packard 51626A Black Ink Inkjet Printhead Specifications

The Hewlett-Packard 51626A Black Ink Inkjet cartridge, shown in Figure 2.8 (a), is a thermal inkjet printhead that uses an array of resistive heating elements as a drop-on-demand mechanism. The droplets emerge from the printhead because of momentum caused by collapsing bubbles that form in the ink chamber. The nozzle heating element produces a momentary vapor bubble that then collapses; a

reaction force is generated that allows a droplet to overcome the ink surface tension and propel out the nozzle. Capillary force then refills the nozzle for another cycle [21]. The droplet frequency can range from 40 Hz to 5,000 Hz, and a maximum distance of 600 microns is recommended for accurate droplet placement. The fluid reservoir capacity is specified as 40 mL [25]. According to the Material Safety Data Sheet, the associated ink chemistry is composed of primarily water (> 85%), 2-Pyrrolidone (< 8%), and other salts (< 4%) with a pH between 8.3 and 8.7 and a density of 1.0 to 1.2 g/mL [26].

The HP printhead uses two chips in its drive circuit to generate and scale its waveform geometry. The HC4538 is a dual retriggerable monostable multivibrator, which takes the TTL level rising edge input from a function generator. The circuit then modifies the square wave to the appropriate printhead waveform. The output from Pin 6 is then fed to Pin 1 of the IRF530, a Metal-Oxide-Semiconductor Field-Effect-Transistor (MOSFET). This transistor amplifies the signal, which is then sent to the printhead at the frequency set by the function generator. A diagram of this waveform generation circuit is provided in Figure 2.9.

For the most part, the HP 51626A printhead provides a functional DOD system for visualizing vector printed geometries. With the addition of a micro switch for activation control of the printhead, the current configuration is fully capable of simulating binder deposition methods onto a substrate using ink and paper. A number of these vector and raster-fill geometries are evaluated and summarized in Section 2.2.6. The printhead does experience problems, however, with occasional nozzle failure. In general, the resistor elements decrease in performance over time and are susceptible to failure when subjected to physical or electrical stress. As noted earlier in Section 2.2.1.1, increased reliability is possible with proper maintenance and caution when cleaning the nozzle plate. In addition, the determination of switch bounce and the designed circuit compensation (see Section 2.2.1.3) are in part due to the efforts from diagnosing nozzle failure.
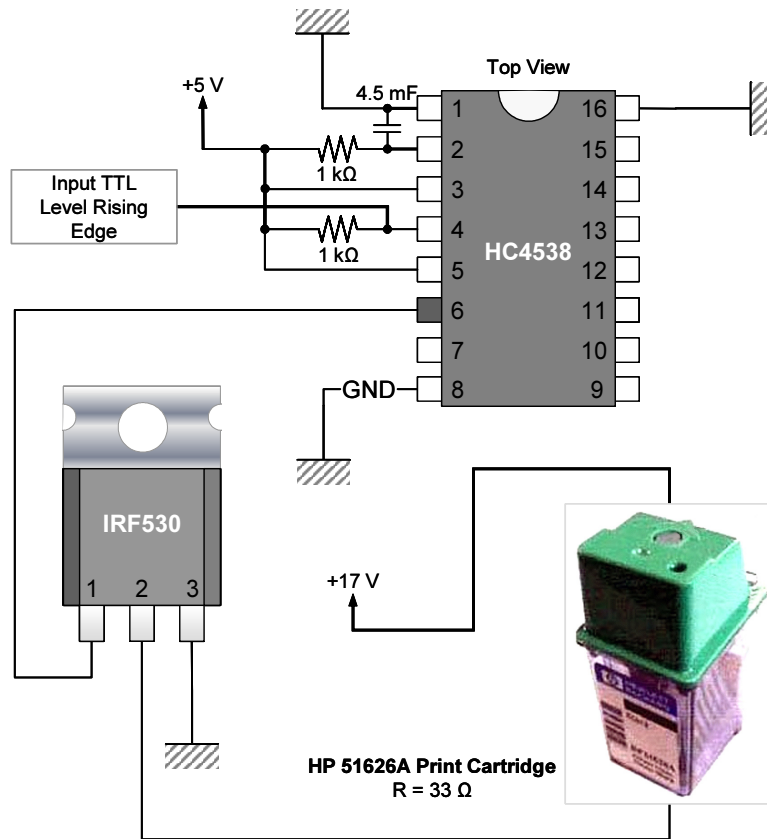
Figure 2.9   Electrical wiring diagram for droplet generation using the HP 51626A DOD print cartridge.   A function generator TTL square wave output signal sent through the HC4538 microchip controls the droplet frequency of the printhead.   The HC4538, a dual retriggerable monostable multivibrator, modifies the voltage waveform input to the proper geometry for droplet generation, and the subsequent MOSFET (Metal-Oxide-Semiconductor Field Effect Transistor) amplifier IRF530 scales the shape to the proper voltage.   The resultant waveform geometry, frequency, and amplitude are verified by observing the MOSFET output with an oscilloscope.

2.2.5.2.   Siemens PT-88S Printhead Specifications

Like the HP 51626A, the Siemens PT-88S is another inkjet printhead, but the droplet generation mechanism is electromechanical instead of thermal. The Siemens PT-88S printhead has eight cylindrical piezoceramic actuators that encase eight corresponding fluid channels. The piezo transducer functions by converting electrical energy to mechanical motion: a positive applied voltage causes the piezo to constrict, while a negative voltage causes it to expand. Based on measurements by Hiro Tsuchiya, the average diameter of each piezoelectric is 1.59 mm. The internal channel has a diameter of 0.69 mm and meets an orifice plate with a hole that tapers from 0.100 mm to 0.080 mm in diameter. The eight nozzles all converge on this single orifice plate with the eight respective holes distributed approximately 350 microns apart. Figure 2.10 provides a cut-away illustration of the printhead that shows this nozzle

configuration. The control voltage for actuating the piezoceramic tube ranges from approximately 90 to 180 Volts with a maximum frequency of 2.9 kHz. A maximum distance of 2 mm between orifice plate and paper is recommended for accurate droplet placement. The material used to encapsulate the printhead is known as Epoxonic HBX 93, a resin produced by Siemens; the orifice plate is believed to be made from Nickel and Chromium, although composition analysis is necessary for certification. An electrochemical process is used to etch the holes and define the orifice plate geometry, while a photoresist layer preserves the remaining material. The accompanying ink provided by Siemens has a viscosity of 23 cP, a surface tension of 46 dynes/cm, a pH of 11.5, and a density of 1.13 g/mL. The MSDS states that the chemical composition includes 73% Ethylene Glycol, 20% Diethylene Glycol, and 7.0% other compounds. Most of this performance and material data is provided by Günther Wöhlert of OCÉ Printing Systems USA, Inc.

To actuate an individual piezo, electrodes must be connected to the corresponding pins--one to the piezo, the other to ground, and a voltage waveform signal must be applied. A wiring diagram, table of pin assignments, and pin orientation illustration are supplied in Figure 2.10. The standard Siemens waveform circuit is only used briefly in the beginning to verify printhead functionality under normal conditions with ink and to test droplet formation stability for a Polyacrylic Acid-based binder system. Because the duration of its use is so short, the design and operation of this circuit is not documented. Instead, because the standard actuation method failed to work with the PAA binder system, the possibility of waveform modification is pursued. In order to conduct this examination, a HP function generator is programmed with arbitrary waveforms of varying times, voltages, and frequencies. The signal is then amplified by 40 dB (100x) gain and connected to the printhead for evaluation. The dependency between waveform resolution and frequency in the single function generator is discovered during this study, and thus the two function generator setup is conceived (also described in Section 2.2.2 with a detailed explanation of this effect in Section 2.3.7). This waveform customization approach towards DOD printing various binder systems using the Siemens piezo-actuated printhead proves to be an effective and potentially versatile process. The study of droplet generation by changing waveform geometry and other printing parameters is presented in Section 2.3. By investigating these relationships, an effort is made to understand how reliable, consistent droplet formation is achieved.

One potentially severe disadvantage related to this printhead is the impending lack of availability, which will increase substantially after November 2000. According to Günther Wöhlert, Siemens will cease production of this printhead at this time. The remaining inventory will be available for some time, but depending on demand, estimates as to when these supplies will be depleted cannot be made. Currently, three Siemens printheads, along with replacement O-rings and orifice plates, are known to be available for further experimentation.

Siemens PT-88S
Nozzle Wiring
Diagram

Pin	Signal Notation	Explanation
1	HZ	Ink–jet Print Head Heater
2	TDK.TF	Temperature Sensor
3	0 V	Ground
4	KFSU9	Selection of Nozzle 9
5	KFSU8	Selection of Nozzle 8
6	KFSU7	Selection of Nozzle 7
7	KFSU6	Selection of Nozzle 6
8	KFSU5	Selection of Nozzle 5
9	KFSU4	Selection of Nozzle 4
10	KFSU3	Selection of Nozzle 3
11	KFSU2	Selection of Nozzle 2
12	KFSU1	Selection of Nozzle 1
13	0 V	Ground
14	WJMT.B	Wiper Motor Terminal B
15	TJEL1	Ink Electrode 1
16	WJMT.A	Wiper Motor Terminal A
17	TJEL3	Ink Electrode 3
18	TDK.TJEL2	Ink Electrode 2

Figure 2.10   Cross-section and diagram of pin connections for actuating each piezo transducer for the Siemens PT-88S printhead. Although nine nozzle connections are indicated in the wiring diagram, only eight are functional. Each of the eight tubes is surrounded by a cylindrical piezoceramic actuator that expands and contracts with corresponding voltage. To activate a nozzle, the positive electrode with amplified waveform signal is connected to the corresponding pin, and the negative electrode is connected to a ground pin (either Pin 3 or 13). All nozzle tubes converge on a common orifice plate.

In terms of reliability, the Siemens PT-88S does not suffer from nozzle failure as seen with the HP printhead. In fact, the default printing conditions using Siemens ink are reliable and considered ideal. Instead, by attempting to adapt the Siemens PT-88S to different fluid systems, extensive investigation into multiple printhead variables is necessary to find a set of stable droplet generation conditions. The correlations between printhead variables are still not well understood, so the prospect of determining optimal binder droplet conditions is relatively low for now. So from a reliability standpoint, the issue of droplet formation instability as the result of many possible factors is of paramount concern. Another potential impediment to DOD printing with various fluids involves the reactivity of binder chemistries with printhead components. During the droplet formation study of binder systems containing PAA, a substantial degree of corrosion on the orifice plate is observed over a short period of time. This gradual

deterioration and increase in orifice diameter manifests itself by causing droplet instability under once acceptable conditions and by directing droplet streams out of alignment. Further details on the orifice plate corrosion that occurs with PAA binder is discussed in Section 2.3.2.

2.2.6. *Ink-Based Vector Drop-On-Demand Test Geometry Results*

To perpetuate efforts towards producing WC-Co tooling inserts with this relatively new approach to Three-Dimensional Printing, the development of a vector DOD printing system using the Bridgeport Series I EZ-Trak DX milling machine as the vector component is commenced. Two different DOD printheads are selected for this system: (1) the Hewlett-Packard 51626A Black Ink Inkjet cartridge and (2) the Siemens PT-88S Inkjet printing mechanism. The HP 51626A cartridge is initially chosen for evaluating and diagnosing the equipment integration. This process involves conducting vector DOD experiments with ink and paper using programmed CNC machine programs. After determining the average ink droplet size on paper to be 115 microns, a multitude of geometries are created and analyzed. A detailed summary of these tests is presented in Table 2-B; other significant results obtained for ink-based vector DOD printing are documented in scans shown in Figure 2.3, Figure 2.11, and Table 2-A.

The geometric complexity of vector printing tasks gradually increases as the capabilities of the milling machine is assessed, more effective programming techniques are used, and DOD control is implemented. Progressing from lines to rectangular shapes to tooling inserts, the results of these early experiments indicate that increasing milling machine speed leads to a decrease in geometric accuracy and droplet spacing with noticeable effects starting at approximately 300 mm/min. These errors occur due to unexpected decelerations during program execution at every change in direction. Section 2.2.1.2 discusses this phenomenon in greater detail. A compromise is made between accurate droplet placement and production rate by allowing for a 50% overlap to occur at a 230-micron droplet spacing. This amount of geometric distortion is deemed acceptable, and the corresponding milling machine speed equates to 600 mm/min. With an effective DOD control micro switch, the tooling insert vector geometry is successfully printed without extraneous ink droplets connecting the exterior diamond perimeter with the center hole.

Afterwards, an examination of interior raster fill methods is also performed in coordination with the now completely functional vector trace. By designing geometries and compiling the resultant machine code with MasterCAM software, the lengthy task of calculating and programming tooling paths is obviated, and a number of different rastering approaches are prepared. For ink-based vector DOD testing, an accurate representation of a tooling insert profile is designed based on a dimensioned sample provided by Valenite, and the majority of raster-fill testing is conducted using this shape. Four different methods are evaluated: (1) section fill, (2) spiral fill, (3) horizontal raster fill, and (4) 130° linear raster fill. Note that the decision to use the 130° angle is not a general recommendation but rather a consequence of

the tooling insert geometry. For rastering tests that include vector outline definition, the profile of the tooling insert is traced consecutively four times with decreasing scale from the exterior to the interior of the geometry. Based on the tooling paths defined in MasterCAM, which rasters from the bottom up (moving in the positive y-axis direction), the ability to activate and deactivate the HP printhead is essential for accurate reproduction of the tooling insert using the section fill. Note that the three latter rastering methods do not include rastering exclusion of the center hole. Figure 2.11 provides scans of actual printed samples that employ these internal fill techniques. A listing of parameters and notes for these experiments is included in Table 2-B.

Table 2-B:
SUMMARY OF VECTOR PRINTING TESTS WITH THE
BRIDGEPORT SERIES I EZ-TRAK DX MILLING MACHINE

Vector Geometry Description	Purpose	Sample CNC Machine Programs	Vector Speed Variations (mm/min)	Droplet Frequency Variations (Hz)	Notes & Summary
Straight Line	To test basic machine vectoring capabilities	`093099.PGM*` `100699.PGM*`	100, 150, 200, 300, 600, 2400	1.67, 2.5, 5, 10, 11	• Lines have accurate length and linearity • Droplet spacings indicate accurate speed * Tests of the DOD micro switch control are conducted later using single & multiple consecutive lines
Rectangle with Sharp & Rounded Corners	To assess standard, multi-sided geometry with sharp and rounded corners; to establish fundamental tooling insert shape definition	`819991.PGM` `825991.PGM`	100, 600	1.67, 10	• No problems performing task • Observed vector deceleration based on droplet spacing near direction change regions
Abstract Shape (refer to Table 2-A for illustration)	To determine vectoring definition versatility and evaluate machine limitations	`819992.PGM` `819993.PGM` `819994.PGM` `819995.PGM` `826991.PGM` `826992.PGM`	150, 300, 600, 2400	2.5, 5, 10, 40	• Also observed deceleration effects for this geometry • Determined that direction change deceleration is a function of vectoring speed and independent of shape orientation (rotation made no difference)
Tooling Insert Vector Outline with Hole (refer to Figure 2.3 for illustration)	To perform actual vector printing of a conventional tooling insert geometry profile	`090799.PGM` `092399.PGM` `0923993.PGM`	120, 150, 300, 360, 450, 600, 1200, 2400	4, 5, 7.13, 10, 10.87, 14.1, 20, 21.71, 26.09, 29.4, 32.61, 40, 43.48, 64.9, 86.96, 120, 173.9	• Initial measurements and programming done manually on Bridgeport on-board GUI • Used data from previous experiments to minimize vectoring deficiencies
Tooling Insert Vector Outline + Raster Fill with No Hole (refer to Figure 2.11 for illustration)	To incorporate and evaluate different raster filling methods for the insert interior	`Tool1012.PGM` `1020991.PGM` `1020992.PGM` `1020993.PGM` `1020994.PGM` `1020995.PGM` `T50R1028.PGM` `TSIO1028.PGM` `TSOI1028.PGM` `T50R1029.PGM`	254, 300, 600, 900, 2400	18.41, 21.74, 43.48, 86.96, 173.9	• Because of deceleration effects, ink concentrations noticeably higher in regions with frequent direction changes • Determined that diagonal 130° raster fill provides most uniform distribution • Programming complications prohibit hole inclusion
Tooling Insert Vector Outline + Raster Fill with Hole & DOD Micro Switch Control (refer to Figure 2.11 for illustration)	To assimilate and test complete functionality required for vector drop-on-demand printing of WC-Co tooling inserts	`T1R1028.PGM` `T2R1028.PGM`	240, 600	17.38, 43.48	• Objective of producing tooling insert layer through vector DOD printing achieved • Optimization of printing parameters with actual powder & binder chemistries required

MasterCAM programming limitations in tool path definition make inclusion of the center hole problematic for some of the raster fill tests, as shown in Figure 2.11. For the spiral fill, the tool path creation routine has difficulty transitioning smoothly between the circular fill pattern in the center to the linear, diamond pattern along the sides. For the linear raster fills, either horizontal or angled, the software appears unable to adjust the z-axis height dynamically—equivalent to turning the DOD printhead off and on—while rastering directly across the circular center. The approach that successfully incorporates the center hole is the section fill method, illustrated in Figure 2.11 (1). This process, while similar to the linear raster fill, does not move across the center hole but instead completes the fill by rastering as much as possible in one pass and then returning to do the remainder. In a similar manner, by rotating the section fill, the 130° raster fill could also be performed with inclusion of the center hole.

Complete Tooling Insert   Vector Trace (4x)

(1) Section Fill   (2) Spiral Fill   (3a) Raster Fill   (3b) 130° Raster Fill
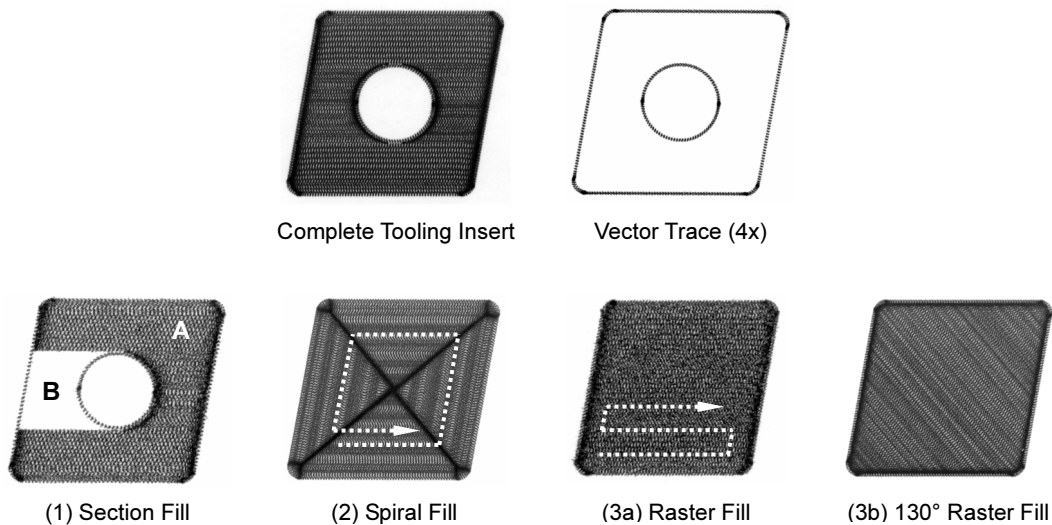
Figure 2.11   Depiction of a completed vector-printed tooling insert drawn with ink along with four different raster fill approaches. These methods are examined as potential rastering techniques for defining the interior after vector perimeter tracing: (1) two sections consecutively, A & B, (2) spiraling inward or outward, or either (3a) or (3b) a single raster fill with printhead start-stop control over the insert hole. The 130° raster fill method shown in (3b) provides more uniform ink distribution along all insert edges in comparison with (3a). Milling machine programming constraints and droplet control issues hinder rastering assessment with inclusion of the center hole for (2), (3a), and (3b). All samples shown are performed at the maximum permitted vectoring speed of 600 mm/min.

In any case, worthwhile conclusions are drawn about each rastering method from the simplified tooling insert geometries produced. For comparison, the raster fill experiments are performed at the maximum acceptable speed of 600 mm/min, which results in deceleration errors around rastered regions with direction changes. The distribution of "binder" is reflected by the darkness of printed regions. Ideally, the entire vector, raster-filled part should have a uniform ink concentration. These ink-based

results highlight the disadvantages of a particular method by clearly denoting the higher binder concentration regions. Using this criteria to evaluate each rastering method, the approach with most uniform binder distribution using current vector printing DOD conditions is the 130° linear raster fill. As shown in Figure 2.11 (3b), the boundaries of the insert geometry have higher relative ink concentrations than the interior, but the gradient along the entire edge remains constant. This result may possibly prove useful in actual 3DP binder printing as a means of reinforcing or refining the edge finish of a part if differential slipcasting does not become a factor. In comparison with the other raster-fill methods, the uniformly distributed, increased ink concentration around the perimeter that results from this process appears to be the most potentially useful. As mentioned earlier, by rotating the section fill to the same angle, the center hole can be included in this rastering process.

Another important consideration in vector DOD printing of tooling inserts is the production rate, an issue addressed with the compromise in maximum milling machine speed. Measurements of the time required to complete the vector outline, interior raster-fill printing of the tooling insert geometry are performed. To complete the section fill tooling insert geometry, which includes the center hole, requires approximately seven minutes at a rate of 600 mm/min. The spiral fill tooling insert without a center hole takes around eight minutes, though it is likely that including the hole would reduce this time since less would be printed. For the linear raster fill tooling inserts, without a center hole, around eight minutes are needed. However, if the center hole were included and the linear raster fill included DOD start-stop control across the hole, the time is expected to be identical, if not more, due to the extra repositioning movements of the z-axis and the same surface area to cover. The times required to complete the vector DOD process can be decreased by increasing the milling machine speed at the expense of droplet placement errors and possible geometry distortion. These effects are machine-dependent, however, and will likely be reduced with the introduction of more advanced, specialized vectoring equipment.

The most efficient method of raster-filling the interior, a linear fill with DOD printhead stops across the center hole, is not performed as the result of several factors. A reliability issue with actuating the micro switch control, which may be attributed to either the switch or the Bridgeport quill positioning, makes consistent stop-and-start operations a concern. In addition, the HP printhead exhibits occasional instability by failing to restart on command. Another obstacle is the lack of properly programmed machine code due to MasterCAM limitations, as mentioned earlier. Though this style of raster fill is technically possible, under ink-based printing conditions, it would be prohibitively time-consuming to manually code the necessary tool paths and, for studying raster-fill variations, would not actually be necessary since conclusions can be made using the no-hole insert geometries. In the future, the need to adapt machine programming to accommodate a tooling insert center hole for vector DOD printing is expected to be unnecessary with the forthcoming slurry, vector 3DP machine from TDK (refer to Section 3.2 for details). In the end, although these problems could be addressed, at this stage in vector DOD

printing development, other issues need to be addressed, such as the integration of binder-based DOD printing discussed in the next section.

Ultimately, the purpose of implementing vector drop-on-demand printing with this milling machine configuration is to demonstrate the ability to produce a WC-Co tooling insert geometry having a vector outline and an interior raster fill. In this regard, the culmination of this effort is successful. The design and integration of a micro switch DOD control and the determination of vector printing parameters based on equipment limitations are also important developments. Although difficulties with machine tool path programming, milling machine speed limitations, occasional micro switch control errors, and HP printhead reliability prevent an optimization of every vector DOD parameter—specifically with rastering methods and production speed, a significant amount of knowledge is acquired. Thus far, experiments with this configuration have measured and validated its vector DOD printing capability. Now, the inclusion of binder-based DOD printing is considered with changes to the printhead and fluid system.

2.3. DROP-ON-DEMAND PRINTHEAD DROPLET FORMATION

With the introduction of 3DP binder systems instead of ink, the previously employed HP 51626A printhead is replaced with a different drop-on-demand printhead, the piezoelectric-actuated Siemens PT-88S, to study droplet formation with different fluid chemistries. In the Siemens PT-88S, eight piezo transducers are used to produce droplets by changing electrical energy, described as a voltage waveform at a certain frequency, into mechanical motion. For these cylindrical piezos, applying a positive voltage causes contraction and shortening, while applying a negative voltage causes expansion and lengthening. The binder within the fluid channel is subjected to an ensuing pressure pulse that moves through the liquid and ideally leads to a volume separation at the orifice. Given the differences in fluid properties for various binder systems, the default Siemens waveform for ink may or may not work for these conditions. Therefore, to establish stable droplet formation conditions requires assessing the influence of and the relationship between the printhead actuation parameters of waveform voltage, timing, and frequency as well as the binder properties of surface tension and viscosity.

The Siemens PT-88S is the primary printhead utilized for droplet formation testing, but a prototype printhead design by Hiro Tsuchiya is also briefly evaluated. Like the Siemens design, Hiro's printhead concept uses a cylindrical piezoceramic actuator. However, several important differences exist. With his single fluid channel and fewer filter stages, no manifold is necessary, and fluid flow has less resistance. The Siemens PT-88S uses an unbonded, removable orifice plate that is held in place by a spring, while Hiro's design uses a permanently bonded orifice plate. This rigid fixation is intended to reduce orifice deflections from the piezo pulses that could prevent droplets from being ejected. The voltage requirements for his prototype design also differ from the Siemens printhead specifications.

Several waveform modification tests conducted with Hiro's printhead provide valuable insight to the droplet formation phenomenon, but since his printhead design remains in development at this time, implementation of vector DOD binder printing and the study of droplet formation are left to the Siemens PT-88S printhead.

The 3DP binder systems examined in this study include (1) a water-based Polyacrylic Acid (PAA) binder in two concentrations, (2) an alcohol-based PAA binder, (3) a PAA binder with a water-and-alcohol solvent mixture, and (4) colloidal silica (CS). The PAA chemistry includes a cross-linking agent that strengthens the binder printed part upon low temperature curing so it can be retrieved during redispersion. The alcohol-based version of this binder is intended to be used with the WC-Co slurry-jetted powderbeds. Note that droplet formation tests performed using the colloidal silica suspension are not directly applicable to the processing of WC-Co. This binder is commonly used for dry alumina powder. Though the colloidal silica does not relate directly to DOD binder printing of WC-Co, the effects of waveform voltage, timing, and frequency on droplet stability for this system appear to share common trends in comparison with the other binder systems tested. Regardless of chemical composition, several conclusions are made concerning droplet stability in relation to performance parameters for the drop-on-demand Siemens printhead. In retrospect, a considerable amount of work is conducted with the CS suspension and a number of droplet formation parameters are analyzed in coordination with the Siemens printhead, so the general relationships observed between droplet formation parameters can be attributed to work with both PAA binder and colloidal silica.

To observe the effects of changing printhead or binder parameters on droplet stability, a specifically designed tool for this purpose known as the Droplet Observation Station (DOS) or Nozzle Test Station is used. Developed by Garth Grover, the test station consists of four component systems: (1) a fluid system for governing binder flow to the nozzle, (2) a motion system for positioning the nozzle and camera, (3) an electronics system for controlling each test station component and setting nozzle parameters, and (4) a video system for droplet visualization [27]. The fluid system is less important due to the independent fluid control inherent with DOD printheads. The setup of this observation station proves invaluable for testing various waveform geometries and observing their effects on droplet formation and stability. The DOS also provides a method for estimating droplet size and speed by referencing the images captured by the visualization system. Further details of this DOS and its implementation are provided in Section 2.3.1.

For tests using the Siemens PT-88S printhead, nozzles four or five are primarily used to evaluate droplet formation and stability, although other nozzles are also tested to diagnose the possible effects of piezo orientation with no apparent difference in droplet formation performance (refer to Section 2.3.8 for details). Based on the printhead assembly discussed in Section 2.2.5.2, the two fluid channels associated with nozzles four and five are the most perpendicular to the orifice plate and thus provide the most

unimpeded route for fluid flow out of the orifice. These nozzle selections guarantee the greatest isolation of piezo actuation performance in relation to droplet generation while minimizing undesired influences from other factors, such as the interaction of printhead components with the fluid along its output path. The performance of droplet generation should not be affected, however, with the selection and use of other nozzles.

With the number of printhead variables to consider, waveform timing and voltage along with frequency, each with a range of possible values, coupled with the influence from binder fluid properties, the task of developing an effective set of DOD printing conditions for generating a fast, stable droplet stream requires extensive experimentation and analysis. Beyond these variables, other effects on droplet stability are observed and assessed. The efforts reported in the following sections attempt to establish a basic understanding of the relationship between each parameter and how these factors contribute toward droplet formation. Currently, a focus on stability is pursued with droplet velocity a secondary consideration. An optimization of droplet size is also important, with smaller volumes allowing for higher resolution part definition at the cost of greater environmental influence. With increases in production speeds, however, the DOD ejection speed may become more influential in determining accurate droplet placement. It should also be noted that the droplet generation conclusions derived from these experiments are believed to apply only to the specific printheads used as indicated. The construction and interaction of the printhead piezoceramic element with surrounding printhead components add another layer of complexity not considered in this study. Limitations of the acquired data and suggestions for further research will be discussed as appropriate.

2.3.1. *Droplet Observation Station Setup*

To pursue an understanding of droplet formation and its contributing factors, a tool for observing and changing these conditions must be developed. Fortunately, such an instrument exists as the result of work done by Grover [27]. The main station components used for this research involve the motion system for orienting the camera relative to the printhead orifice, the electronics setup for inputting various waveform parameters, and the video system for observing and recording the stages of droplet development. As seen in Figure 2.12, the motion system is composed of "three leadscrew linear motion stages driven by stepper motors" [27], two for the "X-Z Axis" that controls printhead positioning and one for the "Y-Axis" that adjusts camera distance. The electronics subsystem includes motor controllers and uses a PC with National Instruments LabView software to control various printing parameters. LabView allows for creation of virtual instruments that control waveform timings and voltages as well as LED pulse width and delay. The video system consists of a CCD camera with LED strobe mounted on the opposite side of the printhead. The LED illuminates at the printhead frequency to capture a specific stage of droplet development, and the camera sends these images to a standard

television screen. Using this configuration, the efforts to determine an optimum set of conditions for a single, uniform droplet stream are considerably enhanced.

In terms of analyzing droplet formation, the Nozzle Test Station or DOS yields many pieces of valuable data. For one, the Droplet Observation Station provides an efficient and versatile method of testing waveform geometries. Through a series of extensive tests using different fluid systems, the effect of voltage, timing, and frequency on droplet stability is examined. To conduct these experiments, first the waveform geometry with appropriate voltages and timings, the droplet frequency, and the LED pulse width and delay are set through a LabView Virtual Instrument (VI). Setting the LED pulse width and delay determines the image brightness and stage of droplet development seen by the CCD camera, respectively. An LED delay of zero measures the point of ejection from the orifice since the delay accounts for waveform propagation and droplet formation within the nozzle. The pulse width determines the length of time the LED stays on to capture a droplet state. If the pulse width is too long, image clarity is affected because of droplet movement. Typically, for the following experiments, a pulse width of 10 microseconds is chosen. The waveform parameters and frequency are sent from the LabView VI to an HP 33120A Arbitrary Waveform Generator (refer to Section 2.2.2 for performance details) for actual printhead application. Originally, only one function generator is used for setting the printhead waveform geometry and frequency, but due to waveform degradation at low frequencies, another function generator is later added for printhead frequency designation only. Details about this phenomenon and its solution are discussed in Section 2.3.7. The waveform signal is sent from the HP 33120A at either its own or another function generator's trigger frequency to the Krohn-Hite Model 7500 Amplifier (refer to 2.2.2 for specifications and settings) which magnifies the waveform voltage by 100 times. The Siemens PT-88S printhead actuates on this amplified signal sent through connector pins to an individual piezo. The resulting droplet behavior is observed in real-time on the monitor, and the camera images can be digitally recorded in TIFF image files for later reference or analysis.

If the printhead conditions specified for testing do not compel immediate droplet production or produce irregular droplet patterns, certain diagnostic procedures can be attempted. First, make sure the binder reservoir level is below the orifice plate to ensure negative pressure within the nozzle; this factor proves to be an important consideration in maintaining droplet stability over time (refer to Section 2.3.6 for more information). Another starting or stabilizing process to try is to clean the orifice plate with a Q-tip wetted with a compatible solvent while waveform actuation is in progress. Alcohol solvents are preferred since they dry quickly and therefore reduce the chance of interference with droplet ejection. Following this attempt or in conjunction, the binder can also be forced through the Siemens printhead and streamed through the nozzles to ensure the binder completely fills the piezo-actuated fluid channel. If multiple attempts fail, as a last resort, a thorough disassembly and cleaning of the printhead may be necessary. Of course, an ineffective waveform or other droplet stability issue, such as orifice plate

corrosion, may be the cause of unstable or non-existent droplet formation failure (refer to Section 2.3.6 for more information).
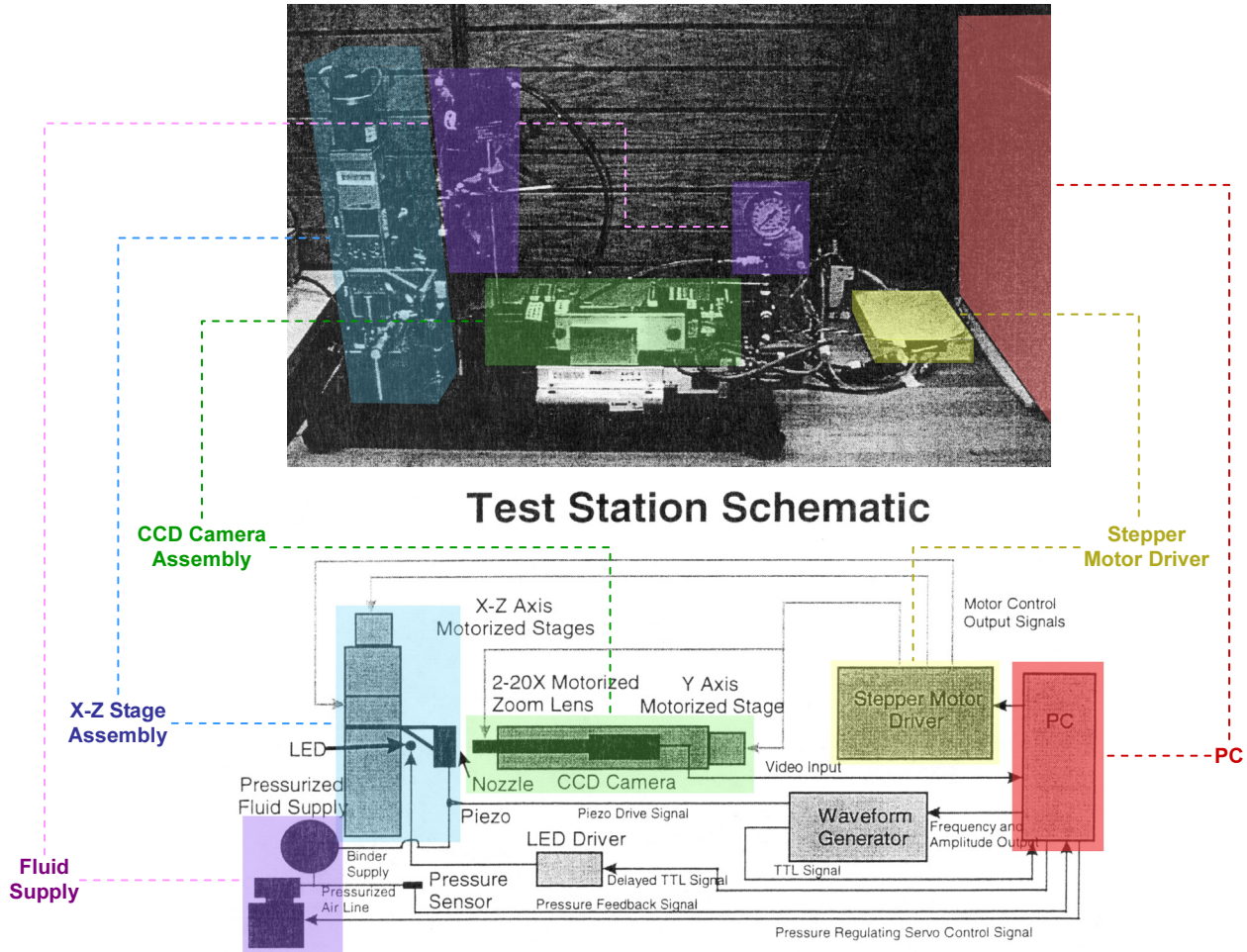
Figure 2.12   Picture and detailed schematic of the Droplet Observation Station. Originally, the nozzle and camera positions are adjusted by using a custom LabView Virtual Instrument (VI) to activate the stepper motor driver (shown above). This automated positioning system is later replaced with a manual set of two precision micrometer translating stages to provide X-Z axis movement. A desired waveform, with its corresponding frequency and varying voltage amplitudes, is then programmed using another designed LabView VI, which sends the information to a function generator. The function generator passes the signal through an amplifier that then connects to the printhead. Note that since the printhead relies on DOD piezo actuation, the binder supply does not require pressurization. The VI also permits LED strobe length and delay designations relative to the original waveform frequency to visualize the different stages of droplet development from the printhead. The base diagram and picture shown above are provided courtesy of Garth Grover [27].

The DOS can also be used to calculate estimates of droplet velocity and diameter by using a known scale calibrated to the magnification shown on screen. Examining the CCD camera output on the

monitor, the distance between two consecutive droplets (if seen) can be measured and the velocity determined based on frequency. Another method involves knowing the LED strobe, or pulse, delay for two image captures of the same droplet. By measuring the distance traveled by the droplet over this change in LED pulse delay, the velocity can be estimated. One final method for estimating the droplet velocity is to find the change in pulse delay for the droplet to travel 1 mm as scaled on the screen. The droplet diameter can be approximated using this same scale. A more accurate calculation of droplet diameter is to measure the binder mass deposited at a set frequency over a known period (refer to Section 2.3.8 for detailed analysis).

2.3.2. *Binder Chemistry and Properties*

Because binder systems can possess a wide range of properties, the process of DOD droplet generation must be customized to each situation, or if possible, the binder system properties can be adjusted. The fluid properties of viscosity, surface tension, and density are most important in developing an effective set of DOD printing conditions. Table 2-C compares these attributes for the binder systems examined in this study. Five different binder systems are tested with the Siemens printhead:

- 2.4 v/o PAA + 0.26 v/o Glycerol + 97.3 v/o Water
- 2.4 v/o PAA + 0.26 v/o Glycerol + 97.3 v/o Ethanol
- 10 v/o PAA + 1.1 v/o Glycerol + 89.5 v/o Water
- 10 v/o PAA + 1.1 v/o Glycerol + 12.1 v/o IPA + 77.3 v/o Water
- Colloidal Silica (Binder "B" Formulation [28])

For this research, the effects of viscosity and surface tension are examined in relation to DOD printhead droplet formation.

In order to produce 3DP parts on alumina substrates with any printing method, the currently established water-based binder composed of Polyacrylic Acid (PAA) is utilized. Typically, the concentration of PAA is 2.4 volume percent (v/o) for use with alumina. This binding solution also includes an amount of glycerol (0.26 v/o for the typical binder), which cross-links with the PAA when cured at 150 °C to allow for subsequent redispersion and part retrieval [29]. This chemical bonding behavior maintains the structural integrity of the printed part until it can be sintered to full density. In an effort to apply this same binding process to WC-Co slurry-based powderbeds, an alcohol version of this binder is created by replacing the water solvent with Ethyl Alcohol. This substitution is necessary to prevent Cobalt oxidation in the presence of water. Although issues with powderbed redispersion may hinder successful implementation of this binder system, the PAA chemistry meets the three criteria for an effective binder system as explained by Sherry Morissette: (1) be removable in a non-oxidizing atmosphere, (2) possess low residual carbon content, and (3) contain minimal contaminating species relative to the powder composition [30]. Refer to Section 3.2 for information about WC-Co slurry-binder developments.

Table 2-C:
COMPARISON OF FLUID SYSTEM PROPERTIES
EVALUATED WITH THE SIEMENS PT-88S PRINTHEAD

Fluid System	FLUID PROPERTIES at Room Temperature (either 20 °C or 25 °C)		
	Viscosity (cP)	Surface Tension (dynes/cm)	Solution Density (g/cm^3)
Siemens Ink (Type 2)	23 cP	46 dynes/cm	1.13 g/cm^3
2.4 v/o PAA + 0.26 v/o Glycerol + 97.3 v/o Water	2.8 cP	72 dynes/cm	1.01 g/cm^3
2.4 v/o PAA + 0.26 v/o Glycerol + 97.3 v/o Ethyl Alcohol	< 2.8 cP[†]	22 dynes/cm[†]	0.800 g/cm^3
10 v/o PAA + 1.1 v/o Glycerol + 89.5 v/o Water	21 cP	72.1 dynes/cm	1.04 g/cm^3
10 v/o PAA + 1.1 v/o Glycerol + 12.1 v/o IPA + 77.3 v/o Water	33 cP	46.3 dynes/cm	1.01 g/cm^3
Colloidal Silica (Binder "B" Formulation)	3.5 cP	43.3 dynes/cm	1.21 g/cm^3
Ethyl Alcohol	1.2 cP	22.3 dynes/cm	0.7849 g/cm^3
Isopropyl Alcohol	2.4 cP	22 dynes/cm	0.7812 g/cm^3
Water	1.0 cP	72.8 dynes/cm	0.998 g/cm^3

[†] Viscosity and surface tension not directly measured; estimates based on properties and proportions of chemical components

Though it would be ideal to formulate a single waveform geometry appropriate for all binder systems, a stable printing condition determined for one composition will most likely not be as effective for another. This variability in droplet generation effectiveness using the same actuation waveform is the result of differences in fluid properties, particularly viscosity and surface tension, for each system. As seen through initial DOD printhead tests, these bulk properties play an important role in the viability of droplet generation. In analyzing Droplet Observation Station results, however, an identical waveform timing is shown to be acceptable for two binder systems—the water-based 2.4 v/o PAA binder and colloidal silica—with similar viscosity, but differing surface tension, which may indicate a stronger

correlation between droplet formation and the former fluid property. Further research is necessary to qualify this statement, since optimizations are still possible for both binder systems to enhance droplet generation performance, which may in turn greatly differentiate printing parameters in relation to their respective fluid properties. As a practical matter for now, this common result, used for subsequent vector printing experiments onto alumina as discussed in Section 2.4, is presented in detail in Section 2.3.8.

The viscosity and surface tension of a binder system have an important effect on droplet formation with a piezo-actuated DOD printhead. If the fluid viscosity is high, then a significant pressure fluctuation is needed to create any droplet because waveform propagation effects dissipate quickly. Alternatively, if the viscosity is low, the pressure waves caused by piezo actuation do not diminish as quickly and tend to induce split streams and errant droplets. Based on Hiro's experience, this low viscosity behavior is confirmed to occur with the Siemens printhead when using the standard ink-based waveform. If the surface tension is relatively high, then the fluid has a difficult time separating to form droplets due to strong intermolecular bonds. If the surface tension is low, then the binder fluid is likely to wet the orifice surface and once again make droplet formation difficult. It is possible, though, that changes in the printhead actuation parameters can reduce these effects and generate a stable droplet.

Through droplet generation tests with the Siemens PT-88S, it is observed that water-based 10 v/o PAA binder is not capable of being printed with the standard Siemens waveform. The relatively high surface tension of this fluid system, in comparison with the standard Siemens ink, is therefore believed to hinder droplet creation under default printhead conditions, although the possibility of successful droplet generation with a more effective waveform is not pursued. Nevertheless, an effort is made to reduce the surface tension of the PAA binder in order to approximate as close as possible the properties of Siemens ink. To increase binder viscosity and decrease surface tension, isopropyl alcohol (IPA) is added in place of water. Another possible method for increasing viscosity, if necessary, is to add more Polyacrylic Acid; greater concentrations of PAA, however, are more likely to lead to differential slipcasting. By adjusting binder viscosity and surface tension to closely approximate the same properties of Siemens ink, the logical prediction follows that the standard waveform used to actuate the Siemens printhead should also produce binder droplets from the PAA system. An optimal mixture of IPA and water as solvent are found that closely match the surface tension of the Siemens ink (refer to Table 2-C for concentrations) with only slightly higher viscosity.

A few unsuccessful attempts are made to generate droplets with the standard Siemens waveform and this modified alcohol + water-based 10 v/o PAA binder. One possible explanation is that the higher viscosity, while only 10 cP higher, plays a significant role in preventing droplet formation. Alternatively, perhaps another fluid property or printing condition must be accounted for. Nonetheless, because of this difficulty, it is decided that modifying the printhead waveform parameters may prove to be a more effective approach. In the end, by looking at the waveform shape, the efforts to manipulate binder fluid

properties become less critical to achieving successful, stable droplet generation, and the negative effects of extreme viscosity or surface tension can be compensated for to some extent. These alternative waveform modification tests are documented in the following sections.

The influence of fluid properties on stable droplet generation is effectively illustrated by experiments conducted with the 2.4 v/o PAA + 0.26 v/o Glycerol + 97.3 v/o Ethyl Alcohol binder. After establishing a functional waveform geometry and frequency for the water-based 2.4 v/o PAA binder and colloidal silica using the Siemens PT-88S printhead (refer to Section 2.3.8 for details), the same DOD printing conditions are applied to this alcohol-based chemistry, which has lower viscosity and lower surface tension. In comparison with the two previous binder systems, the ability to produce a stable droplet stream for the alcohol-based 2.4 v/o PAA binder with these same settings is only moderately successful, with less reliability and questionable longevity. Initially, a higher transition voltage versus the water-based 2.4 v/o PAA binder is determined for optimal single droplet generation—109 Volts versus approximately 97 Volts—though this state deteriorates over time and does not return when the voltage is varied in subsequent tests. After approximately 1.5 hours, the voltage transition threshold between single and multiple droplets increases from 109 Volts to 120 Volts, with the original voltage level no longer consistent. Even at 120 Volts, droplet stability lasts for only a few minutes. Refilling the printhead reservoir lowers the maximum stable droplet voltage to 115 Volts, which remains stable for 15 hours, but the droplet velocity is noticeably lower than the original steady state condition, which still cannot be restored. Though other factors may contribute to this behavior, such as the change in reservoir level relative to the orifice (refer to Section 2.3.6 for an explanation) and the likelihood of orifice plate corrosion, similarities in other important parameters suggest that differences in fluid properties—the lower viscosity and significantly lower surface tension—also affect the binder's droplet generation performance. More extensive testing of this binder system is postponed in order to pursue more important research objectives. Furthermore, due to negative interactions currently being investigated between this binder and the WC-Co powderbed, the continued study of stable droplet formation for this particular binder solution may prove unnecessary.

One important note about binder chemistry involves the issue of corrosion between the binder and the Siemens PT-88S orifice plate material. During droplet formation testing with the Siemens PT-88S, a significant amount of orifice plate corrosion occurred as the result of using the PAA-based and possibly colloidal silica binders. Because of the acidic nature of the PAA binder composition, it is believed that the orifice plate corrosion can most likely be attributed to this reactivity rather than to interactions with the apparently more neutral colloidal silica (refer to [28] for chemical composition). Indicated initially by residual markings on the orifice plate that could not be removed, a degree of corrosion is evidently observed early in droplet formation studies with the PAA binder, but the extent and rate of corrosion are

not explicitly documented at the time. The consequences and influence of orifice plate depletion and hole enlargement are not assessed until severe and unexpected droplet instabilities occur, detailed as follows.

Towards the conclusion of DOS testing, a significant and inexplicable decrease in the transition voltage for a formerly stable droplet waveform is observed. Using the CS binder after months of printhead testing with the same nozzle, the aforementioned voltage decreases from the expected 102 Volts to 92 Volts. Attempts to maintain stable droplets quickly deteriorate and prove immune to other diagnostic adjustments. These unexplained behaviors prompt the thorough cleaning of the Siemens printhead at which time the presence of crooked streams are noted when water is forced through the nozzles. Replacing the orifice plate cures this problem and restores the printhead to its previous functional state.

Based on this apparent change in droplet behavior as the result of orifice plate corrosion, it is possible that over the course of the experiments described in the following sections that expanded or irregularly corroded orifice holes may contribute to or even prove to be the primary causes of performance inconsistencies or degradation over time. This gradual increase in orifice diameter, though not completely understood, is clearly proceeded by the development of crooked and irregular streams with slow moving droplets that eventually prevent correct printhead functioning. The severity of corrosion for an orifice hole can be verified by forcing water through the printhead and checking for proper stream alignment. In addition, visual cues are present as well, such as the development of craters around the orifice hole and permanent stains.

The orifice diameter increases proportionately as a function of operating time; however, the exact correlation requires further investigation. A different orifice plate than the one mentioned above is later examined after approximately 29 hours of total use distributed between four nozzles (numbers three through six) with the water-based 2.4 v/o PAA binder. Starting with the standard 80 micron diameter, the rate of corrosion is apparently inconsistent with nozzle four having a diameter of 104 microns after 6 hours, while nozzle five has a smaller diameter of 90 microns after 11 hours. Nozzle six and nozzle three also exhibit an inverse behavior: 108 microns after 3.5 hours compared to 100 microns after 8 hours. This unexpected trend in corrosion rate indicates that other variables, such as waveform geometry and frequency, most likely also play a role. Nevertheless, corrosion is clearly evident as the result of this PAA binder system.

Further study is necessary to understand this chemical interaction between the PAA binder and the orifice plate and the rate at which the reaction occurs. Until this corrosion process is clearly understood, it is advisable to evaluate the selected orifice hole periodically during operation for structural integrity and diameter accuracy when using this binder chemistry. The associated effects of orifice plate corrosion, such as a continuous change in droplet position towards the orifice at a constant

pulse delay, a reduction in transition voltage, or crooked streams when flushing nozzles, also serve as good indicators of impending nozzle failure.

Note lastly that the three final items in Table 2-C are for comparison only and are not individually tested for droplet formation analysis in the Siemens printhead. These basic solvents are significant and fundamental components of the binder systems tested. They greatly influence the fluid properties of viscosity and surface tension because of their large relative concentration in solution. In addition, these solvents are also used for adjusting these properties. In addition, the benchmark Siemens Ink (Type 2) is not extensively tested but instead serves as an established, functional starting metric for adjusting other fluid systems. Though all of the remaining fluid systems are evaluated with the Siemens printhead, experiments with the two 10 v/o PAA binder systems do not include visual documentation in the form of image captures, because attempts to generate droplets with these particular fluid compositions are largely unsuccessful. All relevant information from each fluid system, however, is considered in the analysis of the following sections.

2.3.3. *Effect of Waveform Timing on Droplet Stability*

The waveform geometry, based on timing and voltage, plays an important role in droplet formation. It defines an actuation process for the piezo that creates pressure pulses in the binder fluid for droplet generation. The typical waveform examined in this study consists of three stages: a ramp up stage (a), a steady state (b), and a ramp down stage (c). Each section describes voltage change over time, and as a whole, the waveform shape appears trapezoidal in nature (refer to Table 2-D for an illustration). In general terms, according to Hiro, the sustained timing segment (b) is believed to be most important for high surface tension liquids. Though many different timings and voltages can be used, this basic actuation process is chosen for its simplicity and similarity to the default Siemens waveform and is sufficient for defining stable droplet generation. Because of the large number of possibilities for waveform definition, continued examination of various timings may yield further improvements in droplet stability and performance.

From experiments with colloidal silica, several conclusions can be made about the effect of long and short timing segments. As seen in comparisons of waveform timing in Table 2-D, the first segment (a) appears to have little affect on droplet speed; this behavior is observed for waveform timings of CS in which only the first segment is changed (1 µs: 8 µs: 1 µs, 2 µs: 8 µs: 1 µs, 4 µs: 8 µs: 1 µs, and 8 µs: 8 µs: 1 µs). The latter two timing segments have a much greater effect on droplet speed. By comparing the two pictures for segment (b), it can be concluded that the longer the middle segment, the greater the droplet speed as indicated by the presence of two drops for the shorter (b) segment on the same scale. When reversing the timing between the two latter segments for CS (4 µs: 8 µs: 1 µs versus 4 µs: 1 µs: 8 µs), by increasing (b) and decreasing (c), the "transition" voltage, or voltage at which a single droplet forms

satellites, decreases (104 Volts versus 121 Volts), and the droplet speed increases (1.5 m/s versus 1.25 m/s). It should be noted that despite the differences in these variables, both waveforms have produced stable droplets for extended periods of time.

While a lack of data prevents conclusive analysis for the water-based PAA binder, the general trends presented above should still apply. Of course, further tests of the PAA system are necessary to verify these trends. As an initial effort into droplet generation with the Siemens DOD printhead, the value and effect of each parameter, such as the timing segment, is unfortunately not consistently accounted for. Many tests are performed with different waveform timings; the ability to compare differences, based on changes in only one segment, is not available with currently compiled data. While this prevents extensive analysis of individual timing segments for the PAA binder, the efforts made at the time did not consider this objective. Instead, the determination of a stable overall waveform is desired, and this goal motivates the experiments and tests performed. The determination of a stable printing condition for the water-based 2.4 v/o PAA binder is discussed in Section 2.3.8.

The Siemens printhead can be successfully actuated based on a certain total timing range. This acceptable length of actuation times is determined in part by the design characteristics of the printhead. Given the maximum piezo ejection frequency specification of 2.9 kHz provided by Siemens, the longest possible waveform timing must fit within this boundary of 344 microseconds, which in terms of the scale of timings examined should not be a problem. Though the absolute minimum is not clearly defined, based on experimental observations, a particular operational interval can be identified. From the experiments conducted for all binder systems, the shortest functional timing length achieved is nine microseconds, while the maximum is 17 microseconds. Many variables can influence the waveform interval, such as the individual timing segments and their corresponding voltage levels as well as the fluid system tested. Therefore, the determination of a conclusive timing range for the Siemens PT-88S requires further study.

In addition, a definite correlation exists between waveform timings, corresponding voltage changes (presented in the following section), and droplet velocity for each binder system. Through numerous waveform experiments, particularly with colloidal silica, images captured on the DOS indicate that the droplet position varies at the same measured time from ejection (set by the LED strobe delay of the DOS) when the printhead is actuated with different waveform timings. The exact measure of droplet speed variation is not currently known, but analysis of the present data and future tests on the DOS will yield valuable insights and quantification of this relation. The effect of each timing segment, its associated length, and the number of segments used are all influential factors that warrant further examination. This relationship is a potentially valuable area for more study as a means for adjusting or maximizing droplet exit velocity, which would aid in accurate binder placement.

Refer to Table 2-D in Section 2.3.8 to view a general summary of droplet formation parameters for the two major binder systems examined, the water-based 2.4 v/o PAA binder and colloidal silica.

2.3.4. *Effect of Voltage on Droplet Stability*

The effect of voltage on droplet stability is multifaceted. The process of voltage actuation as defined in the waveform causes the Siemens piezoceramic to first contract at a constant rate, remain contracted for a period of time, and then expand back to its original state at another constant rate. This cumulative motion causes fluid to pass through the enclose nozzle tube with the piezo expansion inducing droplet cutoff at the end. In one respect, the relationship between stability and voltage can be easily defined. A high maximum voltage leads to multiple droplet streams or satellites and faster droplet speeds. In addition, the greater the applied maximum voltage, the greater the volume of binder ejected, whether as a single stream or as multiple streams. The transition voltage defines the level at which a single stable droplet breaks into multiple drops. Although it is possible that satellite drop formation could occur below the transition voltage at a level that induces sufficient pressure instability in the nozzle, no evidence of this phenomenon is recorded. On the other hand, low voltages (below the transition voltage) generally create a weak, wavering droplet stream that eventually stops completely as the piezo actuation becomes ineffective.

It has been observed that every waveform for every unique binder chemistry appears to have its own voltage transition point whereby a stable single droplet will begin forming satellites. This large variation prevents extensive generalizations about the effect of voltage on droplet stability. It is believed that if droplet formation can be initiated with a particular waveform, then a transition voltage exists at which a single droplet state occurs, though the degree of stability and other performance measures, such as speed, may not be acceptable. Perhaps with further testing, a significantly large sample of different binder systems can establish more broadly applicable and quantitative theories. Several conclusions are made, however, based on observations of the two major binder systems tested.

Based on initial analysis of both the 2.4 v/o PAA + water and colloidal silica binder systems, an unexpected correlation is developed between maximum voltage and droplet frequency. Given a particular waveform, such as the 2 μs : 6 μs: 1 μs for the PAA and colloidal silica binders as well as the colloidal silica 2 μs : 8 μs: 1 μs to a lesser extent, as the frequency increases, the maximum voltage that yields a stable, single droplet stream decreases. For the 2.4 v/o PAA binder, this relationship is most clearly demonstrated. For a frequencies of 300 Hz and 200 Hz, a maximum voltage of 150 Volts is acceptable. However, at 400 Hz the voltage must be reduced to 140 Volts, and at 500 Hz the voltage must be even lower at 135 Volts. Intuitively, these two parameters should not be interdependent. One possible reason for this observation may be the use of only one function generator to perform these waveform tests. By only using one, the waveform resolution decreases as frequency decreases because of a data

point limitation in the equipment, and this change in the waveform geometry is likely to lead to a different piezo actuation behavior than expected (refer to Section 2.3.7 for further details). One other potential explanation may involve the piezoceramic's contraction and expansion capability. Depending upon the rate at which the piezo can change shape, its delayed response to a large voltage increase or decrease as dictated by the waveform geometry may introduce actuation errors since the piezo is unable to react in time and stabilize at higher frequencies.

The other aspect of voltage influence on droplet stability relates to the rate of voltage change. This effect is defined by both waveform voltage and waveform timing. As mentioned in the previous section, testing of actuation timings and voltages on the DOS demonstrate that the associated geometry affects droplet velocity. Waveform timing and the corresponding voltage levels for each segment both contribute significantly to stable droplet development, so the recommended study of droplet velocity must logically take both of these variables into account. In some sense, it is possible to isolate these two waveform variables as attempted in this discussion, but the combined effect must also be considered. Presumably, since large voltage changes lead to large piezoelectric movements, and the corresponding actuation energy is then transferred to the fluid, increasing voltage should lead to a faster droplet speeds, but further qualification and quantification is recommended. Based on current data, higher maximum voltages with the same waveform timings are shown to produce stronger, progressively faster droplet streams, although the voltage level must be restrained at some point to prevent satellite droplets from forming.

The research conducted only examined positive voltage actuation. The possibility of negative voltage waveform segments is recommended as an area for future study and may yield more effective droplet stabilization either as an inverse trapezoidal waveform or as a segment of a positive-negative voltage variation. Hiro has devised a functional waveform for his prototype printhead that starts with a negative voltage, piezo expansion step that then progresses to a positive voltage state before returning to zero. This waveform is demonstrated to be stable for the a wide range of frequencies (between 100 Hz and 1000 Hz) using a water-based 3.5 v/o PAA binder system.

Refer to Table 2-D in Section 2.3.8 to view a general summary of droplet formation parameters for the two major binder systems examined, the water-based 2.4 v/o PAA binder and colloidal silica.

2.3.5. *Effect of Frequency on Droplet Stability*

In general, frequency should not play a significant role in droplet stability but should instead only control droplet spacing in flight and on powderbed deposition. The objective of establishing a stable droplet formation condition involves finding a voltage-timing waveform that preserves a single droplet stream over a wide range of frequencies. Frequency affects droplet speed, however, to a small extent. When the piezo contracts or expands, a pressure pulse is generated through the fluid. It perpetuates

through the nozzle tube that carries the fluid out to the orifice and is reflected at the opposite end, sending back a smaller amplitude wave. If the two colliding pressure waves are in phase, then the resulting wave has greater amplitude and more energy is imparted on the fluid than just the piezo actuation, leading to a droplet with higher than expected exit velocity. The converse is also true: pressure waves with inverse phases act to reduce the droplet velocity. This phenomenon is observed with the DOS for the water-based 2.4 v/o PAA binder when tested using the stable 4 μs: 8 μs: 1 μs: 97 V waveform geometry at 952, 970, and 1,011 Hz. At other frequencies, which are currently unpredictable and not necessarily reproducible, a stable single droplet can suddenly form satellites. This phenomenon is commonly observed among all binder systems when a stable droplet at one frequency is subjected to frequency changes. Through analysis of current data, it appears that droplet instability as a function of frequency is more likely to occur in higher ranges (above 400 Hz), in particular with the waveform timings and voltages tested. The limited scope of data and the extensive interdependencies between waveform variables and frequency suggest further study is needed to validate and quantify this frequency generalization.

Normally, the frequency is a setting that is determined in relation to the vector printing speed to satisfy a desired binder droplet spacing for a powderbed. Because the vectoring equipment possesses a limited speed capability, a droplet spacing designation acts as an external constraint to limit the range of possible frequencies available for achieving droplet stability. Due to the interdependent nature of the waveform timing, voltage, and frequency, a suitable set of droplet formation parameters within a restricted frequency range can most likely be defined. Under stable printing conditions, frequency does not affect droplet velocity. This variable independence is expected and verified through extensive DOS testing using functional single-drop printing parameters. To deal with droplet instabilities that arise within the frequency spectrum, such as satellite droplets, multiple constant or erratic streams, or a crooked, yet stable, droplet jet, a multitude of approaches can be taken.

If a frequency setting results in satellite droplet formation, several options are available to attain a single droplet state. Given an effective waveform geometry, it is believed that residual droplet satellites that occur at a desired frequency can be eliminated by adjusting the maximum voltage level. One potential cause of multiple droplets is the pressure fluctuation within the printhead that occurs at the set frequency. When holding the waveform constant, the frequencies at which multiple droplets form are seen to occur at various intervals between stable droplet states. Thus, another method to eliminate extraneous droplets is to change the frequency. The resulting change in droplet spacing for the printed part can be compensated for by altering the translation speed of the vectoring component. It should be noted that when instabilities emerge at a particular frequency the droplet behavior exhibits a hysteresis effect whereby reverting the frequency back to an originally stable range only a few hertz away will not necessarily eliminate the disturbance. Continued frequency increase or decrease is necessary to return

the droplet condition back to a single state. For example with colloidal silica, experiments demonstrate that when a stable 4 µs: 8 µs: 1 µs: 118 V waveform at 500 Hz is reduced in frequency to 100 Hz, a satellite drop forms. Though a single droplet is present down to this level when the instability develops, the frequency must be raised back to 300 Hz before the multiple droplets recombine. Though it is possible that the satellite droplet would eventually dissipate by changing the frequency up only slightly — to perhaps 101 or 102 Hz, which were originally stable — the amount of time this would require is unknown and reserved for future study. By changing the frequency from 100 Hz up to 300 Hz, the pressure fluctuations in the printhead are gradually counteracted, and the satellite droplets eventually disappear. The rate of frequency change, however, also plays a role in maintaining or establishing droplet stability. Rapid changes in frequency are more likely to create or maintain existing droplet disturbances, so relatively slow frequency modulation is recommended. The effect of frequency rate of change and the degree to which it affects droplet stability are not completely understood, but a comprehensive understanding would require further study.

Certain frequencies cause internal printhead pressure fluctuations that interfere with stable droplet formation. These frequencies result in streams that appear crooked initially but straighten upon further frequency change. This behavior may also be due to orifice plate corrosion, though this contribution is not easily verified from collected data due to a lack of awareness regarding its potential severity until later in the droplet generation evaluation process.

Overall, the most important consideration for frequency is verifying that the desired frequency at which vector printing will take place does not produce droplet instability. This criteria is evaluated and confirmed for droplet formation conditions used in the following vector DOD printing tests discussed in Section 2.4. For the most part, frequency does not play as critical a role in droplet generation as the waveform timing and voltage.

Refer to Table 2-D in Section 2.3.8 to view a general summary of droplet formation parameters for the two major binder systems examined, the water-based 2.4 v/o PAA binder and colloidal silica.

2.3.6. *Other Effects on Droplet Stability*

Several other effects on droplet stability are observed that do not fit into the above categories. The top of the binder reservoir should always remain below the orifice level to maintain a negative pressure in the printhead. This condition is the normal pressure state within the piezo tube of the Siemens printhead as well as in Hiro's similar DOD printhead design. The more positive the pressure within the piezo tube, the slower the droplet ejection speed because of the tendency towards orifice surface wetting. The excess binder on the orifice dissipates the droplet energy as it emerges from the printhead and thus reduces its speed. As the binder supply is depleted and the reservoir level decreases, the more negative pressure and suction into the orifice increases. This prevents wetting of the orifice

surface and thus allows the ejected droplet to travel faster without dissipating energy at the printhead outlet. If the reservoir level progresses too far below the orifice, the negative pressure may eventually cause air to be sucked into the piezo tube, which also causes problems with droplet generation. The effect of reservoir level on droplet speed is clearly demonstrated with Hiro's DOD printhead design. Under stable droplet formation conditions, using a 4 μs: 1 μs: 8 μs: 160 V waveform geometry at 600 Hz, the addition of binder to the printhead reservoir reduces the speed of the droplet by 0.52 m/s, a significant 13% reduction from the initial speed of 3.92 m/s before binder is added. The same behavior can be observed without increasing the reservoir volume, but by only changing its height relative to the orifice. Ideally, the height differential between the reservoir and orifice should remain constant so that pressure changes from binder depletion do not affect droplet generation, although this factor is not closely monitored for every experiment and may unknowingly contribute to observed phenomena. The reservoir level is verified as a diagnostic step when severe printing problems, such as a failure to start with a known functional waveform, occur.

Printhead droplet generation is fairly sensitive to disturbances and vibrations in the fluid supply line and reservoir, as seen in tests on the DOS and when doing vector printing with Bridgeport. Given a stable droplet condition, disturbances, such as the vibration of the milling machine spindle or intentional vibrations of the fluid line, are observed to cause the droplet state to become erratic, although the circumstances under which this instability occurs are not fully understood; the probability of a return to steady state is also difficult to predict. To alleviate this potential effect, it is recommended that (1) the milling machine motor vibrations be minimized by reducing its rotational speed and (2) the connections between printhead and reservoir remain isolated and stationary.

With a progressive decrease in ejection speed over time, the presence of cross-winds can greatly affect proper droplet placement on the powderbed. In some cases, cleaning the orifice plate with a compatible solvent or flushing the piezo tubes with binder or solvent may correct errant droplet behavior. This process eliminates any buildup of binder or contaminant along the fluid path that can affect droplet formation. Orifice plate cleaning in itself introduces another impedance, although usually temporary, to stable droplet formation. A certain amount of time must elapse for residual solvent to evaporate from the orifice plate surface. During this time, lingering solvent around the orifice may interfere with the properties of the ejected drop, notably its speed. This behavior is clearly illustrated by the observed gradual shift in droplet position at a set strobe delay on the DOS after the printhead has been cleaned.

The issue of printing time may also play a role in droplet stability, but the reasons for this dependency require further examination. Over the course of studying droplet formation, observations of droplet stability over extended periods—on the scale of hours—indicate that the speed of the droplet tends to decrease. The exact cause of this variation is uncertain, though many possibilities exist. One or a

combination of (1) change in the reservoir level relative to the printhead, (2) gradual magnification of internal printhead disturbances from the actuation process, or (3) corrosion of the orifice plate (as discussed in Section 2.3.2) could contribute to this phenomenon.

The implementation of drop-on-demand controls through use of the micro switch (discussed in Section 2.2.1.3) presents another source of potential droplet instability. With the current understanding of the Siemens printhead functionality with various binder systems, a consistent, steady droplet stream is less likely to be preserved upon stopping and restarting of the printhead. With the large number of other variables influencing the droplet formation process, maintaining a state of equilibrium already requires considerable effort. Given a functional waveform, however, the likelihood of an immediate single-drop state starting or resuming is increased, though not guaranteed as evidenced by many DOS tests. If the droplet generation process is allowed time to stabilize, then with previously functional conditions, the return to a steady, stable droplet state is highly likely. Another concern is that the probability of inconsistent droplet behavior increases as the time between stopping and resuming the DOD printhead increases, indicating that binder volatility plays a role in DOD control. From observations of the binder systems tested, a reproducible and stable restart is greater for intervals of less than ten seconds. The drying of binder in the nozzle or on the orifice plate surface that affects the droplet formation path may explain this time dependence. The amount of time necessary to reach steady state after restart is currently unpredictable but ranges from several seconds to around a minute based on experimental observations. To understand and quantify this stabilization process will probably involve the correlation of many factors, including those previously discussed, and thus will require further study.

2.3.7. *Effect of Frequency on Waveform Resolution*

Initial tests of droplet formation utilize only one HP 33120A Arbitrary Waveform Generator (detailed in Section 2.2.2), whose output sends the piezo-actuating waveform signal at a particular frequency. Based on the prescribed LabView program settings, only 10,000 points are available per cycle for defining a waveform. Each data point represents an equal increment of time. This limitation affects the resolution, or the number of points, available to represent a particular waveform geometry, whose voltage change typically occurs on a microsecond scale. Using the trapezoidal waveform shape described in Section 2.3.3, the transitions from zero Volts to the steady state maximum voltage and back are ideally smooth and linear. For tests of droplet stability at low frequencies, however, the resolution of the expected waveform is severely degraded due to the lack of data points in the function generator to define a particular time period. For example, at 100 Hz with 10,000 data points to represent this interval, the amount of time per data point ($t_{data\ point}$) is calculated to be

$$\frac{1}{t_{\text{data point}}} = 100\,\text{Hz} \cdot \frac{\text{Max. Data Points}}{\text{cycle}} = \frac{100\,\text{cycles}}{\text{sec}} \cdot \frac{10{,}000\,\text{data points}}{\text{cycle}} = 1{,}000{,}000\,\tfrac{\text{data points}}{\text{sec}}$$

So taking the inverse yields

$$t_{\text{data point}} = 1\,\mu s$$

which is fairly coarse considering the time scale of the voltage waveform. If the voltage goes from zero to 100 Volts in 5 microseconds, then each data point (D_x) would remain constant for 1 microsecond at 20 Volt increments (i.e. D_0 = (0 Volts, 0 μs), D_1 = (20 Volts, 1 μs), D_2 = (40 Volts, 2 μs),… etc.). Therefore, each data point represents a relatively long period of time at a particular set voltage. By generalizing the above equation, it is obvious that lower frequencies increase $t_{\text{data point}}$, and the inverse is true for higher frequencies decrease $t_{\text{data point}}$. As a result, the desired linear increase in voltage becomes more segmented and exhibits a stair step effect. This digitization phenomenon increases as the frequency decreases using the single function generator setup. With each time step increase in voltage, a certain amount of time is required to reach this next voltage level. The rate at which this voltage change can occur is limited by equipment performance so the larger the necessary voltage increase from one time step to the next, the less precise the voltage adjustment and the greater the distortion of the intended waveform.

For approximately the first 40% of the droplet generation tests, this waveform resolution degradation is present. Therefore, increasing waveform irregularities are likely contributors to problems observed with droplet formation during these experiments.

This increasing waveform distortion with decreasing frequency problem is solved with the addition of a second function generator. By using one function generator, specifically the HP 33120A, to set the waveform function, the resolution remains independent of the droplet frequency. To obtain a high-resolution waveform, the frequency chosen for waveform definition is 50 kHz, which provides $t_{\text{data point}}$ = 0.002 μs. As long as the droplet generation setup includes two function generators, one for setting the droplet frequency and the other for waveform definition, the effect of low frequency waveform corruption on droplet stability is eliminated.

The process for setting up and connecting these two function generators for waveform-frequency independence is as follows. The first function generator (FG_1), assuming it is an HP 33120A, is used to set droplet frequency, while the second function generator (FG_2), which must be an HP 33120A, holds the arbitrary waveform defined at 50 kHz resolution. The FG_1 is set to Burst Mode with internal triggering at a user-specified Burst Rate (initially at 500 Hz) and 1 cycle Burst Count. Using the default 50 Ω Output source, FG_1 sends a trigger waveform signal, a standard TTL square wave with 50% duty cycle, that is split between the External Trigger connector on FG_2, the LED for visualization, and an oscilloscope for frequency and voltage verification. The FG_2 is programmed with the waveform and sends the signal at the frequency specified by the External Trigger, set by using Burst Mode with a 1 cycle Burst Count, and

an external trigger source mode. The Single setting activates the External Trigger connector and uses the rising edge of the TTL pulse from FG_1 to send the waveform. The FG_2 output source is set for high impedance and sends the data to the amplifier. The final scaled waveform geometry is subsequently processed by the Siemens printhead.

2.3.8. *Summary of Droplet Formation Parameters*

In studying the process of drop-on-demand printhead droplet generation, a number of important parameters are examined. To observe droplet formation and evaluate its associated variables, experiments are conducted on the Nozzle Test Station. The effects of binder chemistry, waveform timing, voltage, frequency, and other general environmental factors on droplet stability are measured, observed, and analyzed. The problem of waveform resolution as a function of frequency in the single function generator setup may have also contributed to certain instabilities; this low-frequency waveform error, however, is addressed with the addition of a second function generator for separate droplet frequency control. The complex relationships between all of these factors make analysis of behaviors difficult to attribute to a specific cause. Many possibilities for further study are suggested in the course of discussing the preceding sections. An attempt to summarize the relevant concepts and conclusions follows.

In terms of binder chemistry, the fluid properties that most affect droplet formation are surface tension and viscosity. The general influence of surface tension dictates that if high, droplets do not separate easily from the fluid column in the nozzle channel, and if low, orifice surface wetting becomes likely. With high viscosity binder, pressure fluctuations from piezo actuation disappear quickly, hindering droplet formation, while a low viscosity fluid tends to induce split streams and satellite droplets. The difficulty in DOD printing of the water-based 10 v/o PAA binder with the Siemens standard waveform indicates that the relatively high surface tension most likely hinders droplet production under these conditions. By reducing the surface tension to more closely match Siemens Ink (Type 2), it is assumed that droplet generation with the standard Siemens waveform will prove more successful. The surface tension is reduced to the same level as the ink by adding IPA in place of water; this substitution also raises the viscosity, however. Attempts to generate droplets with this new alcohol/water-based PAA binder under the same conditions previously attempted prove unsuccessful, which may be attributed to the increased viscosity relative to ink or the contribution of other droplet formation parameters not accounted for. The viability of droplet generation with this PAA binder may still exist if changes in waveform parameters are studied. This approach of examining printhead actuation parameters is pursued as an alternative to binder property modification. Another example of the effect of viscosity and surface tension on droplet stability is a comparison between alcohol- and water-based 2.4 v/o PAA binder using the same printhead waveform geometry. Although the alcohol-based binder exhibits some signs of eventual stability, irregularities in transition voltage and extremely

low droplet speed indicate that given the similarities in other printing parameters, the large difference in surface tension is likely a contributing factor to this stability reduction. One concern related to binder chemistry is the observed corrosion of the Siemens PT-88S orifice plate when using Polyacrylic Acid-based binders. The amount of corrosion for several nozzles is measured over known periods of operation with no conclusive correlation. An apparent inverse relationship between operation time and orifice diameter corrosion for two of the nozzles indicates that other factors, such as waveform and frequency, are significant in determining corrosion rate. Further study of this phenomenon is recommended so that the degree of corrosion can be more reliably predicted since orifice diameter changes can lead to droplet instability.

Waveform timing and voltage contribute to defining the overall piezo-actuation process. The standard waveform geometry examined is trapezoidal in nature with three stages (refer to Table 2-D for an illustration). In terms of waveform timing, it is believed that the first timing segment is not influential in determining droplet velocity. The second segment (b), however, appears to increase droplet speed with increasing time. If the values of segments (b) and (c) are interchanged so that (b) increases and (c) decreases, it has been observed that the transition voltage decreases and droplet speed increases. In terms of overall timing intervals tested (a + b + c), droplet formation, though not always stable, is observed to occur between 9 and 17 microseconds of total time. Times tested above and below appear to be non-functional, although much more work on this study of waveform timing is recommended. The influence of waveform timing on droplet speed is also an important correlation that requires further analysis. Waveform voltage, if examined by itself, determines the degree of actuation for the Siemens piezoelectric transducer. With the trapezoidal voltage variation, higher maximum voltage settings lead to multiple droplet streams, higher speed, and higher volumes. The transition voltage defines the level at which a stable single droplet will break into satellites. This value varies depending on waveform geometry and binder chemistry, so no conclusive generalizations are possible. One observation of transition voltage in CS and PAA systems indicate that at higher frequencies, the transition voltage decreases, even though a relationship between these two variables is not intuitively expected. This behavior may be dependent on changes in waveform resolution, which for these observations, is affected by low frequencies (refer to Section 2.3.7 for details), or on the ability of the piezo to function accurately at different frequencies. The waveform voltage combined with waveform timing determine piezo actuation rates and influence droplet speed. Further study is required to correlate this relationship. In addition, since this study only examined positive voltage variation, the possibility of negative voltage in waveform definition should also be explored as another means of achieving stable droplet generation conditions.

Ideally, droplet frequency should not affect formation stability. The frequency does affect droplet speed to a small extent. Depending on the phase of actuated and reflected pressure waves in the nozzle channel, greater or less energy can be imparted to the fluid based on the amplification or

interference of these pulses, respectively. Observations suggest that droplet instabilities caused by frequency characteristics tend to occur in higher ranges (above 400 Hz), though further study is needed. Droplet stabilities at certain frequencies can be compensated for by either a small change in frequency or a reduction in voltage. The rate of frequency change is also a factor in maintaining droplet stability. Slow frequency modulation is recommended, although the exact effect is not clearly understood. Generally, the primary concern for a droplet formation setting is ensuring the frequency chosen for vector DOD printing does not exhibit the instability effects previously observed.

The other major effects on droplet stability involve reservoir level, disturbances and vibrations, orifice cleaning, duration of operation, and micro switch start-stop timing. To maintain the expected negative pressure within the Siemens piezo tube, the reservoir level must be kept below the level of the orifice plate. If level is too low, then the high negative pressure can also interfere with droplet stability. Ideally, the relative height difference should remain constant for consistent droplet generation. Disturbances and random vibrations to the reservoir and supply line can also affect droplet stability. Orifice plate cleaning can affect droplet formation by leaving residual solvent that must evaporate from the surface. Printhead operation time also appears to contribute to stability issues, though the exact cause is unknown. Possible time-dependent factors include changes in reservoir level, internal printhead disturbances, and orifice plate corrosion. The DOD micro switch start-stop control function also affects droplet stability by introducing sudden interruptions to an otherwise complex equilibrium condition that depends upon many variables. The amount of time necessary to resume steady state operation depends partly upon the duration prior to resumption of printing and varies from seconds up to a minute, but this stability transition is not currently predictable or guaranteed. It is observed that intervals of less than ten seconds between printhead restarts provide greater reliability.

By adjusting each of the above parameters, a stable droplet printing condition can be achieved. Because of the complex interactions of these variables and the remaining questions to be answered, it is difficult at this time to define an effective droplet formation strategy. Given a particular binder composition, adjusting the remaining variables may yield many possible stable droplet formation conditions. In terms of waveform timing, it appears that a longer holding period at a level voltage relative to the ramping stages yields better results. The ramping up and down of the voltage should also be relatively quick, although the ramping up phase appears to have little effect on droplet velocity. Beyond these generalizations, many possible timings exist. If a particular waveform cycle is unstable at one particular voltage or frequency, changing either or both of these parameters within the performance parameters of the printhead may stabilize the droplet stream. The volume and speed of the droplet under a given set of formation conditions will most likely vary when using another possible stable waveform timing, voltage, and frequency setting. Given the many possibilities for generating a stable droplet, these additional criteria can further serve as limiting conditions for determining an appropriate

waveform geometry and frequency. The exact relationship between these resulting droplet characteristics and the mechanical actuation process, however, is currently unknown and is one possible area for further study.

The fluid properties of viscosity and surface tension are important contributing factors that may also deserve further attention. For the majority of this study, the effort is focused on optimizing printhead operational parameters with no adjustments to binder chemistry. In one sense, it would be ideal to establish stable DOD printhead parameters for any desired fluid composition. By determining fluid properties that facilitate stable droplet generation, however, the variability of other parameters may be reduced and lead to faster development of desired operating conditions. The dependencies between fluid properties, the particular DOD printhead, and the piezo-actuation variables, however, are likely to complicate such an investigation.
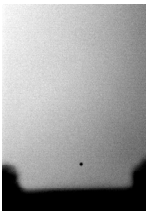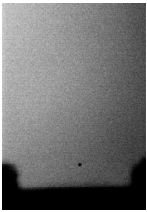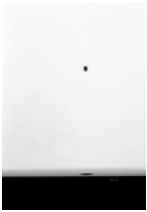
Note that Table 2-D: *Droplet Formation Parameters & Results* is separated over the following three pages for reference.

Table 2-D:
DROPLET FORMATION PARAMETERS & RESULTS

	Water-based 2.4 v/o Polyacrylic Acid Binder [2.4 v/o PAA + 0.26 v/o Glycerol + 97.3 v/o Water]		Colloidal Silica Binder [Binder "B" Formulation]	
	Viscosity	Surface Tension	Viscosity	Surface Tension
Relative to Water-based 2.4 v/o PAA*	n/a	n/a	Slightly Higher (0.7 cP more)	Significantly Lower (28.7 dynes/cm less)
Relative to Colloidal Silica*	Slightly Lower (0.7 cP less)	Significantly Higher (28.7 dynes/cm more)	n/a	n/a

* Refer to Table 2-C for Fluid Property Values

Waveform Geometry Notation

$a : b : c : h$

Voltage (V) — Time (μs), with segments a, b, c and height h

Waveform Timing (microseconds)

Water-based 2.4 v/o Polyacrylic Acid Binder results:

a — Long: 4 µs — **4 µs** : 8 µs : 1 µs : 97 V, 300 Hz • 500 LED Delay, Nozzle 3 — Short: 1 µs — **1 µs** : 8 µs : 1 µs : 97 V, 300 Hz • 500 LED Delay, Nozzle 3 — No Data for Valid Comparison

b — Long: 8 µs — 4 µs : **8 µs** : 1 µs : 97 V, 150 Hz • 500 LED Delay, Nozzle 3 — Short: 1 µs — 4 µs : **1 µs** : 1 µs : 97 V, 150 Hz • 500 LED Delay, Nozzle 3 — No Data for Valid Comparison

c — Long: 8 µs — 4 µs : 1 µs : **8 µs** : 160 V, 600 Hz • 600 LED Delay, Nozzle Hiro — Short: 1 µs — 4 µs : 1 µs : **1 µs** : 160 V, 600 Hz • 600 LED Delay, Nozzle Hiro — No Data for Valid Comparison (Hiro Printhead ONLY)

Colloidal Silica Binder results:

a — Long: 8 µs — **8 µs** : 8 µs : 1 µs : 150 V, 500 Hz • 700 LED Delay, Nozzle 4 — Short: 1 µs — **1 µs** : 8 µs : 1 µs : 150 V, 500 Hz • 700 LED Delay, Nozzle 4

b — Long: 8 µs — 2 µs : **8 µs** : 1 µs : 150 V, 500 Hz • 300 LED Delay, Nozzle 4 — Short: 1 µs — 2 µs : **4 µs** : 1 µs : 150 V, 500 Hz • 300 LED Delay, Nozzle 4

c — Long: 8 µs — 8 µs : 1 µs : **8 µs** : 145 V, 500 Hz • 1000 LED Delay, Nozzle 4 — Short: 1 µs — 8 µs : 1 µs : **1 µs** : 145 V, 500 Hz • 1000 LED Delay, Nozzle 4 — No Data for Valid Comparison
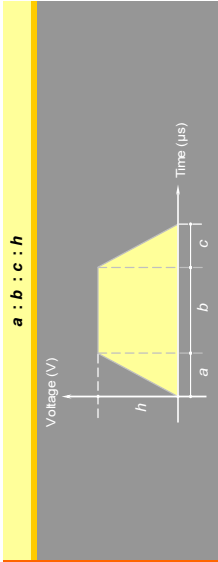
Table 2-D (Cont.):
DROPLET FORMATION PARAMETERS & RESULTS

Waveform Voltage (Volts)

Low
4 µs : 8 µs : 1 µs : **92 V**
500 Hz • 500 LED Delay
Nozzle 4

Transition
4 µs : 8 µs : 1 µs : **104 V**
500 Hz • 1000 LED Delay
Nozzle 4

High
4 µs : 8 µs : 1 µs : **150 V**
500 Hz • 500 LED Delay
Nozzle 4

Low
4 µs : 8 µs : 1 µs : **78 V**
500 Hz • 500 LED Delay
Nozzle 4

Transition
4 µs : 8 µs : 1 µs : **97 V**
500 Hz • 500 LED Delay
Nozzle 4

High
4 µs : 8 µs : 1 µs : **102 V**
500 Hz • 500 LED Delay
Nozzle 4

Siemens Orifice Corrosion

Severe Corrosion
11 Hours of Use

Moderate Corrosion
6 Hours of Use

Initial Droplet State
4 µs : 8 µs : 1 µs : 97 V
500 Hz • 500 LED Delay
Nozzle 5

Frequency Response (Hz)

Reduce Voltage
2 µs : 8 µs : 1 µs : **119 V**
500 Hz • 500 LED Delay
Nozzle 4

Adjust Frequency
4 µs : 8 µs : 1 µs : 118 V
700 Hz • 1000 LED Delay
Nozzle 2

Satellite Droplets
4 µs : 8 µs : 1 µs : 118 V
1500 Hz • 1000 LED Delay
Nozzle 2

2 µs : 8 µs : 1 µs : **150 V**
500 Hz • 500 LED Delay
Nozzle 4

Reduce Voltage
2 µs : 6 µs : 1 µs : **140 V**
400 Hz • 800 LED Delay
Nozzle 4

Adjust Frequency
4 µs : 8 µs : 1 µs : 97 V
1686 Hz • 1500 LED Delay
Nozzle 4

Satellite Droplets
4 µs : 8 µs : 1 µs : 97 V
1678 Hz • 1500 LED Delay
Nozzle 4

2 µs : 6 µs : 1 µs : **170 V**
400 Hz • 800 LED Delay
Nozzle 4

Table 2-D (Cont.):
DROPLET FORMATION PARAMETERS & RESULTS

Water-based 2.4 v/o Polyacrylic Acid Binder
[2.4 v/o PAA + 0.26 v/o Glycerol + 97.3 v/o Water]

	Viscosity	Surface Tension
Relative to Water-based 2.4 v/o PAA*	n/a	n/a
Relative to Colloidal Silica*	Slightly Lower (0.7 cP less)	Significantly Higher (28.7 dynes/cm more)

Colloidal Silica Binder
[Binder "B" Formulation]

	Viscosity	Surface Tension
Relative to Water-based 2.4 v/o PAA*	Slightly Higher (0.7 cP more)	Significantly Lower (28.7 dynes/cm less)
Relative to Colloidal Silica*	n/a	n/a

* Refer to Table 2-C for Fluid Property Values

Waveform Geometry Notation

Voltage (V)
Time (µs)
a : b : c : h

CURRENT OPTIMAL CONDITIONS

	High	Low	Startup Condition
Waveform Timing	4 µs : 8 µs : 1 µs		
Frequency Range	650 Hz @ 97 Volts, 1500 LED Delay, Nozzle 4	75 Hz @ 97 Volts, 500 LED Delay, Nozzle 3	500 Hz @ 150 Volts, 500 LED Delay, Nozzle 4
Maximum Stable Voltage	Typically 97 Volts		

	High	Low	Startup Frequency
Waveform Timing	4 µs : 8 µs : 1 µs		
Frequency Range	1000 Hz @ 104 Volts, 200 LED Delay, Nozzle 4	15 Hz @ 104 Volts, 5000 LED Delay, Nozzle 4	500 Hz @ 150 Volts, 500 LED Delay, Nozzle 4
Maximum Stable Voltage	Typically 100 to 104 Volts		

Note that the pictures shown in Table 2-D depict the printhead orifice plate surface on the left with the droplet traveling to the right. In reality, the printhead is oriented on top with the droplets moving downward. In addition, the brightness and contrast of each picture are adjusted for clarity. Though the table above provides a characterization of droplet formation behavior as influenced by particular variables, the other factors not depicted above but discussed in the preceding sections also contribute significantly to droplet stability.

Based on the results of extensive experimentation with both the water-based 2.4 v/o PAA and colloidal silica systems, an "optimal" set of stable droplet formation parameters for each binder is defined. These droplet generation conditions are not guaranteed to be completely reliable for either system, as evidenced by the occasional instabilities observed during testing, but for the most part, many experiments are successfully conducted using these settings. In comparing the results of these experiments, the choices made for these two systems are the most effective and most scrutinized. The determination of efficacy for droplet generation is defined as a repeatable set of conditions that permit continual DOD printhead output without complete failure through the course of each test and that maintain droplet uniformity as verified by visual inspection beforehand and afterwards. Some speed variation and occasional instability are expected. The parameter values listed at the bottom of Table 2-D for droplet formation meet these criteria. Coincidentally, the most functional waveform timing developed for both the water-based 2.4 v/o PAA binder and colloidal silica are identical. In addition, the droplet diameter (D_x) based on mass deposited over time are also similar, with D_{PAA} = 44.0 μm and D_{CS} = 44.6 μm. The calculation of droplet radius ($0.5 \cdot D_{CS}$) for colloidal silica is performed as follows:

VARIABLES

$$X_{CS\,Solid} = \text{Mass fraction of colloidal silica solids} = 0.30$$
$$\rho_{CSSn} = \text{Density of colloidal silica solution} = 1.21\,\text{g/mL}$$
$$m_{CSDried} = \text{Mass of dried colloidal silica}$$
$$m_{CSSn} = \text{Mass of colloidal silica solution}$$
$$V_{CSSn} = \text{Volume of colloidal silica solution}$$
$$Q_{CSSn} = \text{Flow rate of colloidal silica solution}$$
$$t = \text{Amount of time to collect } m_{CS\,Sn}$$
$$F = \text{Droplet Frequency}$$
$$V_{CS\,Drop} = \text{Volume of colloidal silica drop}$$
$$r_{CS\,Drop} = \text{Radius of colloidal silica drop}$$

Starting with $m_{CS\,Dried}$ measured from the dried collected solution,

$$m_{CS\,Dried} = 0.771\,g$$

$$m_{CSSn} = \frac{m_{CS\,Dried}}{X_{CS\,Solid}}$$

$$= \frac{0.771\,g}{0.30} = 2.604\,g$$

$$V_{CSSn} = \frac{m_{CSSn}}{\rho_{CSSn}}$$

$$= \frac{2.604\,g}{1.21\,g/mL} = 2.15\,mL$$

Since it took $t = 25.58$ hours to collect m_{CSSn} at frequency, $F = 500\,Hz$,

$$Q_{CSSn} = \frac{V_{CSSn}}{t}$$

$$= \frac{2.15\,mL}{25.58\,hr} = 0.0841\,\frac{mL}{hr} = 2.34\times10^{-5}\,\frac{mL}{s}$$

$$V_{CS\,Drop} = \frac{Q_{CSSn}}{F}$$

$$= \frac{2.34\times10^{-5}\,\frac{mL}{s}}{500\,Hz} = \frac{2.34\times10^{-5}\,\frac{mL}{s}}{500\,\frac{Drops}{s}} = 4.67\times10^{-8}\,\frac{mL}{drop}$$

$$= \frac{4}{3}\pi\left(r_{CS\,Drop}\right)^3$$

Therefore,

$$r_{CS\,Drop} = 2.23\times10^{-3}\,cm = 22.3\,\mu m$$

The droplet radius calculations for the water-based 2.4 v/o PAA binder are performed similarly. These printing parameters are also observed to be nozzle independent as seen with the PAA binder system. Based on DOS tests, four different nozzles (numbers 3, 4, 5, and 6) produce the same initially stable behavior—before corrosion affects the orifice diameter—when these settings are applied.

Two main differences exist in the stable droplet conditions of these two binder systems: droplet speed and corrosion concerns. Using the estimation based on the change in droplet position over a known time delay (as seen on the DOS), for colloidal silica, the droplet speed is calculated to be 1.5 m/s, while for water-based 2.4 v/o PAA binder, droplet speed is calculated to be much faster at 3.6 m/s. In terms of corrosion, the Siemens orifice plate composition is particularly sensitive to the effects of the PAA binder chemistry and requires vigilant inspection, while the reactive nature of colloidal silica is not as evident, based on current knowledge, though further evaluation may be needed.

Note that the high and low frequency capabilities stated for these optimal waveforms are observed to produce stable droplets for only a short duration (on the order of minutes) and therefore require extended periods of testing to ensure reliable long-term operation. Due to the complex, and

sometimes seemingly fickle, nature of drop-on-demand printhead droplet formation for various fluid systems, additional research into this process and its associated elements is recommended and will likely yield greater optimizations or a different, more effective set of printing conditions. Nevertheless, the currently functional DOD printing conditions outlined above are utilized in the following vector printing experiments of water-based 2.4 v/o PAA binder into alumina powderbeds and produce a valuable data set for analysis.

The primary objective of this investigation is to determine a set of stable printing conditions that allow for binder-based vector DOD printing. In addition, a greater understanding of process variables for DOD droplet generation is obtained, although many issues exist for further exploration. Ultimately, with advances in the slurry-binder interactions of the WC-Co, this 3DP production process can be adapted to WC-Co tooling inserts. The general consensus states that an optimal waveform will produce a droplet 0.25 times the orifice diameter. Based on the research reported above, this goal is still far from being realized. Nevertheless, further progress into 3DP vector drop-on-demand development is pursued in the next section.

2.4. VECTOR PRINTING TEST GEOMETRIES & PRIMITIVES ONTO ALUMINA POWDERBEDS

The next step in the vector DOD development process for Three Dimensional Printing involves combining the previous equipment implementations discussed in Section 2.2 with the stable DOD printing conditions for the Siemens PT-88S specified in Section 2.3.8. Using this largely functional configuration, with the exclusion of the DOD control, two sets of experiments are conducted by DOD printing the 2.4 v/o PAA + 0.26 v/o glycerol + 97.3 v/o water binder solution into slurry-jetted alumina powderbeds. An initial series of tests are performed using slipcast alumina powderbeds, primarily for analysis of DOD printing line quality, but apparent powderbed composition issues prevent successful extraction of binder-printed regions, thereby making meaningful analysis of results difficult. In order to compose a representative powderbed substrate for binder printing, a standard 30 v/o alumina slurry is jetted on the Hood Machine, an established slurry 3DP production device, to produce two rastered powderbeds (discussed in Section 2.4.1). The jetted samples are distributed on rectangular borous silicate pieces and separated for individual vector DOD printing tests. The first set of experiments, presented in Section 2.4.3, use these as-jetted alumina powderbeds to produce two series of lines at different droplet spacings, a square with linear raster fill, and a tooling insert geometry with no center hole and 130° raster fill. Several problems experienced through the course of completing and analyzing these binder-printed samples prompt another set of experiments to be done. Issues with failed single line extractions and an incomplete tooling insert geometry are analyzed. The major conclusion of the first set of experiments is that the slurry powderbed topography contributes significantly to final part quality—too much, in fact, to

clearly assess the product of vector DOD printing. One of the major alterations to the vector DOD process, then, is to begin with sanded alumina powderbed top surfaces to create an ideal, smooth profile for binder printing. In addition, a grid with support structure is designed to preserve individual lines for subsequent line width analysis. The results from these experiments provide more effective insights into vector DOD printed edge quality and surface finish. In addition, measurements of individual line widths indicate potential line resolution improvement versus standard slurry-based parts with conventional 3DP. The second set of experiments are discussed and analyzed in Section 2.4.4. Finally, a comparison of these two sets of experiments is performed.

The initial set of DOD printing tests using slipcast alumina powderbed substrates is not particularly effective. The experiments are also conducted on the Droplet Observation Station to simplify vector functionality since only the evaluation of single lines is desired. Though not an ideal model of a slurry-printed surface, slipcast beds are relatively simple and quick to produce and, if nominally effective, would prove much more efficient to use than constructing properly jetted powderbed surfaces. Refer to [8] for detailed information about both the slipcasting and the standard slurry-jetting process. Although the absorption and composition characteristics of slipcast powderbeds differ from conventional jetted powderbeds [31], an attempt to use this type of powderbed is made based on past success with binder droplet testing.

The experiment seeks to observe line quality with four different droplet spacings: 5 μm/drop, 10 μm/drop, 15 μm/drop, and 20 μm/drop. The droplet spacings are determined by altering the droplet frequency while keeping the vector speed constant. The water-based 2.4 v/o PAA binder is used with the Siemens printhead and the optimal droplet formation settings described in Section 2.3.8. In order to provide a smooth horizontal layer height for printing, the top surface of each slipcast sample is sanded. The tests are performed successfully without droplet instability. After the samples are cured for one hour at 150 °C in Argon (refer to [29] for details about the curing process), the following attempts at extraction fail. The binder lines are visible on the treated powderbed surface, but the redispersion process is unsuccessful. Potential problems may have resulted from the slurry slipcasting process. Besides having a higher packing density, slipcast alumina powderbeds possess a lower concentration of Polyethylene Glycol, the chemical used for redispersion, than jetted powderbeds because the dissolved redispersant is more effectively removed from the slurry when poured onto a porous plaster substrate [31]. In addition, a discoloration in certain regions of several slipcast samples may indicate that contamination or decomposition of the slurry occurred. Unfortunately, no significant data is obtained from these slipcast powderbed experiments. These results do indicate, however, that a properly processed, slurry-jetted powderbed would be much more effective for binder-based vector DOD printing experiments. Thus, a set of two powderbeds is produced using a standard 30 v/o alumina slurry and the Hood Machine.

Afterwards, the vector DOD printing setup, illustrated in Figure 2.1 and described in detail within Section 2.2, is used for further experimentation. Two alterations are made from the original complement of assembled equipment. One significant modification involves the substitution of the default Siemens PT-88S orifice plate with a gold-plated version in an attempt to prevent, or at least retard, corrosion from exposure to the PAA binder. Fortunately, through the course of experimentation, no difference in droplet formation performance is observed. The other adjustment is the removal of the Honeywell 1SM2 Micro Switch DOD control. As discussed in Section 2.3.6, the complications and instabilities from stopping and starting the printhead outweigh the benefits of retaining drop-on-demand control; thus, preservation of stable droplet generation is simplified.

Only single layers of vector-printed binder are produced for this initial study. Though multiple layers for significant three-dimensional part production are the eventual goal, a single layer provides fundamental insight into the binder-powder interaction on an isolated level and also provides base measurements of layer thickness, line widths, and feature size for comparison with future experiments. With the advent of technology being developed by TDK, the possibility for multi-layer, DOD, vector-printed parts is presented in the final chapter, Conclusions & Future Work.

2.4.1. *Alumina Slurry Processing and Powderbed Jetting*

Due to the problems with slipcast alumina powderbeds outlined in the previous section, two representative 3DP slurry-based powderbeds are produced using the conventional, raster slurry-jetting technique on the Hood Machine. Located in the Ceramics Processing Research Laboratory (CPRL), the Hood Machine is an essential tool for slurry powderbed production. Depicted in simplified form within Figure 2.13, the Hood Machine uses a rastering technique with a fast and slow axis to build a powderbed in sequential layers. Each layer is formed as a merged assembly of individual slipcast lines. The slurry is jetted from a 127 micron nozzle onto a porous substrate with flow rate controlled by air pressure. A two-pump recirculation system is used to keep the slurry suspension uniform in composition and to prevent settling or agglomeration of powder particles over time. A computer controls the rastering motion mechanism, the powderbed layer dimensions, and z-axis control. After each slurry layer is jetted, a drying cycle removes excess liquid from the powderbed to prevent defects from forming. The description provided above is general in scope; a detailed explanation of the slurry-jetting process for powderbed formation using the Hood Machine can be found in [29].

In order to manufacture the powderbed on the Hood Machine, a standard 30 v/o alumina slurry is prepared. The slurry is composed of submicron alumina powder along with Polyethylene Glycol (PEG), Nitric Acid, Methanol, and water. Four additions are used to introduce the alumina powder into the slurry mixture with subsequent ball milling between additions. After 18 hours of total milling time, the slurry is filtered and then jetted on the Hood Machine. For more details about the slurry chemistry

and the associated preparation process, consult the work of Jason Grau and Scott Uhland in [8] and [29], respectively.
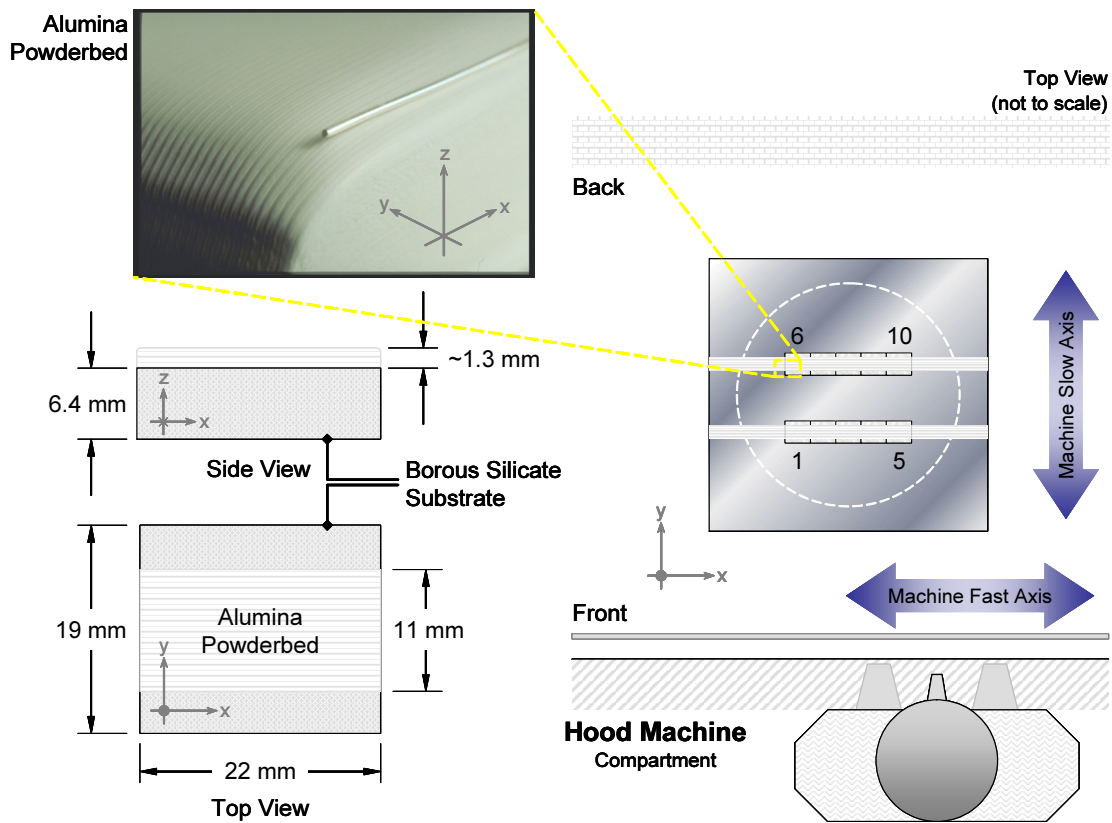
Figure 2.13   Illustrations and process information related to the two slurry-jetted alumina powderbeds constructed for the proceeding vector printing experiments. The inset picture, though taken from a different alumina powderbed, accurately characterizes the powderbeds' appearance and texture. A standard 30 v/o alumina slurry is jetted onto two sets of five rectangular borous silicate (BS) substrates. The diagram includes dimensions for an individual BS piece and for the corresponding jetted powderbed on each substrate. A unique number is assigned for each BS piece for future identification in the experiments (refer to the following sections). A set of axes for each item above indicates the powderbed orientation relative to the Hood Machine designated axes (labeled "Machine Fast Axis" and "Machine Slow Axis") for slurry jetting. In addition, the same axes correspond to the powderbed orientation for vector DOD printing. Note that the origins shown are not accurately identified. Due to the relatively symmetrical designs to be evaluated, the smallest x-y powderbed dimension (11 mm) acts as a limiting size factor for vector DOD printed geometries.

As shown in Figure 2.13, the two linear powderbeds are jetted onto ten individual, rectangular borous silicate substrates. Each piece has approximately 19 mm x 22 mm in area for powderbed definition; five pieces are aligned together to form one powderbed substrate for slurry jetting. This powderbed will be disassembled into its composite pieces so multiple vector DOD binder printing tests can be conducted. The borous silicate substrates are therefore numbered for future identification. The

two powderbeds are comprised of 46 layers with a layer height of approximately 56 microns, defined by a mass flow rate of 4.2 to 4.3 g/min. The powderbed deposition process is completed without incident. The texture of the powderbed surface is relatively smooth and uniform, although the artifacts from a linear, raster process are clearly present as illustrated in Figure 2.13. These surface features from the slurry jetting process will play a role in determining the final part quality in the first set of experiments described in Section 2.4.3.

The smallest horizontal powderbed dimension (i.e. neglecting vertical height) of 11 mm places a limitation on the size of the vector DOD print geometry. Since all of the MasterCAM designs are fairly symmetrical, caution is required to ensure the entire binder deposition process remains on the alumina powderbed surface by limiting geometry measures to less than 11 mm. This maximum dimension requires several of the geometries to be scaled down in order to fit, and this reduction affects the size of the sample and its corresponding programmed line spacings.

2.4.2. *Binder Droplet Formation Parameters*

The Siemens PT-88S printhead is used for drop-on-demand printing of 2.4 v/o PAA + 0.26 v/o glycerol + 97.3 v/o water binder. The functional waveform parameters chosen for binder droplet formation are 4 µs: 8 µs: 1 µs: 97 V (refer to Section 2.3.8 for discussion about this selection). Using these conditions, the droplet speed is determined to be 3.6 m/s, and the average droplet diameter in the air is estimated to be 44 microns. The droplet size is determined and verified using two different methods: (1) by measuring the mass of dried binder deposited over time and then calculating backwards based on density and frequency (refer to Section 2.3.8 for details) and (2) by visual inspection of droplets on the monitor during tests with the Droplet Observation Station. The second method provides a quick, though slightly less accurate, droplet diameter calculation due to the granularity of the scale used. For further discussion about the measurement and development of these parameters, refer to Section 2.3.

2.4.3. *Vector Printing Using Unsanded Alumina Powderbeds*

Following the difficulties of DOD printing onto slipcast powderbeds using the Nozzle Test Station, a more effective, but complex, examination of vector drop-on-demand printing for 3DP with the water-based 2.4 v/o PAA binder starts with a set of experiments that implement the Bridgeport milling machine vector printing configuration, Siemens PT-88S DOD printhead, and slurry-jetted alumina powderbeds. The Siemens printhead is actuated using the stable droplet generation parameters provided in Section 2.4.2, and the alumina powderbeds are the products of the standard powderbed deposition process described in Section 2.4.1. Using a slightly modified vector DOD setup as detailed in Section 2.4, four different tests are used to characterize the now adapted 3DP binder-based process: (1) five lines with different droplet spacings determined by vectoring speed, (2) five lines with different droplet spacings

determined by frequency, (3) a square block with linear raster fill, and (4) a tooling insert geometry based on a Valenite CNMA 432 Insert. The powderbeds do not require much preparation, other than referencing and orientation confirmation. Five powderbeds on separate borous silicate substrates are used for these experiments with one sacrificed as a calibration piece. Previously used for ink-based vector DOD printing with the HP 51626A printhead, two geometries designed on MasterCAM, the square and the tooling insert, are adapted to the 2.4 v/o PAA binder droplet parameters and converted to appropriate CNC programs for execution on the milling machine (refer to Figure 2.14 for illustrations). The other two five-line droplet spacing experiments are input manually with the native Bridgeport GUI. The first three vector DOD experiments are completed successfully, but the tooling insert geometry fails unexpectedly during raster definition. The first two line droplet spacing tests exhibit strange redispersion behavior during the extraction process, while the latter two geometries redisperse effectively. The failure to extract line width measurements from the two five-line droplet spacing experiments necessitates further experimentation and formulation of a more effective design for line preservation. Observations of the extracted vector DOD printed geometries suggest that the powderbed linear raster deposition process creates a dominant geometric anisotropy that affects the surface finish and edge quality of the printed part. The irregular, undulating profile created by slipcasting individual, consecutive slurry lines poses significant problems for consistent binder placement and thus considerably reduces geometric accuracy. The results and conclusions from these experiments create impetus for the next round of testing described in Section 2.4.4.

2.4.3.1. Alumina Powderbed Preparation

Before experimentation can begin, several steps must be taken to allow for correct printhead positioning and, after testing, correct piece identification. To prepare the alumina powderbed samples for experimentation, the five samples from the first powderbed are taken, and a record of each numbered piece used is made. The borous silicate substrates are numbered from one to five. The alumina sample is checked for correct orientation relative to the machine axes prior to printing (refer to Figure 2.13 for identification of corresponding powderbed axes). Neglecting height, the smallest dimension of 11 mm, corresponding to the width perpendicular to the slurry-jetted powderbed x-axis, is oriented parallel to the machine default y-axis. One of the five alumina samples, identified as Piece 4, is designated as the "calibration" powderbed, which is used only for defining the correct z-axis positioning of the Siemens printhead. This calibration sample is not used for experimentation because the z-axis level is checked between each vector DOD test, and since the printhead remains continuously operational without a DOD micro switch control, the powderbed is therefore subjected to numerous random binder droplets that would invalidate any potential results.

2.4.3.2. Vector Drop-On-Demand Printing Parameters and Observations

As previously explained, four experiments are conducted to examine various vector DOD printing parameters: (1) individual line characteristics as a function of vectoring speed, (2) individual line characteristics as a function of droplet frequency, (3) edge quality and surface finish of a vector outline trace, linear raster fill square block, and (4) edge quality and surface finish of a vector outline trace, 130° raster fill tooling insert with omitted center hole. The first two droplet spacing tests to evaluate individual line quality are programmed directly into the Bridgeport EZ-Trak milling machine. The latter two geometries are designed and exported as machine programs using MasterCAM. The corresponding powderbed samples follow the same numbering designation as listed above, except for Piece 5, which is used for the tooling insert geometry since z-axis calibration is performed with Piece 4 (discussed in the previous section). Piece 1, or also Test (1), examines the effect of droplet spacing on line width by varying the milling machine speed. The same droplet spacing parameter is tested with Piece 2, except that frequency is varied instead. For both tests, five droplet spacings are selected: 10 μm/drop, 20 μm/drop, 30 μm/drop, 40 μm/drop, and 45 μm/drop. Each spacing specification is performed on a separate parallel line across the entire length of the powderbed. Formerly used for ink-based testing, the square block for Test (3) is re-programmed in MasterCAM for the water-based PAA binder system and compiled with tool paths that define four consecutive vector traces shifting from the exterior to interior and a horizontal linear raster fill (refer to Figure 2.14 (a) for an illustration and parameters). The tooling insert is also adapted from ink-based experimentation and implements an identical four vector trace (refer to Figure 2.14 (b) for an illustration and parameters). The interior raster fill is likewise linear but oriented at 130° from horizontal. The reason for selecting this raster method is to ensure the most evenly distributed binder concentration gradient along the geometry edge as seen during ink-based vector DOD testing (refer to Section 2.2.6 and Figure 2.11).

Common line spacing parameters are used for both the square and tooling insert. Based on the droplet size of the PAA binder in air, the tool diameter in MasterCAM is defined to be 44 microns. A 50% overlap is present between all parallel adjacent lines and is equivalent to a 22-micron line spacing. Although the droplet diameter does not represent the binder behavior upon powderbed impact and absorption, which would be a more accurate line spacing assessment, this nominal droplet diameter designation and degree of overlap guarantees stitching between two adjacent printed lines. Used with ink-based testing as well, the four vector profile traces defined in both the square and tooling insert machine programs are designed to impart the desired vector characteristic to the geometry boundary and to diminish, if not eliminate, the effects of the interior raster fill.

To achieve reasonable geometric accuracy at an acceptable production rate, the milling machine speed is maximized for both Tests (3) and (4) at 600 mm/min or 10 mm/s (refer to Section 2.2.1.2 for an explanation). Given this speed, the spacing between consecutive droplets is controlled by the frequency,

and this value is adjusted to establish a fairly uniform droplet spacing in all directions. Note that for proper implementation, the CNC programs generated by MasterCAM require that additional stop commands be injected at the beginning and end of the program to allow for vector printing equipment adjustments, such as z-axis height verification to prevent damage from incorrect calibration.

	Tooling:	44 μm Diameter Droplets
	Z-axis:	Origin – top of powderbed +0.5 mm – printhead
Feed Rate:		600 mm/min
Raster Fill:		Horizontal Linear Line
Spacing:		22 μm

(a)

	Tooling:	44 μm Diameter Droplets
	Z-axis:	Origin – top of powderbed +0.5 mm – printhead
Feed Rate:		600 mm/min
Raster Fill:		∡130° Linear Line
Spacing:		22 μm

(b)
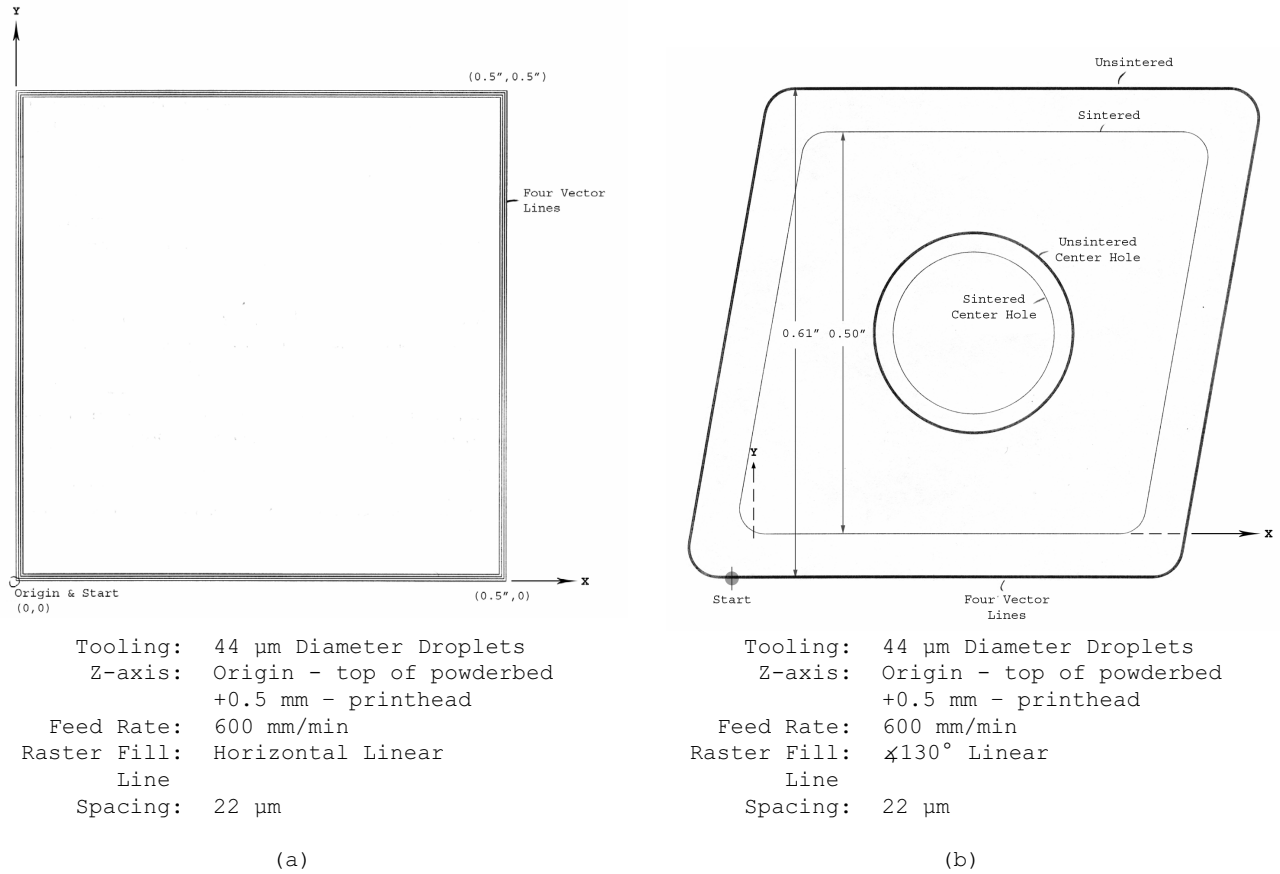
Figure 2.14   Annotated illustrations of (a) the square and (b) the tooling insert shapes rendered in MasterCAM. The tooling insert outline contains both sintered and unsintered dimensions for comparison. Based on calculations presented in Section 2.2.4, the unsintered dimensions are 22% larger than sintered. Each geometry outline is defined by four consecutive vector traces 22 μm apart that transition from their respective exterior boundaries to the interior. These geometric boundaries define a single layer to be vector printed, and parsing input for tooling properties (droplet size), z-axis depth, feed rates, and raster-fill style (spiral or linear), MasterCAM automatically generates a CNC machine program in plain text. The execution order for both (a) and (b) are identical: four vector traces along the exterior perimeter followed by linear interior raster fills. Minor editing of this program is then performed to permit necessary equipment adjustments particular to the Bridgeport milling machine setup. Note that the center hole of the tooling insert is not included in the machine program used. These programs are transferred via 3.5" floppy disk to the Bridgeport milling machine computer for execution.

The origin of the programmed geometry is determined by using a sacrificial "calibration" powderbed, Piece 4, for these tests. The z-axis origin is defined as the top of the powderbed surface, and
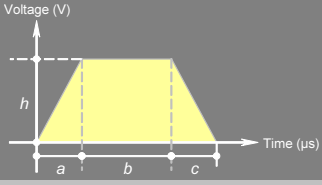
the vertical spacing between the printhead and powderbed is expected to be 500 microns. This orientation is determined manually by slowly lowering the milling machine quill until the printhead contacts the powderbed sample. Note that the separation distance between the orifice plate and powderbed is actually greater than expected because the z-axis origin is located at the interface between the lowest point on the Siemens printhead—the orifice plate holder, not the orifice plate—and the powderbed. Considering the variability of each calibration, the presence of the orifice plate holder only adds to the actual z-axis distance, and this total quantity, which is not clearly quantified, is reflected in the separation distance shown in Table 2-E. The x- and y-axis zero points are also set using this piece. As stated in the previous section, due to serving this function and the associated exposure to random binder droplets, Piece 4 cannot be used for experimentation.

Nozzle 5 on the Siemens PT-88S is chosen for binder droplet production. The printhead remains active during the entire experimental set (Pieces 1, 2, 3, and 5) to minimize potential instabilities caused by evaporated binder on the orifice plate, internal pressure fluctuations, inconsistent re-activation, etc. Based on observations of DOD behavior during tests with the Droplet Observation Station, it is believed that a steady equilibrium droplet state, once established, is easier to maintain with a continuously operational printhead. This constant condition therefore contaminates the "calibration" powderbed. To minimize differences in powderbed placement after calibration, a consistent positioning of the borous silicate substrates is ensured by locating pieces along two perpendicular edges, the edge of the support block and a secured metal strip.

Some changes are necessary for the effective execution of these experiments. Due to powderbed size limitations (discussed in Section 2.4.1), scaling modification to the square and tooling insert geometries is required. The square block, originally 0.5" per side, must be reduced by 10% to 0.45" per side to fit onto the alumina powderbed sample. The tooling insert must be scaled down by 20% to preserve the entire geometry. This reduction in overall size decreases the associated line spacing for each geometry by the same amount. Therefore, instead of 22 microns, the square has a line spacing of only 20 microns, while the tooling insert has a spacing of 18 microns. Another operating adjustment relates to droplet formation. The stable printhead voltage, while originally specified as 97 Volts, increases to 99 Volts at 500 Hz for these experiments. Many factors can influence the stability of droplet formation, as noted in Section 2.3, so some degree of variability is expected.

Table 2-E:
VECTOR PRINTING PARAMETERS FOR UNSANDED ALUMINA POWDERBEDS WITH PAA BINDER

	Alumina Powderbed Piece Reference Number†				
	1	2	3	4	5
Vector Geometry Description	Five Individual Lines with Different Droplet Spacings by Varying Vector Speed	Five Individual Lines with Different Droplet Spacings by Varying Frequency	Square Block 0.45" x 0.45"	Calibration Powderbed	*Incomplete* Tooling Insert CNMA 432
Binder Composition	2.4 v/o Polyacrylic Acid (PAA) + Glycerol + Water				
Droplet Diameter (microns)	44.0 microns				
Droplet Frequency (Hz)	500 Hz	Line 1: 1000 Hz Line 2: 500 Hz Line 3: 333 Hz Line 4: 250 Hz Line 5: 222 Hz	500 Hz	n/a	500 Hz
Vector Speed (mm/s)	Line 1: 5.0 mm/s Line 2: 10.0 mm/s Line 3: 15.0 mm/s Line 4: 20.0 mm/s Line 5: 22.5 mm/s	10 mm/s	10 mm/s	n/a	10 mm/s
Consecutive Droplet Spacing (µm/drop)	Line 1: 10 µm/drop Line 2: 20 µm/drop Line 3: 30 µm/drop Line 4: 40 µm/drop Line 5: 45 µm/drop	Line 1: 10 µm/drop Line 2: 20 µm/drop Line 3: 30 µm/drop Line 4: 40 µm/drop Line 5: 45 µm/drop	20 µm/drop	n/a	20 µm/drop
CNC Machine Program	0302001.PGM	n/a	0302003.PGM	n/a	0302005.PGM
Adjacent Line Spacing (µm/line)	n/a	n/a	20 µm/line	n/a	18 µm/line
Printhead-Powderbed Separation (microns)	750+ microns		500+ microns	Variable	500+ microns
Droplet Waveform Function (*a*:*b*:*c*:*h*)	4 µs : 8 µs : 1 µs : 99 V				

† Refer to Figure 2.13 for powderbed piece identification and printing orientation

Observations recorded throughout indicate that droplet generation remains fairly stable for the duration of testing. The first two droplet spacing experiments, Tests (1) and (2), detailed in Table 2-E above are completed successfully. A note from Test (1) indicates that droplets "vibrate" due to spindle motor rotation. Test (2) requires several changes in frequency. After all five lines are printed, some fluctuations in droplet speed are observed at 222 Hz, but increasing frequency restores stability. Creation of the 90% scaled square block is successful with droplet consistency verified afterwards. Some concern is expressed about the proximity of the back side to the powderbed edge. Approximately eight minutes elapse for completion of vector DOD printing on Piece 3. During the tooling insert geometry print with Piece 5, unforeseen problems arise during program execution, and the 130° linear raster is terminated

prematurely leaving only partial definition of the insert interior. An examination of the associated CNC code indicates that the final, expected commands for the raster fill are missing. In reviewing the program preparation process, it appears that an incomplete transfer of the machine code occurs when the data is saved from one version of the program file to another using the embedded Bridgeport User Interface. Based on the relatively large file size of the original, complete tooling insert program, it is conjectured that a buffer limitation exists within the Bridgeport software and therefore causes the truncation error. In addition, the assignment of incorrect timestamps for saved files may also have contributed to this unexpected alteration by affecting the installed software's behavior. Manual verification of the machine program within the Bridgeport UI could also have prevented the error prior to actual execution. Droplet stability is verified at the conclusion of Test (4).

After these samples are printed, the binder droplet diameter in air is calculated for verification using the mass of dried binder deposited in a set amount of time at a certain frequency. After four hours of DOD printing with the Siemens PT-88S at 500 Hz, the mass of dried PAA binder is 0.013 g. Calculations, as shown in Section 2.3.8, yield an average droplet diameter of 44.0 microns. The results validate the expected value used under these given conditions.

2.4.3.3. Extraction of Printed Layers

The removal of each vector-printed geometry from its powderbed substrate follows the established extraction procedure implemented for PAA + glycerol binder into alumina as described in [29]. The four test samples (Pieces 1-3 and 5) are cured at 150 °C for one hour in Grade 5 Argon gas using a VWR Scientific vacuum oven located in the CPRL. Temperature variations must be minimized to prevent PEG decomposition [29] that can affect redispersion, so a convection fan is used for circulation. Temperature levels as measured by a thermocouple (TC) indicate some fluctuations between 142 °C and 150 °C, but differences in temperature measurement may also be attributed to TC placement relative to the alumina substrates.

Subsequent redispersion is conducted by placing each borous silicate sample separately in a glass Petri dish and slowly introducing deionized water into the dish. The water is absorbed into the borous silicate through capillary action and eventually reaches the alumina powderbed on top. The water causes the PEG from the alumina slurry to expand and break apart the unbound powder. The remaining excess powder is removed by subsequent spraying of the sample with water from a wash bottle. For Piece 1 droplet spacing Test (1), odd behavior is observed with the top layer of the alumina powderbed staying as one solid piece while the remainder redisperses completely. No indications of binder-printed lines are evident. After discussions with Uhland, this unexpected layer delamination may have been caused by PEG decomposition that occurred because of a temperature gradient in the oven; in terms of sample orientation in the oven during curing, Piece 1 is the closest to the edge from the center where theoretically

it would be hotter, so this explanation is plausible. In contrast, Piece 3 with the square block is redispersed successfully (refer to Figure 2.16 for documentation pictures). The powderbed used for droplet spacing line tests on Piece 2 is successfully redispersed. The individual lines, however, are not recoverable because they are too weak to withstand the redispersion process. Only fragments of the 10 μm/drop line appear to survive, although the actual pieces are difficult to identify. The incomplete tooling insert geometry on Piece 5 redisperses effectively with a clear indication of where the raster fill stopped. The entire vector trace also remains intact, although the areas missing the raster fill are fragile. Documentation of this vector DOD printed part is shown in Figure 2.15. As discussed in the next section, the most dominant feature observed from the successfully redispersed geometries (Piece 3 and 5) is the effect of the powderbed texture on the surface finish.

2.4.3.4. Edge Quality & Surface Finish of Printed Layers

Since line quality measurements are unavailable due to the redispersion problems with Pieces 1 and 2, the effort to produce a line primitive for examination by vector DOD printing is continued in the following set of experiments discussed in Section 2.4.4. In order to strengthen the individual line structure for post processing, a support frame and grid are designed to print and preserve single lines for evaluation. The description and relevant details of this structure are provided in Section 2.4.4.2.

In terms of the edge quality and surface finish of the successfully extracted square and tooling insert, several observations can be made. The primary characteristic of these extracted layer geometries is the prevalent linear powderbed texture that results from the slurry-jetting process. For both samples, this linearity dominates the surface finish and edge quality definition, although in macroscopic terms, the geometric accuracy is acceptable. The fact that the complete vector trace of the tooling insert survives indicates that the programmed vector definition process works and provides a potential method for studying the quality of vector-versus-raster printing by setting an initial benchmark for geometry vector line thickness that is required for successful extraction in a single layer. The oscillating nature of these powderbed features is particularly evident when observing part definition perpendicular to the slurry lines as seen in pictures ❻ through ❽ of Figure 2.15 and ❷ and ❹ of Figure 2.16. The regularity of this undulating edge does show that binder droplet vector placement remains fairly consistent across z-axis height variation. In examining pictures ❷ and ❹ of Figure 2.16, the resulting intermittent separation between the vector trace and horizontal linear raster fill, which runs parallel to the slurry lines, also demonstrates the effect the powderbed surface profile has on binder droplet placement and/or absorption. The influence of vector DOD printing on edge quality can be more easily assessed when observing regions parallel to the alumina powderbed lines, especially in pictures ❶ and ❸ of Figure 2.16. The straightness appears to deviate to a small degree, and this irregularity may be attributable either to the powderbed texture or to vector DOD printing errors.
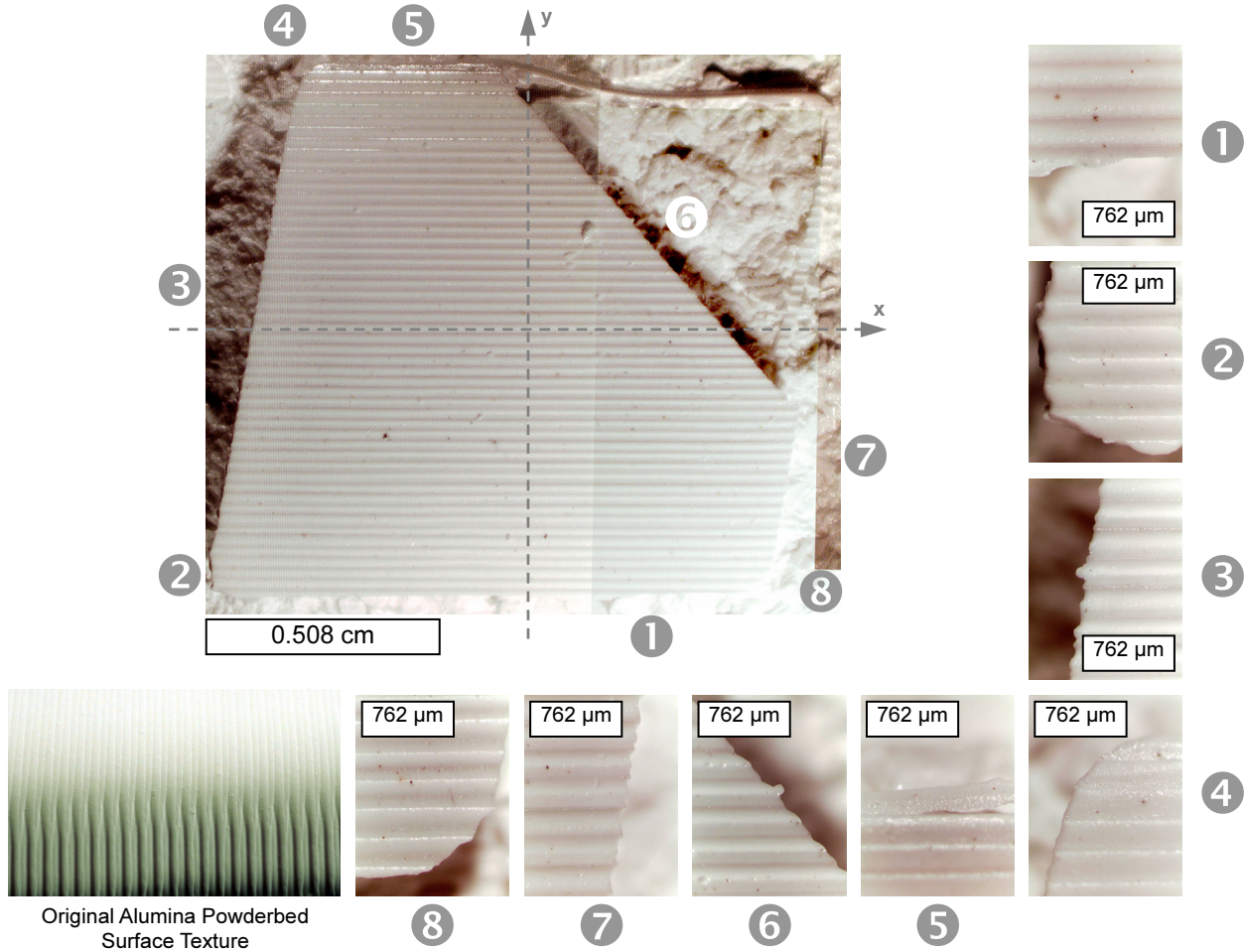
Figure 2.15 Pictures demonstrating edge quality and surface finish for a partially filled, vector-printed, PAA binder tooling insert into an *unsanded* alumina powderbed. Incomplete command transfers between CNC machine program versions (detailed in Section 2.4.3.2) prevent complete raster-fill execution. The superimposed axes indicate the printed part orientation relative to the programmed machine tool path (the y-axis points towards the milling machine, parallel to the default machine y-axis). Note that the origin is not accurately identified. The irregular edges, shown in the eight surrounding magnified pictures, occur in part because of changes in the height of the powderbed, which affect the distribution and placement of binder. The rough, grooved profile of the original powderbed surface, included above, is a direct result of the linear, layered slurry deposition process.

In terms of process explanations for defects, such as deviations in linearity along the edge, several possibilities exist. One likely cause arises from issues with droplet formation stability. For the most part, using the waveform determined from analysis in Section 2.3, the reliability of DOD printing should be fairly high, but the possibility of random fluctuations still exists and cannot be verified during vector DOD printing operations. Errors may also result from droplet vibration that occurs due to spindle motor operation. In addition, since the powderbed is not firmly mounted to the X-Y table, any disturbances from or affecting the translation table could cause the substrate to shift. Since the printhead is

continuously operating to maintain an equilibrium state, the deposition of extraneous binder droplets at the beginning or end points of the process is possible when the printhead is elevated relatively high above the powderbed. Finally, defects may occur due to the Bridgeport positioning accuracy limitations (± 0.025 mm), especially at corners or changes in direction, since this error is within range of one binder droplet (0.040 mm).
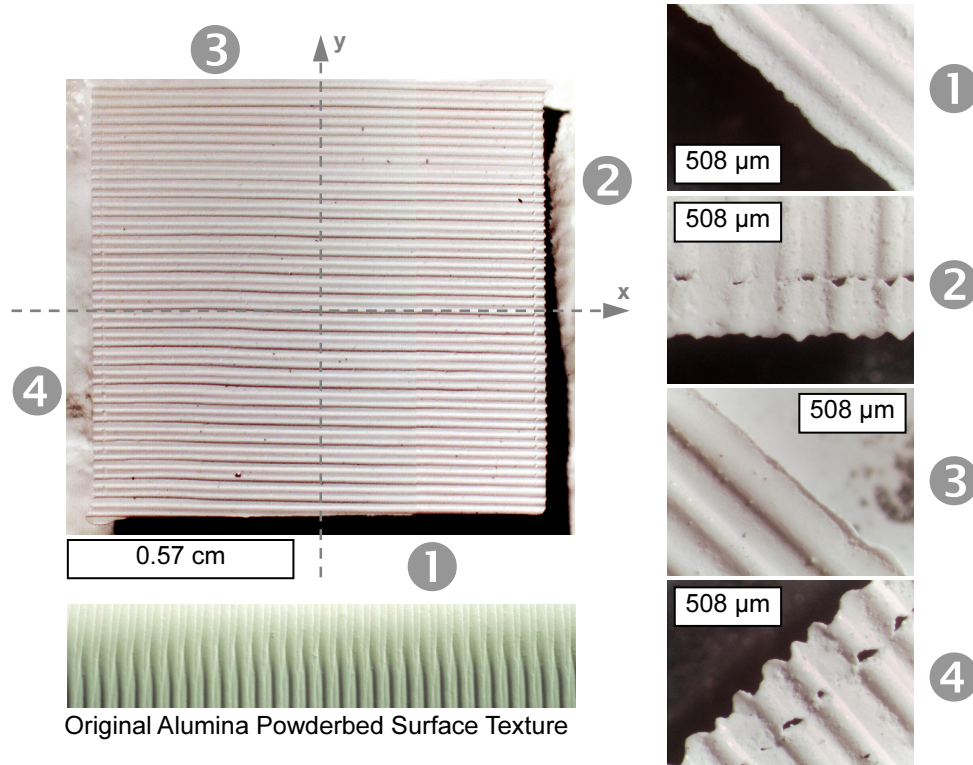
Figure 2.16 Pictures demonstrating edge quality and surface finish for a vector–printed, PAA binder square into an *unsanded* alumina powderbed. The superimposed axes indicate the printed part orientation relative to the programmed machine tool path (the y-axis points towards the milling machine, parallel to the default machine y-axis). Note that the origin is not accurately identified. The irregular edges, as seen on the four magnified pictures on the right, occur in part because of changes in the height of the powderbed, which affect the distribution and placement of binder. This fluctuating surface also causes incomplete binder merging between the vector outline and raster fill, even with a conservative droplet spacing. The rough, grooved profile of the original powderbed surface, included above, is a direct result of the linear, layered slurry deposition process.

Overall, the edge quality and surface finish, although not ideal, preview the potential benefits for 3DP parts created using the vector DOD printing method. The primary issue to resolve with part quality is the large influence of the slurry linear deposition process. The texture that normally results from sequentially slipcast slurry lines prevents a consistent binder droplet placement due to oscillating height variation. These powderbed surface conditions can perhaps be improved using the current jetting

process by changing relevant powderbed formation conditions, such as mass flow rate, line spacing, raster speed, or slurry composition. Alternatively, as in the case of the TDK slurry-vector machine under development, an entirely new approach to slurry powderbed deposition can be designed (refer to Section 3.2 for details). As a result of these experiments, further tests are conducted with sanded powderbed tops to eliminate the influence of the slurry-based deposition process on the surface finish and edge quality of extracted parts.

2.4.4. *Vector Printing Using Sanded Alumina Powderbeds*

In order to better evaluate the effect of vector DOD printing on 3DP part line quality, edge quality, and surface finish, another round of experimentation is pursued. Based on the dominant effects of the powderbed slurry-jetting process as seen in the previous experiments, the need to better isolate the process of vector DOD printing prompts a slight adjustment to the powderbed surface prior to printing. Using the same equipment, printhead, and water-based 2.4 v/o PAA binder combination again, four new tests are conducted with the five remaining alumina powderbeds generated as described in Section 2.4.1. The Siemens PT-88S printhead is assumed to use the same stable droplet formation parameters as before (4 μs: 8 μs: 1 μs: 97 V). The modifications outlined in Section 2.4 to the Bridgeport machine-based vector DOD setup are still applied. The powderbeds, however, require more preparation in order to remove the slurry-jetting artifacts from the top surface. The top surface is sanded, buffed, and then dusted off in order to create as smooth a surface as possible. A new MasterCAM-designed geometry is created, hereafter referenced as a Single-Line Grid design (SLG) with frame support, to reinforce and preserve individually DOD printed binder lines for extraction. The four new experiments seek to examine more effectively the same issues as before through the production of the following: (1) a 22 μm/drop SLG with frame support, (2) a 40 μm/drop SLG with frame support, (3) a 32 μm/drop SLG with frame support, and (4) a square block with linear raster fill. For comparison, the square block is repeated under the same conditions previously used. All machine programs for this study are configured and compiled with MasterCAM. All four tests are completed successfully in terms of reliable droplet generation; errors in z-axis calibration may contribute to printed part defects and significantly affect the value of measurements taken. Extraction of the cured, single-layer part from each powderbed sample is successful with the exception of the grid structure for the 40 μm/drop SLG design. The final part quality is substantially improved in comparison with previous results primarily from the removal of the linear powderbed features. In addition, measurements of single line widths suggest that the vector DOD printing process is capable of producing high-resolution parts with features smaller than those currently possible with 3DP.

2.4.4.1. Alumina Powderbed Preparation

A similar preparation procedure to that described in Section 2.4.3.1 is performed with additional steps to refine the powderbed top surface. First, the five alumina samples from the second powderbed produced in Section 2.4.1 are identified for future reference. These borous silicate substrates are numbered six through ten. The alumina samples are checked for correct orientation on the milling machine prior to printing (refer to Figure 2.13 for powderbed axes identification). Once again, the smallest powderbed dimension (11 mm) is oriented parallel to the machine y-axis. One of the five samples (identified as Piece 8) though originally intended for possible experimentation, eventually becomes the "calibration" powderbed used for setting the z-axis origin for the Siemens printhead. Since printhead droplet formation is continued without interruption, Piece 8 is no longer useful for collecting data. Finally, the top surfaces of these five powderbeds are gently dry sanded with 1200-grit sandpaper on a rotating polishing machine and then buffed with a Kim Wipe to obtain as smooth a surface as possible by visual inspection. Excess, loose powder is then removed with short blasts of compressed air.

Note that the attempt to use Piece 4 from the previous experimental set for calibration leads to severe miscalculations of z-axis height since it is later realized that (1) the two powderbeds produced in Section 2.4.1 do not have the same height and (2) the lack of top surface removal causes the height of Piece 4 to be presumably greater than the actual test samples, which already suffer from some variation as a result of the smoothing procedure.

2.4.4.2. Vector Drop-On-Demand Printing Parameters and Observations

Using the improved powderbed substrate surface for binder printing, the following experiments are conducted to further evaluate the performance of vector DOD printing: three for line quality characteristics, (1) a SLG_1 with square frame support & 22-μm drop spacing, (2) a SLG_2 with square frame support & 40-μm drop spacing, (3) a SLG_3 with square frame support & 32-μm drop spacing, and (4) a square block with vector profile trace & horizontal, linear raster fill for comparison with previous results (as seen in Figure 2.16). Note that compared with the previous set of experiments with unsanded alumina powderbeds, the parameters and reasons for such choices are identical. Therefore, for further background regarding chosen conditions, refer to Section 2.4.3. All geometries are designed and compiled in MasterCAM to obtain appropriate machine programs for execution on the Bridgeport EZ-Trak milling machine. The Single-Line Grid design is developed as a potential solution to preserve individually printed lines for analysis. The structure is 0.40" x 0.40" in size and consists of an external square frame 0.15" thick that encompasses a square grid with sixteen 0.025" x 0.025" cells. The borders of each cell represent a single binder printed line. An illustration of this SLG design with relevant dimensions and an explanation of the programmed tool path is shown in Figure 2.17. The square block uses the same parameters described in Section 2.4.3.2 and Table 2-E. Note that for each of these
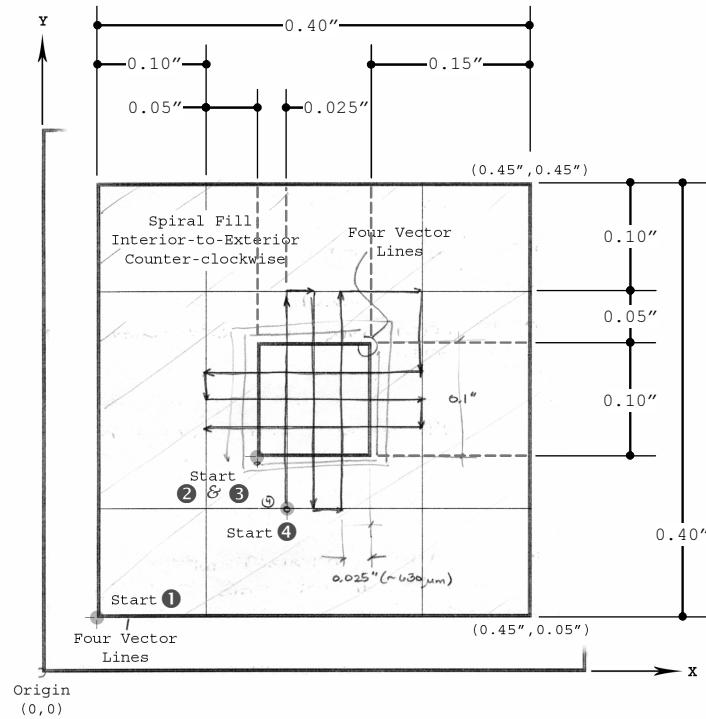
geometries, a vector trace is executed four times from the exterior perimeter to the interior, except for the center grid portion of the SLG design, with gradually decreasing radii for boundary reinforcement (refer to Figure 2.14 (a) and Figure 2.17). The powderbed samples, referenced as Pieces 6 to 10, are selected to correspond with the following tests listed above: Piece 6 for Test (1), Piece 7 for Test (2), Piece 9 for Test (3), and Piece 10 for Test (4). Piece 8 is later used as the "calibration" powderbed.

As in the experiments described in Section 2.4.3.2, the line spacing parameter used for these experiments is based on the droplet size of the water-based PAA binder in air (44 microns) as generated under stable formation conditions. The MasterCAM tool diameter is equivalently set, and a 22-micron spacing (50% overlap) between adjacent parallel lines is used. Though this diameter is not representative of actual binder conditions in the powderbed, based on previous experiments, the droplet diameter and percentage overlap are shown to provide sufficient merging to produce a cohesive binder-printed part. Similar to the previous set of experiments described in Section 2.4.3, the exterior profile traces are repeated again for all geometries in order to separate vector definitions of the part shape from its interior raster fill. For the SLG_x design experiments with Pieces 6, 7, and 9, the droplet spacing is determined by changes in frequency with machine speed kept constant (refer to Table 2-F).

For future reference, the drop-on-demand control process using the micro switch and quill is partially implemented in the machine programming of the SLG geometry. As stated before, due to concerns about droplet stability during reactivation and to better guarantee the successful completion of a vector DOD printing experiment, the micro switch control is not, however, applied to these experiments. Minor adjustments to the current z-axis movement will be required for complete and proper DOD control.

The milling machine speed is maximized for all four experiments at 600 mm/min or 10 mm/s (refer to Section 2.2.1.2 for an explanation), the speed compromise between accuracy and production rate.

Like the situation discussed in Section 2.4.3.2, the errors associated with z-axis calibration are once again present but also potentially magnified. The origin for all three powderbed axes is determined by using the "calibration" powderbed. Ideally, the distance between the Siemens orifice plate and the powderbed can be accurately set. Since the Siemens orifice plate holder adds to the distance between the orifice plate and the powderbed, the desired z-axis distance of 500 microns is underestimated. In addition, calibration variability can also introduce differences in printhead separation distance for each powderbed sample. In addition to these factors, an attempt to use Piece 4 for calibration leads to considerable error in z-axis distance for printing with Pieces 6 and 7 (refer to Section 2.4.4.1 for causes). The change to Piece 8 for calibration provides some improvement, but error is also introduced from the inconsistent top surface removal process that creates slight height variations in Pieces 6 through 10. These variable increases in z-axis separation between powderbed and printhead are reflected in the values given in Table 2-F. The consistent positioning method for locating powderbed samples is retained.
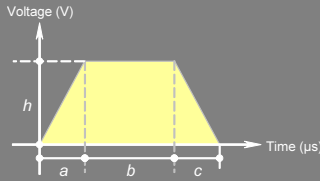
Tooling:	44 µm Diameter Droplets	Feed Rate:	600 mm/min
Z-axis:	Origin – top of powderbed	Line Spacing:	22 µm
	+0.5 mm – printhead	Droplet Spacings:	20 µm/drop
Raster Fill:	Spiral In-Out		32 µm/drop
	Counter-clockwise		40 µm/drop

Figure 2.17 Annotated illustration of the proposed Single-Line Grid (SLG) design rendered in MasterCAM. This structure is intended to support individual, vector-printed PAA binder lines onto alumina so that layer quality and line width limitations can be explored. With the exception of the single-line grid, the outer and inner square frames are defined by four consecutive vector traces 22 µm apart that transition from their respective exterior boundaries to the interior. Using the same input conditions for tooling properties (droplet size), z-axis depth, and feed rates as the square and tooling insert geometries seen in Figure 2.14 along with a spiral raster-fill style, MasterCAM once again generates a CNC machine program in plain text. The execution order proceeds as follows: (1) four vector traces of the exterior square frame, (2) four vector traces of the internal square frame, (3) spiral in-out raster fill of the interior section between (1) and (2), and (4) single-line grid definition. Minor editing of this program is performed to permit necessary equipment adjustments particular to the Bridgeport milling machine setup. These programs are transferred via 3.5" floppy disk to the Bridgeport milling machine computer for execution. Line width and layer quality are evaluated as a function of droplet spacing. Three droplet spacings are selected for testing: 20 µm/drop, 32 µm/drop, and 40 µm/drop. Using the same edited CNC program, droplet spacing variation is achieved by changing the droplet frequency.

The Siemens printhead is again deployed with steady state conditions. Using Nozzle 5 for the four experiments with Pieces 6, 7, 9, and 10, the printhead is kept operational once stable droplet formation equilibrium is established to minimize instabilities. This continual operation keeps the calibration Piece 8 from being used as an experimental sample.

Only one unique adjustment is necessary for performing these experiments. The suggested droplet generation voltage (97 Volts) is slightly modified once again for stable printhead operation. The waveform geometry (4 μs: 8 μs: 1 μs) is initially applied to Nozzle 5 at a transition voltage of 100 Volts and a frequency of 500 Hz. The square block must once again be scaled to 90% of its original size.

Table 2-F:
VECTOR PRINTING PARAMETERS FOR SANDED ALUMINA POWDERBEDS WITH PAA BINDER

	Alumina Powderbed Piece Reference Number[†]				
	6	7	8	9	10
Vector Geometry Description	Single-Line Grid Design with Square Frame Support 0.4" x 0.4"	Single-Line Grid Design with Square Frame Support 0.4" x 0.4"	Calibration Powderbed II	Single-Line Grid Design with Square Frame Support 0.4" x 0.4"	Square Block 0.45" x 0.45"
Binder Composition	2.4 v/o Polyacrylic Acid (PAA) + Glycerol + Water				
Droplet Diameter (microns)	44.0 microns				
Droplet Frequency (Hz)	455 Hz	250 Hz	n/a	313 Hz	500 Hz
Vector Speed (mm/s)	10 mm/s	10 mm/s	n/a	10 mm/s	10 mm/s
Consecutive Droplet Spacing (μm/drop)	22 μm/drop	40 μm/drop	n/a	32 μm/drop	20 μm/drop
CNC Machine Program	BLL31600.PGM	BLL31600.PGM	n/a	BLL31600.PGM	0302003.PGM
Adjacent Line Spacing (μm/line)	22 μm/line		n/a	22 μm/line	20 μm/line
Printhead-Powderbed Separation (microns)	1000+ microns *Error due to z-axis calibration with Piece 4*		Variable	500+ microns	1000+ microns
Droplet Waveform Function ($a:b:c:h$)	4 μs : 8 μs : 1 μs : 100 V				

[†] Refer to Figure 2.13 for powderbed piece identification and printing orientation

Using these parameters, the four experiments are performed and noted with the following observations. Throughout these tests, just like before, a constant droplet vibration is observed as the result of spindle motor operation. Test (1) for a 22-μm drop SLG_1 design is printed successfully in approximately seven to eight minutes with a stable droplet seen after completion. The SLG_2 design for Piece 7 is performed successfully in eight minutes; a stable droplet is once again verified. The process of completing SLG_3 requires the machine program to be stopped prematurely and restarted because the z-axis origin is set too low. Following z-axis elevation, Test (3) is completed successfully in around seven minutes with subsequent confirmation of droplet stability. The square block for Piece 10 is printed in eleven minutes, and a stable droplet is later observed. The concern for this final test is the proximity of the square to the back edge of the powderbed and whether this positioning will lead to distortion or curvature of the printed part. Throughout all four tests, the separation between printhead and powderbed is greater than the desired 500 microns; Piece 9 has the lowest separation distance, while Pieces 6 and 7 incorrectly use Piece 4 to calibrate printhead separation, leading to more substantial error.

Tests with Pieces 6 and 7 have a rather large printhead separation distance because Piece 4 from the other powderbed is used to determine the z-axis origin. As explained earlier in Section 2.4.4.1, using Piece 4 does not take into account the height discrepancy between powderbeds that results from the powderbed formation process and subsequent surface sanding. For these two pieces, the measurement given in Table 2-F is considered a minimum, though actual distance between powderbed and orifice could be as high as 1.5 mm. As the distance between powderbed and printhead increase, the droplet placement accuracy decreases. The magnitude of this inaccuracy, though, is dependent on the ejection speed of the droplet. Given that DOS measurements of the 2.4 v/o PAA binder droplet using this waveform with the Siemens PT-88S indicate an ejection speed of 3.6 m/s, the effect of such a relatively large separation distance may be negligible, although for general vector DOD experimentation the recommended distance should be 500 microns. After Piece 8 is used for calibration, this source of error is removed, and the maximum distance between the powderbed and the printhead is reduced. The z-axis calibration, however, is also affected by differences in sample height resulting from the sanding process. This variability occurs because each top surface is removed separately instead of sanding all samples at once. Fortunately, despite the potentially severe consequences of these errors, the extraction of these vector DOD prints provides useful results for analysis.

2.4.4.3. Extraction of Printed Layers

The process of extraction for these four experiments is the same as that conducted for the vector prints onto unsanded alumina powderbeds (see Section 2.4.3.3). First, the four samples, Pieces 6, 7, 9, and 10, are cured and then redispersed in deionized water. Based on the redispersion problems with Piece 1 in the first set of experiments, closer attention is paid to the positioning of powderbed samples within the

oven by attempting to place all four as close to the center as possible. The samples are cured for one hour in Argon with a temperature range that varies between 147 °C and 149 °C.

Overall, the redispersion of each piece progresses as expected and in a similar fashion. For three of the four tests using Pieces 6, 9, and 10, the process of powder infiltration, swelling, and subsequent cleaning off with a water bottle removes all of the unbound powder in approximately eight minutes, leaving a clearly defined printed part for examination. Unbound powder lodged between the center grid lines of Pieces 6, 7, and 9 does not redisperse immediately, but after approximately seven minutes, subsequent spraying with a deionized removes the excess powder. For the largest droplet spacing (40 µm) SLG_2 tested, however, the redispersion of the line structure is not successful.

For the 40-µm droplet spacing SLG_2 design, the internal grid is either destroyed or not clearly present during redispersion. After a significant amount of redispersion around the exterior is complete, with the wash bottle cleaning only the exterior portions, parts of the grid structure are roughly delineated though not completely redispersed. Upon subsequent spraying of the center portion, the grid structure fails to appear, with only a small corner section remaining intact. Though it is uncertain whether the SLG_2 is complete and well-defined prior to extraction, the force of the water bottle spray used to remove the final unbound portions of powder is believed to be one contributing factor for the 40-µm droplet spacing SLG failure. Since the droplet spacing almost matches the droplet diameter in air, the binder concentration per unit area of powderbed (or percentage overlap) is less than the other samples tested so, with the assumption that the binder diameter does not increase significantly upon powderbed impact, the effect of any defect or error is more significant compared to a sample with closer droplet spacing. Of course, the strength of this droplet spacing grid structure could also be enhanced with further vector DOD binder printing onto multiple layers, which is the next step in terms of developing this 3DP process.

It is also possible that a different, gentler redispersion method could better preserve the fragile, if existent, single-line, single-layer structure. Another possible contributing factor for effective redispersion may depend upon the effects of the sanding process. In order to prevent extensive damage to the fragile powderbed structure, only a minimal amount of the top surface is removed. Using sandpaper and a Kim Wipe to smooth the surface may, in addition to removing alumina, introduce artifacts into the powderbed, and this contamination may affect binder-powderbed interactions and thus the final properties for the vector-printed part. Though this possibility does not appear to play a role in the redispersion of Pieces 6, 9, and 10, with the low binder concentrations present in the SLG_2 of Piece 7, the contributions of contaminants, or perhaps even loose powder on the surface, may have affected grid development. The significant printhead-powderbed separation distance for Piece 7 mentioned in the previous section may also have played a role by affecting droplet placement accuracy.

2.4.4.4. Line Quality of Printed Layers

From the successful extraction of two SLG designs, one for 20-µm spacing and another for 32-µm spacing, measurement of the resulting line widths are performed. For the 40-µm SLG_2, measurements are made from fragments that are found in the redispersed powder to evaluate line width potential. As seen in Figure 2.18, the increase in droplet spacing results in a decrease in line width as expected.

In comparisons of line quality, lines in the 32-µm droplet spacing SLG_3 appear to possess more uniform linearity than the lines at 22-µm droplet spacing. Based on this conclusion and the fact that the ends of potential lines can be seen in the 40-µm SLG_2, it is possible that the line quality is even greater for this higher droplet spacing. In the 22-µm SLG_1, the presence of extraneous droplets seen along lines in the upper right grid corner may indicate that droplet instability occurred during this stage of binder deposition and distorted line development. It is also possible, however, that random droplets are deposited before or after the program is complete (see the explanation at the end of this section). The horizontal lines for the 22-µm SLG_1 appear smoother and more uniform than the vertical lines, and based on the process of grid definition as described in Figure 2.17, the similarity among vertical lines as well as the similarity among horizontal lines should exist. An experiment to recreate the 22-µm SLG_1 may yield better results with greater linearity and fewer line defects. For obtaining small feature, high-resolution part definition, the trend suggested by the observed decrease in line width and smoother, more uniform line at higher droplet spacings is a promising development. If the 40-µm SLG_2 design is not functional, then by considering this trend, an effective range of droplet spacings with increasing line quality can be determined between the 32- and the 40-µm level, with 40-µm being the maximum possible spacing, although further research is necessary to firmly establish the maximum spacing limitation (refer to the following section for an argument refuting 40-µm as the maximum droplet spacing)..

In comparison with line widths obtained by the standard continuous-jet (CJ) binder printing method, these results for vector DOD printing using a specific waveform (4 µs: 8 µs: 1 µs: 100 V) and specific printhead (Siemens PT-88S) yield considerably smaller line width measurements that point towards the possible advantages of this production process for 3DP parts. According to measurements shown in Figure 2.18, the line widths measured from these experiments range from 140 to 170 microns. The typical, continuous-jet printing method for depositing water-based 2.4 v/o PAA binder into an alumina powderbed produces an average line width of 350 microns, more than twice the size of the new vector DOD process values. The CJ binder line is formed by using a 40-µm ruby tip nozzle to eject an 80-µm drop at a speed of 9-10 m/s and a 10-15 µm droplet spacing (equivalent to an 80-90% overlap). Based on the set of performance parameters provided for continuous-jet binder printing, it is obvious that many measurements for vector DOD binder printing must still be determined, such as the actual binder droplet size upon impact, to understand and improve the performance of the vector DOD printing process.

Droplet Spacing: 22 µm
Line Width: 160-170 µm

Droplet Spacing: 32 µm
Line Width: 145-150 µm

Droplet Spacing: 40 µm
Line Width: 140-150 µm
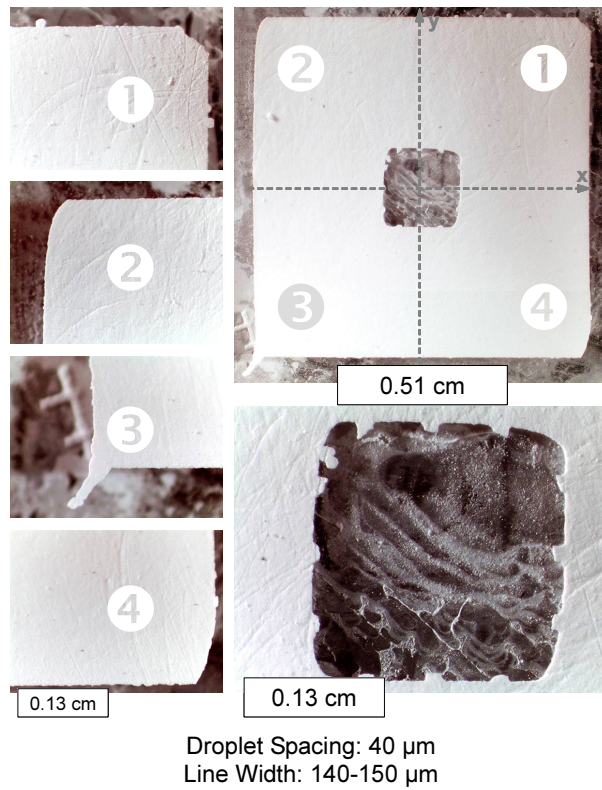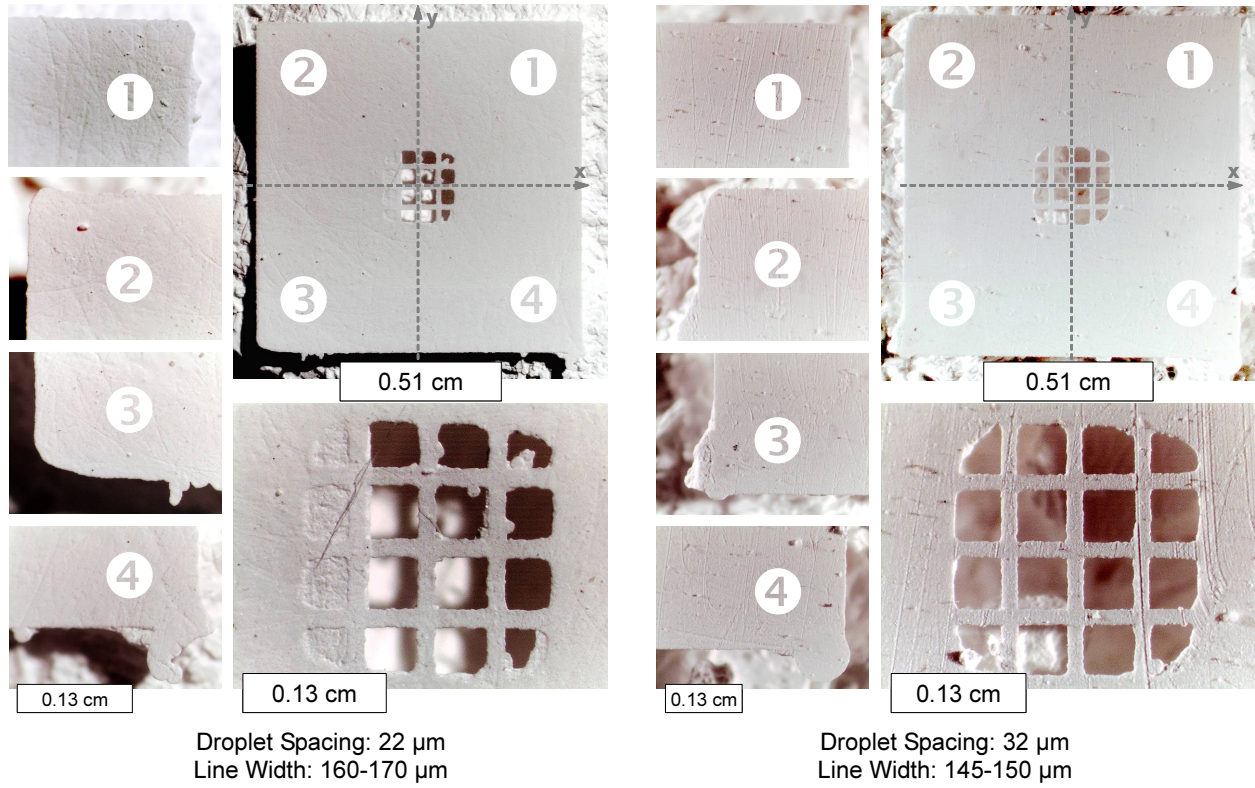
Figure 2.18　Pictures and corresponding line width measurements for three sets of the vector-printed, PAA binder single-line grid design. A surrounding square base structure is constructed along with an interweaving perpendicular

grid to support individual lines (refer to Figure 2.17 for technical details). These lines, based on different droplet spacings, are examined for definition quality and respective widths. The superimposed axes indicate the printed part orientation relative to the programmed machine tool path (the y-axis points towards the milling machine, parallel to the default machine y-axis). Note that the origin is not accurately identified. From qualitative examination of the three line widths measured, the smallest linear feature that could be created with vector printing under these conditions (printhead, powderbed, and binder) would most likely have a minimum width of 140 microns at a 40 micron droplet spacing.

To verify and test the independence of these experimental results, it would be worthwhile to vary the vectoring speed instead of the frequency, which is the determining factor for results shown in Figure 2.18. In addition, many other variables can be examined to affect line quality, such as the DOD waveform, binder chemistry, or the printhead, all of which would greatly affect droplet performance. In the end, many more aspects of this printing process are opened for development as the result of this preliminary study.

As seen in Figure 2.18, the left portion of the 22-μm SLG$_1$ structure contains a column of grid lines still filled with excess powder. Several factors may have contributed to this incomplete redispersion. One possibility may be the presence of a temperature gradient in the oven during the curing that increased the temperature in this region and therefore decomposed a significant amount of PEG required for redispersion (as discussed in Section 2.4.3.3). Another possible explanation may be that further time or intensive exposure to water is necessary, although it is believed that a thorough attempt is made to remove the unbound powder during the extraction process and that further efforts may risk damaging the internal grid structure. Droplet instability or inaccuracies in binder placement that occur from the rapid and multiple direction changes specified in the grid design may also have affected this region.

Furthermore, many other sources of error exist to explain part defects. One potential source of error is the degree of top surface flatness, which is only visually inspected before testing. The possibility of a skew printing surface may affect binder placement accuracy. One unforeseen error in machine path programming may also lead to errant droplet placement. The final endpoint for the SLG design at (0.8", 0.8", 0.9") is potentially specified too close to the powderbed so that random drops dispersed through the air could be deposited onto the powderbed. As always, the manual errors in z-axis calibration may contribute to errors in droplet placement since the height exceeds normal DOD recommendations. In addition, the errors described in Section 2.4.3.4 still apply to these operating conditions.

One concern regarding these results is the correlation between measured line widths and specified droplet spacings. As a result of incorrect calibration, the large discrepancy in printhead-powderbed separation from those intended for normal DOD operation (500 μm) may affect the droplet behavior and alter these results. Changes in impact behavior, relative droplet placement, and velocity could all potentially affect line formation in the powderbed. It is a testament to process and droplet

durability that relatively straight and uniform lines are formed under such conditions. Additional testing for verification of these results is nonetheless recommended.

It is important to note that although these results of line width and quality are not representative of WC-Co powderbeds, they portend great potential for future efforts in tooling insert development with this printing process.

### 2.4.4.5. Edge Quality & Surface Finish of Printed Layers

In a comparison of surface finish between SLG experiments, the uniformity and smoothness of each square support frame appear identical. In one sense, this result is expected since the appearance of this top surface is determined in part by the powderbed preparation process (refer to Section 2.4.4.1). Nevertheless, another factor that determines the cohesiveness of this surface is the droplet spacing. If the spacing between droplets is too large, then insufficient binder merging occurs and the resultant surface finish is affected because unbound sections between droplets redisperse and leave pockets. Based on the MasterCAM specifications, one parameter remains constant between all experiments in this section: the line spacing of 22 microns. With this setting, the consecutive droplet spacing is varied for each of the SLG designs by changing the frequency. This difference in spacing between consecutive droplets and neighboring line droplets creates a dimensional variation for comparison. For Piece 6 - SLG_1, the line spacing x consecutive spacing setting is defined as 22 μm x 22 μm. For Piece 7, SLG_2, the values are 22 μm x 40 μm, and for Piece 9, SLG_3, 22 μm x 32 μm. Since the square support frame for Piece 7 appears solid, it follows that a 40 μm x 40 μm setting, or 40 μm line spacing, should also work since a pattern of empty regions would have resulted otherwise. This reasoning establishes the basis for re-testing the 40-μm SLG_2 design on another sanded alumina powderbed and indicates that a different approach to redispersion may be necessary to preserve the single-layer grid structure.

A more effective measure of surface finish is the result of printing multiple layers and examining the qualities of the interface between layers to form a solid surface. This third dimension is not currently available with vector DOD printing using this setup, although by studying the layer depth and how it corresponds to droplet spacing, valuable insights into multi-layer slurry and binder deposition is possible. This information should help improve the inter-layer surface finish when multiple layers can be processed. The problem with examining multi-layer results is that the surface finish of the printed layer would exhibit the effects of linear, slurry-rastering as seen in Figure 2.15 and Figure 2.16 if current slurry printing technology is used. This type of surface, as seen in the previous experimental results, can interfere with smooth edge definition and proper binder merging. Until the layer surface finish is similar to those approximated in Figure 2.18 and Figure 2.19, the evaluation of surface finish between multiple powderbed layers may prove difficult or, if compared to this current state, at the very least disappointing.

The comparison between the two equivalent square blocks produced with vector DOD printing, one using a sanded powderbed and the other without, shows considerable improvement in surface finish and linear edge quality in the sanded alumina sample. Both vector printed squares have accurate overall geometry, and both exhibit distinct corners with the starting corner at the lower left of Figure 2.16 and Figure 2.19 having the most agglomeration of binder, which is expected from the defined tool path and the lack of DOD printing control. The edge quality of the sanded alumina square block is considerably better than the unsanded alumina square block, whose edges are highly influenced by the variation in powderbed height and corresponding droplet placement. Closer examination of both blocks shows that the sanded alumina sample still has some irregularity in edge definition (refer to ❶ and ❹ in Figure 2.19), most likely attributable to droplet instability, but the unsanded alumina sample even has regions where powderbed height prevents the vector and raster-fill sections from merging (refer to ❷ and ❹ in Figure 2.16).

Edge quality among the SLG designs all appear good with little variation between droplet spacing samples. All SLG designs exhibit defects along the external perimeter, but the z-axis depth of these edge defects differs with the 40-μm SLG_2 showing the thinnest layer depth and thinnest defects. In contrast, examining corner ❹ of the 22-μm SLG_1 and corner ❸ of the 32-μm SLG_3 indicates that these print conditions have a degree of associated thickness in the powderbed that increases in regions where droplets aggregate (defect regions). It is expected that corner ❸ of all SLG designs and the square should have a some defect, since the vector trace begins and ends in this region. With a continuously running printhead, it seems likely that droplet collection would occur in this region. For the 22-μm SLG_1, this defect is surprisingly not observed.

The issue with edge quality for vector DOD printing, as observed in the results of these tests, is the sharpness of corners. The three SLG designs and the square block all clearly exhibit roundness at corner interfaces, though not for every instance. Corner ❶ for the 22-μm SLG_1 and 32-μm SLG_3 both appear reasonably sharp. The remaining corners, even the internal corners of the SLG grid structures, all exhibit a rounded shape, which is believed to be a function of the deceleration error in milling machine speed. The exact relationship of this behavior is not known; a recommended experiment to assess this effect is to vector trace, consecutively several times to preserve the line structure, only the external geometry of a shape with sharp corners. This test may provide greater insight, if the other vector DOD printing variables can be controlled. By comparing the sanded alumina samples with the square block from the unsanded alumina powderbed, the square with surface texture appears to have better corner definition. This corner sharpness may be the result of better z-axis calibration (closer to 500 μm) for these prior set of experiments. Since the powderbed-printhead separation varies and tends to be closer to 1 mm for these sanded alumina samples, errors introduced by this distance may play a role.
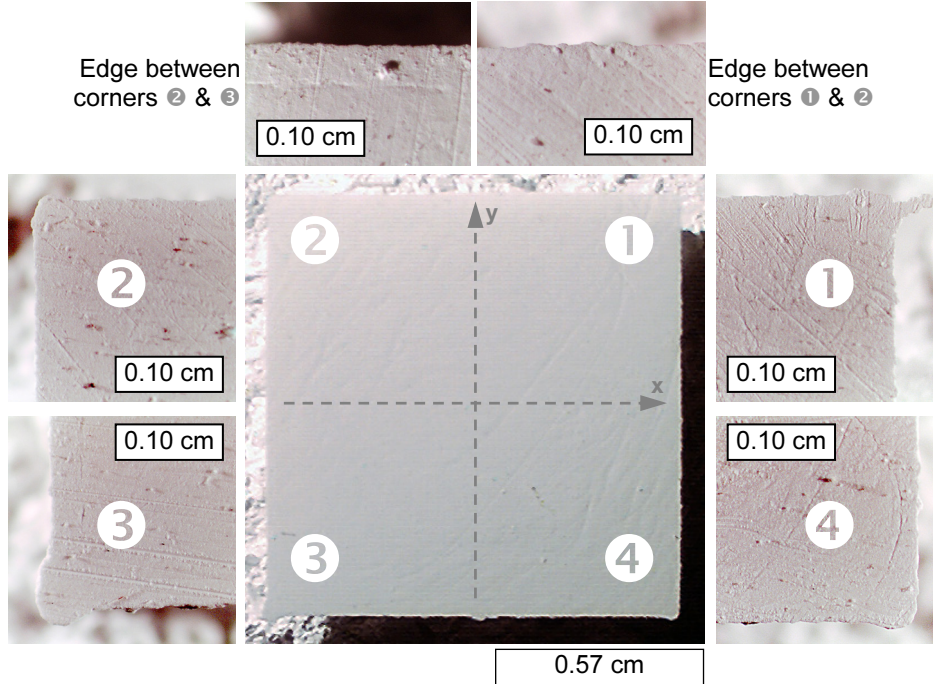
Figure 2.19 Pictures demonstrating the edge quality and surface finish for a vector-printed, PAA binder square into a *sanded* alumina powderbed. For comparison, all printing parameters are equivalent to those used in Figure 2.16. The superimposed axes indicate the printed part orientation relative to the programmed machine tool path (the y-axis points towards the milling machine, parallel to the default machine y-axis). Note that the origin is not accurately identified. Mild sanding and buffing of the top powderbed surface removes the uneven remnants of the linear slurry deposition process and prevents the consequential edge variation depicted in Figure 2.16. Thus, the edge quality and surface finish are independent of the slurry deposition process and more clearly illustrate the effect of the vector printing parameters (i.e. vector speed, droplet frequency, droplet separation, etc.).

The surface finish of all powderbed samples, Pieces 6 to 10, appear smooth to a great extent. The remnants of powderbed preparation are occasionally evident when observed on a smaller scale. The roughness in the surface finish of these alumina samples primarily comes from the sanding process used prior to vector DOD printing. Random scratches throughout the powderbed layer, seen in the corner close-ups of the square block in Figure 2.19 and the internal grid structure of the 32-µm SLG_3 in Figure 2.18, appear as a result of the polishing process with 1200-grit sandpaper and subsequent buffing with a Kim Wipe. These surface defects cannot be completely removed using the manual polishing methods and the level of visual inspection available for processing. Smoothing the surface completely by sanding would be inordinately time consuming and likely impossible. The distinct presence of these scratches under magnification indicate that these random pits and grooves may influence the printed part quality if they are severe, especially as seen in the large scratch of the grid in the 32-µm SLG_3; therefore, it is

recommended that even higher grit sandpaper be used in the future for "powderbed preparation," or removal of the top surface, to minimize the effect of random surface scratches.

Refer to previous discussions throughout Section 2.4.4 for details on other possible explanations for defect formation, which inevitably affect edge quality and/or surface finish.

2.4.5. *Summary of Vector Drop-on-Demand Printing Experiments*

The implementation of vector drop-on-demand printing for production of 3DP parts is explored based on the parameters for stable droplet generation and the functional assembly of equipment for this purpose. Eight vector DOD printing experiments are performed in two sets of four.

FIRST EXPERIMENTAL SET
- Five single lines with different droplet spacings (speed variation)
- Five single lines with different droplet spacings (frequency variation)
- Square block with horizontal linear raster fill
- Tooling insert with 130° linear raster fill

SECOND EXPERIMENTAL SET
- Single-line grid design with support frame for 22 µm/drop spacing
- Single-line grid design with support frame for 40 µm/drop spacing
- Single-line grid design with support frame for 32 µm/drop spacing
- Square block with horizontal linear raster fill

The design of experiments started first from the desire to determine line widths of the Siemens DOD printhead droplets onto alumina. Initially, slipcast powderbeds are used to evaluate DOD printed lines on the Droplet Observation Station. After the standard curing process for alumina powderbeds, redispersion attempts on these slipcast samples failed. Changes in slurry composition, such as the loss of the redispersant PEG, that occur from the slipcasting process may have affected the processing of these samples. In order to create more functional, reliable powderbeds, a standard 30 v/o alumina slurry is jetted on the Hood Machine to create two powderbeds composed of ten borous silicate substrates (five per powderbed) that are used for the eight vector DOD experiments. In addition, the Siemens PT-88S functions as the DOD printhead with stable droplet formation conditions determined in the previous Section 2.3. The original printhead parameters (4 µs: 8 µs: 1 µs: 97 V) are adjusted to slightly higher voltage levels for each set of experiments to achieve the maximum stable droplet condition.

The first set of experiments attempt to produce single lines, a square block, and a tooling insert to evaluate vector DOD printing. The vector drop-on-demand setup developed and evaluated in Section 2.2 is used with a few changes: the removal of the micro switch DOD control, the use of a gold-plated orifice plate, and the addition of a droplet visualization system. The Siemens PT-88S printhead is employed as the DOD mechanism for depositing the water-based 2.4 v/o PAA binder into the slurry-jetted alumina powderbed. The first four experiments above are conducted. The tooling insert geometry fails to

successfully complete the raster-fill procedure. After curing and attempted redispersion, the two sets of five single lines fail to survive the extraction process. The square and tooling insert are successfully removed from original powderbed substrate, but exhibit dominant slurry line artifacts that make it difficult to distinguish the effects of vector DOD printing. Some useful data is obtained. The consistency of droplet placement by the Siemens printhead is evidenced by the periodic line oscillation along edges perpendicular to the jetted slurry line. These experiments also confirmed that a 44 micron binder droplet size estimate, based on calculations for droplet diameter in the air while neglecting powderbed interaction, and a 50% overlap or 22-micron line spacing are sufficient for merging portions of an alumina powderbed to form a solid shape. Throughout the experiments, DOD printhead is fairly reliable based on the effective waveform geometry and frequencies used. Once an equilibrium droplet formation condition is established the printhead remains in continuous operation for the duration of the experiments. From these experiments, the performance of the droplet generation conditions are validated, but the possibilities for random instability and errors are still present as indicated by defects along edge of printed parts. One defect that is specifically related to the slurry-jetted powderbed lines is the incomplete merging between the vector and raster-fill printing steps caused by the powderbed height variation. Due to problems with individual line extraction and the prevalence of slurry-based powderbed effects on printed part quality, another series of experiments are performed with appropriate adjustments. The top surfaces of the alumina powderbeds are sanded to create a smooth substrate that will illustrate the effects of vector DOD printing effectively. In addition, a new grid structure is developed to support and preserve individually printed lines for subsequent line width measurement.

The second round of experimentation examines the relationship between droplet spacing and line width using the Single-Line Grid (SLG) design and evaluates the general performance of vector DOD printing by repeating the square block geometry for comparison. Powderbed preparation involves sanding the powderbed top surface with 1200-grit sandpaper, buffing with a Kim Wipe, and finally removing excess powder with air. The same vector DOD setup from the previous experiments is used. The four tests are completed successfully, but calibration of the z-axis origin proves fairly inaccurate, with a distance between printhead and powderbed ranging from 500 to 1500 microns, with distances closer to 1 mm likely. The distance calibration error more than likely contributes to errors and defects in the printed parts, but results still provide useful data. Redispersion of the 40-µm/drop SLG causes grid structure to fail; the reason for this failure could be from binder weakness, line defects, or redispersion method. The most significant result is the measurement of line width for vector DOD printing of the 2.4 v/o PAA binder, which ranges from 140 to 170 microns based on the grid structures of the three SLG designs. The possible error in correlating measured line width with set droplet spacing prompts further testing to be performed. Using the sanded alumina powderbeds, vector DOD printing quality is clearly evident. Comparing line width measurements, the continuous-jet binder printing produces lines widths

of 350 microns while vector DOD printing form lines with less than half this dimension. Lines possess good linearity; similarly, edge definition also good, except for corner sharpness. This lack of precision may be the result of deceleration effects of the milling machine. These general results for vector DOD printing bode well for the future production of high-resolution, small feature parts. The application towards WC-Co tooling inserts will be possible once slurry-binder issues are resolved.

Many possible factors contribute to vector DOD printed part errors. Defects and random droplets observed in the grid structure and along edges for the second set of experiments may be caused by incorrect z-axis calibration. In addition, potential deviations in powderbed flatness as the result of sanding may lead to droplet placement errors. One major contributor is droplet instability (refer to Section 2.3 for discussion of its complex contributing factors). Vibrations or disturbances from the Bridgeport milling machine, especially the spindle motor, influence droplet placement during testing. Inaccuracies in milling machine movement also lead to possible errors in geometry or droplet accumulations in one region. Since the powderbed is not firmly mounted onto the milling machine, possible movements during testing could introduce errors. Finally, since the Siemens PT-88S printhead is continuously operating, random droplets are likely to be deposited when beginning or ending an executed machine program.

Several recommendations are suggested for further development in this area of vector drop-on-demand printing for 3DP part production. The research performed by Vedran Knezevic relates to binder droplet placement strategy in slurry printed powderbeds [21]. By examining the effects of the droplet deposition process as discussed by Knezevic, such as performing an iterative construction of the vector trace by merging multiple droplet segments, it may be possible to further improve part quality. In order to improve reliability for the experiments conducted, the micro switch DOD control is not implemented for binder-based DOD printing. Incorporation of this feature is recommended once droplet stability is better understood in order to achieve full vector DOD functionality. The use of a gold-plated orifice plate to reduce corrosion from PAA does not affect the operating performance of the Siemens printhead during experimentation. The corrosive effect of PAA on the coated orifice plate has not yet been assessed, so analysis of the current orifice plate condition will provide a valuable measure of effectiveness for the gold-plating. Furthermore, material analysis of the Siemens orifice plate will improve understanding of potentially reactive chemistries and provide possible methods to eliminate or mitigate corrosive effects. Finally, when the technical issues have been resolved, the process of producing 3-D parts with vector drop-on-demand printing should be examined.

3 CONCLUSIONS & FUTURE WORK

3.1. SUMMARY OF WORK

In reference to the long-term goal of manufacturing WC-Co tooling inserts by Three Dimensional Printing, three fundamental steps required for successful implementation are examined:

- Tungsten Carbide-Cobalt slurry development
- Tungsten Carbide-Cobalt powderbed production
- Vector drop-on-demand printing of Tungsten Carbide-Cobalt tooling inserts

The initial two objectives are performed in conjunction with the assistance of another colleague. The first requirement for producing a part from sub-micron powder is to develop a stable, jettable slurry. Two different approaches are considered: (1) water-based slurries composed of WC powder only with Co salt as a binder and (2) alcohol-based slurries using WC-Co powder and an organic binder. For each type of system, a dispersant is necessary to suspend the powder particles in solution to prevent flocculation. Various measurement, such as settling density and viscosity, are made to evaluate the stability of each slurry chemistry. Based on the rate of progress with these two approaches, the decision is made to focus on alcohol-based slurries. The most effective dispersant evaluated up to this point is Emphos PS-21A. Further developments after the conclusion of this research alter the dispersant selection and are discussed in Section 3.2. As stated previously in the Section 1.6, detailed information concerning the development of a stable WC-Co slurry can be found by referencing the Diplomarbeit document by Olaf Dambon [18].

Once a jettable, alcohol-based slurry is developed, relevant parameters are examined in an effort to produce smooth, uniform powderbeds. To devise an effective powderbed formation process requires an understanding of the relationship between slurry dwell time, line spacing, flow rate, and its effect on powderbed development. In the end, functional parameters are optimized to produce a smooth, uniform powderbed structure. Once again, for extensive data and analysis of these issues, refer to the Diplomarbeit document by Olaf Dambon [18].

The primary focus of this thesis relates to the third objective, vector drop-on-demand printing. To investigate this possibility, three steps are taken. Each process step is covered in a major subsection of Chapter 2. First, an effective combination of equipment is assembled to perform the required functions. The capabilities and limitations of this setup are then evaluated. The problems identified are addressed or compensated for. From Section 2.2, the nominal operating conditions for this setup are then characterized, and the next step is initiated. The vector DOD setup consists of a Bridgeport Series I EZ-Trak DX milling machine for vector movement, a Honeywell micro switch for DOD control, a function

generator for frequency specification and initial waveform generation input, a camera-LED system for verifying printhead operation, and two different DOD printheads. A Hewlett-Packard 51626A Inkjet printhead is utilized initially for analysis of equipment performance. The printhead is connected to the quill of the milling machine and traces shapes described by machine programs designed to simulate vector motion. Output from the HP printhead is recorded as ink on paper. Through this work, the micro switch control is successfully implemented with the addition of a switch debouncing circuit, and a limitation in vectoring speed is identified for the Bridgeport milling machine. A series of geometry experiments are conducted with CNC programs developed natively on the Bridgeport and later, with the implementation of raster-fills, using MasterCAM software. The visualization system is developed by using a circuit to adjust LED brightness and delay for droplet imaging on the milling machine. After developing a functional configuration for vector drop-on-demand printing, the efforts to generate a stable droplet using the Siemens PT-88S printhead and various binder systems is pursued and covered in Section 2.3. The variables affecting droplet formation, including binder viscosity and surface tension, waveform timing and voltage, droplet frequency, and various other factors, are examined to find a correlation between these settings and a steady droplet state. Through many tests using the Droplet Observation Station to check various conditions, a better understanding of the relationship between the printhead and its parameter settings is obtained, though many questions remain unanswered. By far, the complex nature of drop-on-demand droplet generation warrants further research. In the end, a stable waveform geometry based on timing and voltage is established for the water-based 2.4 v/o PAA binder and the Type "B" colloidal silica binder. After stable droplet formation parameters are established, vector DOD printing of 2.4 v/o PAA binder into alumina powderbeds is conducted and is discussed in Section 2.4. The two prior studies are integrated and multiple alumina prints are generated for analysis. Two different sets of experiments are conducted, one with normal, as-jetted alumina powderbeds and the other with sanded alumina powderbeds. The final results of these experiments provide a good comparison for the effectiveness of binder-based vector DOD printing versus standard 3DP part production methods.

The important conclusions from this research include: (1) the printing of the first 3DP vector printed parts using 2.4 v/o PAA binder with alumina powder, (2) the development of a highly functional, though speed limited, vector drop-on-demand printing configuration using the Bridgeport milling machine for vector motion and either a HP inkjet or Siemens printhead for DOD printing, (3) the analysis of DOD droplet generation parameters and the determination of a fairly stable waveform & voltage operating condition for two binder systems using the Siemens PT-88S printhead, and (4) the production and measurement of vector DOD binder printed individual lines from the PAA and alumina system, whose line widths are considerably smaller (140-170 µm) than conventional 3DP binder printing methods (350 µm).

The major issues that need to be resolved include: (1) the lack of a slurry-printing component for the vector DOD configuration to allow for multiple layer analysis, (2) the powderbed surface texture so that the highly anisotropic line features from slurry deposition do not dominate the surface finish and edge quality of printed parts, (3) the milling machine limitations of speed and programming so that higher production rates and more complex geometries can be effectively tested, (4) droplet stability analysis and optimization, which will lead to reliable implementation of the micro switch DOD control function, and (5) the limited development of vector DOD printing applications at this point. In terms of studying WC-Co tooling insert part production, further development of the slurry-binder system is necessary due to redispersion and binder interaction issues and afterwards must be followed by stable droplet formation analysis for DOD printing of the binder.

3.2.   RELATED DEVELOPMENTS & PROGRESS

Several important projects are concurrently under development that relate to the future direction of this research. One vital study involves revisions to the WC-Co slurry & binder formulation to increase compatibility and facilitate redispersion. Chosen based on experiments conducted by Olaf Dambon [18], the non-aqueous dispersant Emphos PS-21A was later shown to be reactive with the WC-Co powder so it was replaced. The current dispersant, Polyvinylpyrrolidone (PVP), and binder, Polyacrylic Acid (PAA) with Glycerol, react to form a incompatible gel. A new dispersant, known as Zephrym, does not react with the PAA binder but does not exhibit effective redispersion characteristics. Due to the difficult and complex task of developing this slurry-binder system, ongoing research involves investigating new dispersants, addition of redispersant(s), or binder systems that do not require curing. Another related development is the design and construction of a TDK Slurry-Vector Printing Machine currently underway. This machine implements multiple new approaches to 3DP part production. The slurry deposition mechanism consists of a spring-actuated, fast rastering arm that moves slurry across the substrate at a rate that allows lines to merge into a smooth uniform layer. The machine will also incorporate eight DOD nozzles currently being developed by Hiro Tsuchiya. The primary application of this new tool will be for electronics-related 3DP research. The possibility of conducting vector DOD printing experiments with WC-Co will also exist. Finally, the progress of 3DP tooling insert development will continue through experiments with the conventional slurry-binder printing tool known as the Hood Machine. Using this functional 3DP machine to study slurry jetting and binder printing conditions will provide a valuable foundation for future work once a slurry-jetting, vector DOD printing machine is available.

3.3. RECOMMENDATIONS FOR FUTURE WORK

From the discussion and analysis of the experiments performed in this research, various questions and concepts are posed that may warrant further investigation. The following recommendations are drawn from the innumerable considerations and ideas that follow from conducting such preliminary research. The process of vector printing the exterior profile is assumed to require multiple passes with slight changes in scale to adequately define the geometry. Currently, the number of passes used is four, though this choice is somewhat arbitrary. Research into determining the effects of each vector pass will provide a better understanding of how many are necessary and the benefits each contributes to the final part quality. Beyond the number of passes, the vector definition process can be done either from the exterior to the interior of the shape by gradually scaling down or vice versa. A comparison of these possibilities is also recommended to determine which method provides the best resulting edge definition. Many issues and variables, in addition to those outlined in Section 3.1, can be investigated to further the understanding and optimization of vector drop-on-demand printing for 3DP. These possibilities have been discussed throughout Chapter 2. One complex and highly variable aspect of this process is droplet generation and its corresponding parameters, such as waveform geometry and binder chemistry, both of which have numerous possibilities for adjustment. Another important consideration is the sequence of vector profiling versus interior raster fills. In terms of continuing the study of vector DOD printing of PAA binder into alumina, the size of a primitive drop size should be measured as well as the depth of infiltration. Eventually, it would be valuable to extend the examination of vector DOD printing from a single layer to a fully three-dimensional part to study its surface, edge, and line characteristics. In the end, the production of WC-Co tooling inserts through 3DP vector drop-on-demand printing would be the most worthwhile development.

REFERENCES

[1]   Ashley, Steven, "Rapid Prototyping Is Coming of Age," *Mechanical Engineering*, Vol. 117, No. 7, July 1995, pp. 62-68.

[2]   Grau, J., Cima, M.J., and E. Sachs, "Fabricating Alumina Molds for Slip Casting with 3-D Printing," *Ceramic Industry*, Vol. 140, No. 7, July 1996, pp. 22-25.

[3]   Sachs, E., Haggerty, J., Williams, P., and M. Cima, *United States Patent*, No. 5204055, 1993.

[4]   Sachs, E., Cima, M.J., Williams, P., Brancazio, D., and J. Cornie, "Three Dimensional Printing: Rapid Tooling and Prototypes Directly from a CAD Model," *Transactions of the ASME: Journal of Engineering for Industry*, Vol. 114, No. 4, November 1992, pp. 481-488.

[5]   Sachs, E., Wylonis, E., Cima, M.J., Allen, S., Michaels, S., Sun, E., Tang, H., and H. Guo, "Injection Molding by Three Dimensional Printing: A Desktop Manufacturing Process," *ANTEC*, 1995.

[6]   Lauder, A., Cima, M.J., Sachs, E., and T. Fan, "Three Dimensional Printing: Surface Finish and Microstructure of Rapid Prototyped Components," *Material Research Society Symposium Proceedings*, Vol. 249, 1992, pp. 331-336.

[7]   Sachs, E., Cima, M.J., Bredt, J., and A. Curodeau, "CAD-Casting: The Direct Fabrication of Ceramic Shells and Cores by Three Dimensional Printing," *Manufacturing Review*, Vol. 5, No. 2, June 1992, pp. 117-126.

[8]   Grau, Jason, "Fabrication of Engineered Ceramic Components by the Slurry-Based Three Dimensional Printing Process," Ph.D. Thesis, Massachusetts Institute of Technology, June 1998.

[9]   Heinzl, J. and C.H. Hertz, "Ink-Jet Printing," *Advances in Electronics and Electron Physics*, Vol. 65, 1985, pp. 91-171.

[10]   "Cemented Carbides and Cermets," *Metals Handbook*, Second Edition, Edited by J.R. Davis, ASM International, 1998, pp. 634-638.

[11]   *VT9000-02 Valenite: A Promise Worth Something, Die and Wear Products* [9:45 Documentary], Madison Heights, MI: Cincinnati Milacron Marketing Company, 1997.

[12]   Shimada, F. and T. Kainuma, *United States Patent*, No. 5288676, February 1994.

[13]   Benjamin, M.L., Dobbs, R.J., and M.E. Shaffer, *United States Patent*, No. 4478888, October 1984.

[14]   Benjamin, M.L., Dobbs, R.J., and M.E. Shaffer, *United States Patent*, No. 4456484, June 1984.

[15]   Benjamin, M.L., Dobbs, R.J., and M.E. Shaffer, *United States Patent*, No. 4397889, August 1983.

[16]   Caradonna, Michael A., "The Fabrication of High Packing Density Ceramic Powder Beds for the Three Dimensional Printing Process," S.M. Thesis, Massachusetts Institute of Technology, June 1997.

[17]   Sachs, E., "Prototyping and Manufacturing of Cutting Tool Inserts," *Proposal to Valenite and Kennametal*, January 1999.

[18]   Dambon, Olaf, "Development of a Rapid Fabrication Process for Tungsten Carbide-Cobalt Tooling Inserts by Slurry-Based Three Dimensional Printing," Diplomarbeit, Massachusetts Institute of Technology & RWTH Aachen, September 1999.

[19]   *Bridgeport Series I EZ-Trak DX: Installation, Maintenance, and Parts Breakdown Manual*, Code No. 1104-2900, Bridgeport Machines, Inc., Revision A: September 1996.

[20]   *EZTRAK 3-AXIS: Programming and Operations Manual*, Code No. 1104-2740, Bridgeport Machines, Inc., Revision A: November 1995.

[21]   Knezevic, Vedran, "Effect of Binder Drop Placement Strategy on Surface Finish of Fine Ceramic Parts by 3D Printing," S.M. Thesis, Massachusetts Institute of Technology, June 1998.

[22]   "Applying Precision Switches," *MICRO SWITCH General Technical Bulletin No. 14*, Honeywell Inc., 1998.

[23]   *HP 33120A Function Generator / Arbitrary Waveform Generator: User's Guide*, Part No. 33120-90005, Hewlett-Packard Company, August 1997.

[24]   "Krohn-Hite Model 7500 1 MHz Wideband Power Amplifier," Krohn-Hite Corporation. 2004. <http://www.krohn-hite.com/htm/amps/mod7500.htm> (10 May 2004).

[25]   "HP 26 Black Inkjet Print Cartridge Specifications: HP Home & Home Office Products," Hewlett-Packard Development Company, L.P. 2004. <http://h10010.www1.hp.com/wwpc/us/en/ho/WF06c/A10-12771-69422-56983-69422-56985-12809-12810.html> (20 April 2004).

[26]   "HP 51626 Series – No. 26 Black: MSDS," Hewlett-Packard Development Company, L.P. 2004. <http://www.hp.com/hpinfo/globalcitizenship/environment/productdata/pdf/ij_51626series_eng_v1.pdf> (20 April 2004).

[27]   Grover, Garth A., "Ink Jet Nozzle Test Station," S.M. Thesis, Massachusetts Institute of Technology, June 1999.

[28]   Bredt, James F., "Binder Stability and Powder/Binder Interaction in Three Dimensional Printing," Ph.D. Thesis, Massachusetts Institute of Technology, January 1995.

[29]   Uhland, Scott A., "Fabrication of Advanced Ceramic Components Using Slurry-Based Three-Dimensional Printing," Ph.D. Thesis, Massachusetts Institute of Technology, June 2000.

[30]   Morissette, Sherry, "Tailoring Suspension Chemistry for Three-Dimensional Printing of WC-Co Tooling Inserts," *Consortium Presentation*, June 2000.

[31]   Uhland, Scott A., Personal Communication, Massachusetts Institute of Technology, Cambridge, MA, February 18, 2000.